



Norwegian University of
Science and Technology

Back Calculation of Measured Settlements for an Instrumented Fill on Soft Clay.

Stian Berre

Master of Science in Civil and Environmental Engineering

Submission date: June 2017

Supervisor: Steinar Nordal, IBM

Norwegian University of Science and Technology
Department of Civil and Environmental Engineering



NTNU – Trondheim
Norwegian University of
Science and Technology

MSc Thesis
TBA4900 – Geotechnical Engineering, 2017

By

Stian Skjeldnes Berre

Title:

Back calculation of measured settlements for an instrumented fill on soft clay

BACKGROUND

The mechanical response of natural soft clays are complex and cause considerable challenges for geotechnical design and construction. Sampling of soft sensitive clays often results in low quality samples and uncertainty in soil properties. Back calculation of observed field measurement can give better understanding of in situ soil behaviour. For this purpose an instrumented embankment for a bridge abutment at the road project E6 Klett is going to be studied in this MSc project.

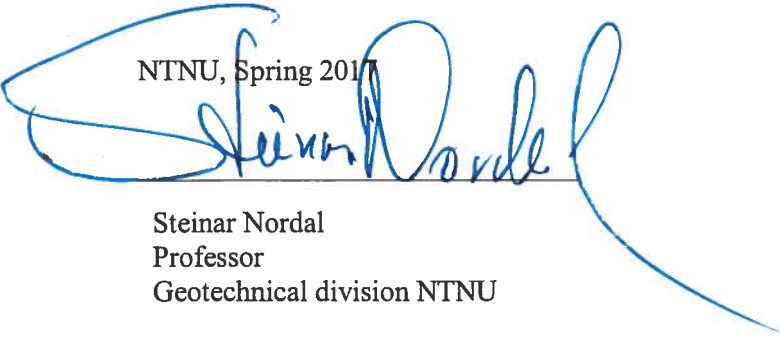
PROBLEM FORMULATION

The work proposed is to back calculate measured settlements and porepressures for the selected E6 Klett embankment constructed on soft clay and to investigate soil behaviour based on available data.

This is to be achieved by performing FEM analyses of the construction sequence of the embankment over time, reproducing the actual geometry, the installation of wick drains and the actual loading history. The simulations are to be compared to observed settlements as well as measured pore pressure over time. Soil models and soil parameters are to be selected to give the best possible fit. As part of the back-calculations it is also suggested to simulate laboratory tests using Soil Test in Plaxis. A discussion around what soil models and parameters are needed to provide a good fit with the observations, is welcomed.

The construction of the embankment involves a preload that is to be removed before the bridge abutment is constructed. Time for removal of the preloading is determined based on excess pore pressure dissipation and accumulated settlements. It is in Statens Vegvesens' interest to remove the preloading as soon as possible. The outcome of this study should contribute to documentation of sufficient consolidation before preloading removal.

NTNU, Spring 2017


Steinar Nordal
Professor
Geotechnical division NTNU



Report Title: Back Calculation of Measured Settlements for an Instrumented Fill on Soft Clay	Date: 15.06.2017
	Number of pages: 106
	Master Thesis x
Name: Stian Skjeldnes Berre	
Professor in charge/supervisor: Steinar Nordal (NTNU)	
Other supervisors: Arnfinn Emdal (NTNU) and Jon A. Rønningen (NTNU)	

Abstract:

Settlement problems in areas with soft sensitive clays are encountered in many parts of Norway and especially in areas of central Norway. Sampling of sensitive soft soils is challenging and often results in low quality samples which are hard to interpret. Back-calculations of observed field measurements and re-evaluation of laboratory samples can give better understanding of soil behavior for soft clays.

This study describes the performance of a full-scale fill constructed on soft clay, stabilized with pre-fabricated vertical drains in Klett, central Norway. A section of the fill has been investigated in detail using the finite element software Plaxis, where exact geometry and load application of the fill has been recreated through available data. Predictions of vertical displacement and pore pressure development are made and compared with field measurements.

A large number of laboratory tests have been investigated through background theory, and characteristic soil parameters have been interpreted. Two material models were used in the numerical analysis. In addition to a conventional model that accounts for creep, a more advanced user defined model was utilized to investigate the effect of destructuration.

This study has shown that a very good agreement between calculated and observed settlement can be achieved with an exact reconstruction of the fill in Plaxis. Both vertical displacement and pore pressure development are in line with field measurement, but deviations occur for first predictions. Verification against laboratory test data shows that both material models underpredict pore pressure development. Modifications and the use of the user defined model show very good fit for the first 280 days and the final prediction show almost an identical settlement development.

Keywords:

- | |
|------------------------|
| 1. Settlement |
| 2. Porepressure |
| 3. Ground improvements |
| 4. Numerical analysis |

Preface

This master thesis was written at the Norwegian University of Science and Technology, NTNU, in Trondheim during spring 2017. The work in this report represents 30 credits and completes my Master in Science degree in Civil and Environmental Engineering. The supervision in this master thesis was given by the geotechnical department at NTNU.

This report was developed in collaboration with Statens Vegvesen, Norwegian Geotechnical Institute and Finmeas OY. Large amount of data was supplied for the work in this report and they also contributed with interesting discussions and evaluation regarding the work in this report.

The idea of the project was brought up by me as I performed the installation of field measurements, used in this study, in collaboration with Finmeas OY. After a discussion with my main supervisor, Steinar Nordal, I contacted the involved companies and we defined the problem together.

Trondheim, 2017-06-12

Stian Skjeldnes Berre

Acknowledgment

I would like to thank my main supervisor Steinar Nordal and co-supervisor Arnfinn Emdal for good help during the work. I would also like to send a special thanks to Ph.D-candidate Jon A. Rønningen for all his support and guidance.

This thesis is written in collaboration with Statens Vegvesen, NGI and Finmeas OY. I would like to thank Eivind Juvik at Statens Vegvesen and Bjørn Kristian Bache at NGI for many interesting discussions and for all data supplied related to the previous work and site conditions in general. I would like to thank Finmeas OY for all data related to the field measurement.

Last, but not least I would like to thank my family for supporting me throughout the whole process and this report is a team effort from all of us.

S.S.B.

Sammendrag

Setninger i naturlig bløt leire er et problem som forekommer mange steder i Norge, spesielt i Midt-Norge. Prøvetaking av sensitiv bløt leire er utfordrende og resulterer ofte i prøver med lav kvalitet og usikkerheter rundt materialeegenskaper. Tilbakeregning av observerte setninger kan gi større forståelse av oppførselen til naturlig bløt leire.

Denne studien beskriver opptreden til en fullskala fylling på leire, stabilisert med prefabrikkerte vertikaldren på E6 Klett, sør for Trondheim. Et snitt tvers gjennom fyllingen er studert i detalj ved bruk av elementmetode programmet Plaxis. Geometrien av terreng og fylling, samt lastforløp er modellert på en realistisk måte gjennom tilgjengelig data slik som lasermålinger og dronebilder. Beregninger for setninger og poretrykksutvikling er sammenlignet med instrumenterte målinger.

Et stort antall undersøkelser fra laboratoriet er evaluert gjennom teori og karakteristiske parametere for leire er blitt tolket. To materialmodeller er benyttet i den numeriske analysen. I tillegg til en konvensjonell modell som implementer kryptformasjoner, er en mer avansert materialmodell benyttet for å studere effekten av degradering av stivhet rundt flytepunktet.

Denne studien viser analogi mellom beregnet og observert setning oppnådd gjennom en eksakt rekonstruksjon av fyllingen i Plaxis. Både vertikale deformasjoner og poretrykksutviklingen er i samsvar med målte verdier, men avvik observeres for de første antakelsene. Gjennom modifikasjoner og implementering av en bruker-definert modell oppnås veldig god overensstemmelse for de første 280 dagene og en tilnærmet identisk setningsutvikling.

Contents

Preface	i
Acknowledgment	iii
Sammendrag	v
1 Introduction	1
1.1 Background	1
1.2 Objectives	2
1.3 Limitations	3
1.4 Approach	3
1.5 Structure of the Report	4
2 Area and Site Conditions	5
2.1 Site Conditions	5
2.2 Field Measurements	8
2.3 Previous Work	9
3 Background Theory	11
3.1 Consolidation Theory	11
3.1.1 Primary Consolidation	11
3.1.2 Secondary Consolidation	12
3.2 Ground Improvements	14
3.3 Sample Disturbance	15
3.4 Anisotropy and Structure	19
3.5 Time Resistance Concept for Volumetric Creep	20
4 Methods	23
4.1 Plaxis	23
4.2 Soft Soil Creep Model	23

4.3	User Defined - Unified Enhanced Soft Clay Creep Model	24
4.3.1	Rotational Parameter β_{0NC}	25
4.3.2	Rotational Parameter μ	25
4.3.3	Destructuraion Parameter χ	25
4.3.4	Destructuration Parameter a_v	27
4.3.5	Destructuration Parameter ω	28
4.3.6	Compression Parameter g^*	28
5	Soil Parameters	29
5.1	General	29
5.2	Permeability Parameters	31
5.2.1	Numerical Modelling of Prefabricated Vertical Drains	32
5.3	Compressibility Parameters λ^* , κ^* and $r_{si}(\mu^*)$	33
5.4	Initial Stress	36
5.5	Strength Parameters	37
5.6	Back Calculation	37
5.7	USDM Input	40
6	Plaxis 2-D Model	43
6.1	Geometry	43
6.2	Mesh	44
6.3	Loading	46
7	Numerical Analysis	49
7.1	Simplifications and Assumptions	49
7.2	Settlement	49
7.3	Pore Pressures Beneath Fill	54
7.4	Modifications	59
7.5	Unloading	61
7.6	State Parameters	63
7.7	Mesh Analysis	64
8	Summary	67
8.1	Summary and Conclusions	67
8.2	Discussion	68
8.3	Recommendations for Further Work	70

A Acronyms	73
B Permeability	75
B.1 Vertical Drains Calculations	75
C Methods	81
C.1 Interpreted Oedometer Tests	81
C.2 Tri-axial Tests	89
C.2.1 Block Sample 1502 at Depth 14.91 m. and 9.99 m.	90
C.2.2 72mm Sample 2015 at Depth 16.40 m.	92
C.2.3 72mm Sample 2015 at Depth 9.55 m.	94
D 2-D Model	97
D.1 2-D Model	97
D.1.1 Measured Heights	97
D.1.2 Drone Photos	99
E Settlement	105
E.1 Settlement plates	105
Bibliography	107

List of Figures

2.1	Project site location	6
2.2	Field investigations for project site (Modified after (NGI, 2015)	7
2.3	Project site with cross sections, PVD and fill extension(Modified after (NGI, 2015) .	8
2.4	Piezometers and field settlement measurements in site area (Shaded area is fill in plane view). Sensor 9 is marked in blue (Modified after data from Statens Vegvesen	9
2.5	Settlement NGI	10
3.1	Definition of primary and secondary consolidation (After Mesri et al.).	12
3.2	Settlement diagram (After Bjerrum (1973)).	13
3.3	Compression (After Bjerrum (1967)).	14
3.4	Vertical drains (Modified after Steinar Hermann (1996)).	15
3.5	Example of oedometer test results on block sample and 54 mm sample (After Karl- srud and Hernandez-Martinez (2013)).	16
3.6	Modulus relationship from oedometer test (After Karlsrud and Hernandez-Martinez (2013)).	17
3.7	Oedometer test on block sample, Klett 10m (After Amundsen et al. (2015)).	18
3.8	Triaxial tests on block sample, Klett 10 m. (Modified after (Amundsen et al., 2015)).	18
3.9	Behaviour of natural clay in e - p'_c space (After Liu and Carter (2003)).	19
3.10	Surfaces during loading (After Liu and Carter (2003)).	20
3.11	Time resistance number for oedometer tests (After Grimstad (2016)).	21
4.1	Illustration of vertical pre-consolidation stress in relation to in-situ vertical stress (After Plaxis (2016)).	24
4.2	Surface definitions in p' - q plot (Karstunen and Koskinen (2008)).	26
4.3	One-dimensional behaviour of intact and reconstituted samples of soft sensitive clays(Karstunen and Koskinen (2008)).	26
4.4	Concept for finding χ for sample 2010 at depth 9.40 meter.	27

5.1	Cross section through embankment with vertical drains (After NGI (2015)).	32
5.2	CRS oedometer test 1210 at depth 9.40 meter (Modified after NGI (2015)).	34
5.3	CRS oedometer test 1210 at depth 9.40 meter zoomed in (Modified after NGI (2015)).	34
5.4	Stress and pore pressure distribution in depth for profile 260 (Modified after NGI (2015)	37
5.5	Stress-strain relationship and pore pressure development for SSC and USDM . . .	39
5.6	Stress-strain relationship and pore pressure development from lab tests (Modified after NGI (2014a))	39
5.7	Effective stress path SSC and USDM	40
5.8	Effective stress path lab (Modified after NGI (2014a))	40
5.9	Destructuration oedometer	42
6.1	Geometry plaxis model	44
6.2	Layer description	44
6.3	Mesh	45
6.4	Refined mesh areas	45
6.5	Loading	48
7.1	Settlement with and without correction for settlement plates	50
7.2	Load sequence	51
7.3	Effective stress development	51
7.4	Settlement with and without correction for settlement plates	52
7.5	Settlement	53
7.6	Settlement	53
7.7	Settlement compared with no ground improvements	54
7.8	Pore pressure development 2102 12m.	55
7.9	Pore pressure development 2105 12 m. depth	56
7.10	Pore pressure development 2105 12 m. depth	56
7.11	Pore pressure development 2101 5 m. depth	57
7.12	Pore pressure development 2102 12m.	58
7.13	Excess pore pressure at 183 days (Fill part 11) and 400 days (Consolidation 1 year)	58
7.14	Excess pore pressure at 183 days 400 days (Consolidation 1 year) for SSC without drains	59
7.15	Excess pore pressure with and without vertical drains for compressed loading . . .	59
7.16	Settlement compressed loading	60

7.17 Pore pressure development 2101 5 m. with compressed loading	61
7.18 Settlement modified structure	61
7.19 Settlement for unloading preloading after 300 days	62
7.20 Pore pressure unloading after 300 days	62
7.21 Destruction of structure after phase 11	63
7.22 Destruction of structure after consolidation phase	64
7.23 SSC with normal and very fine mesh	64
7.24 SSC with updated mesh and water pressure	65
7.25 Stress point and node for output results	66
8.1 Relation between volumetric strain and mean stress (After (Plaxis, 2016))	69
8.2 Elastic stress development for oedometer simulation in Soil Test	70
8.3 Pore pressure development 2105 12m.	71
B.1 Degree of consolidation over time (After NGI (2015)).	76
B.2 Conversion of axi-symmetric radial flow to 2-D plane strain flow (After Lin et al. (2000)).	77
B.3 Pre-fabricated vertical drains (PVD)	77
C.1 Interpreted oedometer 1510 18.67 m. depth. (Modified after NGI (2015)).	82
C.2 Interpreted oedometer 1210 9.40 m. depth (Modified after NGI (2015)).	83
C.3 Interpreted oedometer 1502 14.91 m. depth (Modified after NGI (2015)).	84
C.4 Interpreted oedometer 1504 10.35 m. depth (Modified after NGI (2015)).	85
C.5 Interpreted oedometer 1505 13.55 m. depth (Modified after NGI (2015)).	86
C.6 Interpreted oedometer 2015 9.40 m. depth (Modified after NGI (2015)).	87
C.7 Interpreted oedometer 2058 11.36 m. depth (Modified after NGI (2015)).	88
C.8 Interpreted oedometer 2059 9.5 m. depth (Modified after NGI (2015)).	89
C.9 Stress-strain relationship and stress diagram for SSC and USDM sample 1502 14.91 m. in Soil Test	90
C.10 Stress strain relationship and stress diagram laboratory tests sample 1502 (Modified after NGI (2015))	91
C.11 Stress-strain relationship and stress diagram for SSC and USDM sample 1502 9.99 m. in Soil Test	91
C.12 Stress-strain relationship and pore pressure-strain for sample 2015 16.40 m. in Soil Test	92

C.13 Stress strain relationship and pore pressure development laboratory tests sample 2015 16.40 m. (Modified after NGI (2015))	93
C.14 Effective stress path SSC and USDM 2015 16.40 m. in Soil Test	93
C.15 Laboratory tests sample 2015 16.40 m. (Modified after NGI (2015))	94
C.16 Stress-strain relationship and pore pressure development for sample 2015 9.55 m. in Soil Test	94
C.17 Laboratory tests sample 2015 9.55 m. (Modified after NGI (2015))	95
C.18 Effective stress path SSC and USDM 2015 9.55 m. in Soil Test	95
C.19 Laboratory tests sample 2015 9.55 m. (Modified after NGI (2015))	96
D.1 Cross section through embankment with vertical drains (After NGI (2015)).	98
D.2 Drone photo 04.08.2016 (Statens Vegvesen, 2016).	100
D.3 Drone photo 09.02.2016 (Statens Vegvesen, 2016).	101
D.4 Drone photo 10.10.2016 (Statens Vegvesen, 2016).	102
D.5 Drone photo 10.10.2016 (Statens Vegvesen, 2016).	103

List of Tables

5.1	Input parameters for Soft Clay Creep model and the Unified Enhanced Soft Clay Creep model	30
5.2	Assumed permeability values based on oedometer tests	31
5.3	Permeability 2D plane strain	33
5.4	Interpreted modulus numbers and pre-consolidation pressure	35
5.5	Input parameters	36
5.6	Sample 2010 depth 9.40 m. tri-axial data	38
5.7	Calibrated parameters USDMM	38
5.8	Calibrated input parameters USDMM	41
6.1	Construction history of fill in staged construction	47
6.2	Phase options	47
6.3	Compressed loading phases in staged construction	48
B.1	Permeability 2D plane strain	79
C.1	Input data for calibration	90
C.2	Calibrated input parameters USDMM	92
C.3	Calibrated input parameters USDMM	96
D.1	Load layers	99
E.1	Settlement Plates	106

Chapter 1

Introduction

1.1 Background

Large natural soft clay deposits are found in areas south of Trondheim, in central Norway. During last ice-age the area around Klett was below sea level and sensitive soft clays are encountered here. According to seismic examinations, performed by NGU ([Tønnesen, 1991](#)), there are measured distances of 400 meter to rock close to the outlet of the river Gaula.

In conjunction with the new European road, E6, an embankment for a bridge abutment is under construction. Challenging ground conditions with sensitive soft clays made it is necessary to monitor the settlement under the embankment to avoid differential settlements on the bridge. The settlements has already been predicted in a report by NGI in collaboration with Statens Vegvesen ([NGI, 2015](#)), but the predicted settlement are not completely in line with measured settlements.

The work proposed in this MSc research is to back calculate measured settlements and pore-pressures for the embankment constructed on soft clay and to investigate soil behaviour based on available data. This is achieved by performing FEM analysis with actual geometry and construction history for the fill in two dimensions and by verification of the FE-model against laboratory tests. The aim of the analysis is to reproduce the observed settlement development and achieve good fit with measured pore pressure over time. Time for removal of the preloading is determined based on excess pore pressure dissipation and accumulated settlements. It is in Statens Vegvesens' interest to remove the preloading as soon as possible. The outcome of this

study could contribute to documentation of sufficient consolidation before preloading removal.

Several studies of settlement of embankments on soft clays with vertical drains has been done during the last 20 years. It is shown in (Aalto et al., 1998) that 2D plane strain model can give good results when comparing calculated and measured settlement. The same conclusion can be made from a full scale embankment in Malaysia shown in (Indraratna et al., 1994), but it also indicates that the effectiveness of vertical bands in improving soil permeability plays a significant role in estimating settlements correctly. The excess pore pressure conditions and the vertical drainage must be correctly accounted for in order to predict an acceptable settlement development.

As mentioned, much research on this field has been done. All from classical Janbu (Janbu, 1969) and (Bjerrum, 1967) to state of the art research today. Still, problems occurs when predicting settlement especially in soft clays. New research lead to new methods for interpretation of soil behavior, but fundamental features such as anisotropy, destructuration and creep are still hard to hard to interpret from soil sampling. Later years more advanced material models that accounts for this features has been developed. It remains to apply this models to realistic problems and back calculations based on field measurements give valuable verification of new research. A new advanced constitutive model was used utilized on a test embankment on soft normally consolidated clay (Karstunen et al., 2005) and indicate significant improvement compared to conventional models, such as the MCC model.

1.2 Objectives

The main objectives of this project are:

1. Assemble theory and data to evaluate soil behaviour for project site.
2. Literature study of soft clay behavior.
3. Develop a representative plane strain model with exact geometry and load progress.
4. Investigate the performance of the model.
 - (a) Model with assessed parameters from soil samples.
 - (b) Model calibration against soil test and field measurements.

1.3 Limitations

This study is limited to settlement and pore pressure analysis of the fill on Klett. The earlier mentioned soil models are used and the advanced soil model is briefly investigated. The embankment recently ended construction phase and the consolidation (rest) phase is at an early stage, which means that the observed field measurements are still in progress. The level of settlement at the end of consolidation (1 year) will be a predicted value and the agreement with field measurements will not be available in this study. This limits the end conclusion.

Limitations has also been made for investigations of the fill performance. One cross section is investigated in detail and it could be interesting to compare against several settlement sensors, not only the one with biggest deformation. This limitations are based on the desire to obtain good results for the section under investigation and not risking quality reduction. Modelling several cross section would require a large amount of work additional to the work done in this report.

Another limitation made for this study is the investigations of horizontal displacement. In order to verify the results for excess pore pressure and vertical displacement it is necessary to monitor lateral displacement as well. Previous studies has shown that the accurate prediction of lateral displacement is a formidable task. This will not be evaluated in this report.

1.4 Approach

Previously evaluated soil samples from the project site will be used as basis for this study. These samples will be re-evaluated through a literature study. A realistically reconstructed model of the fill will delimit error sources in the numerical analysis.

The available soil samples from the project area will be assessed and used as input parameters in an advanced finite element model in the software Plaxis 2-D. After first prediction soil parameters will be re-evaluated again and calibrated against laboratory tests. Modified parameters will be implemented in the material models in the numerical analysis and a best possible fit between measured and calculated settlement will be the objective.

1.5 Structure of the Report

The main part of the report will be divided into following chapters with a short description for of each chapter:

- Chapter 2 - Area and site conditions
 - This chapter describes the location, ground conditions and the site in general.
- Chapter 3 - Background theory
 - This chapter contains a literature study of settlements in soft natural clays and show background theory for the important parts that affects the object of this study.
- Chapter 4 - Methods
 - This chapter describes the methods used in the analysis. Plaxis, Soft Soil Creep model and the Unified Enhanced Soft Clay Creep model.
- Chapter 5 - Soil parameters
 - This chapter describes how soil parameters used as input for the numerical analysis are found. Methods and calculations are shown for permeability and settlement input. Verification against laboratory tests is showed and calibrated parameters are presented.
- Chapter 6 - Plaxis 2D-model
 - This chapter contains descriptions of geometry, loading and mesh for the 2D-model in Plaxis and how exact geometry and load history has been developed.
- Chapter 7 - Numerical analysis
 - This chapter contains a predicted analysis based on soil parameters from the assessed soil samples. Discussions of performance and modifications are made. A mesh analysis is done.
- Chapter 8 - Summary and recommendations for further work
 - This chapter give a summary of the findings in this study, discusses the results and give recommendations for further work.

Chapter 2

Area and Site Conditions

The purpose of this chapter is to present the area and site conditions that are relevant to this study. Soil characteristics, soil sampling locations and field measurements used for comparison later in the study will be described.

2.1 Site Conditions

As a part of the the new European route, E6, a large embankment is constructed at Klett near Trondheim in Norway, see figure [2.1](#)

Site investigations reveals a dry crust layer of 1-3 meter above 6 meters of reconstituted clay from previous soil slides. Below 8 meter soft silty clay is detected down to unknown depth. The soft silty clay can be divided into a top layer of very soft sensitive clay with a thickness of 20 meter from 8 meter below ground surface. The ground water level is approximately 1-2 meter below ground surface. The pore pressure is artesian increasing 9.2 kPa to 50 meter depth. From 50 meter depth pore pressure is assumed to be hydro static ([NGI, 2014b](#)).

In situ tests evaluated in ([NGI, 2014b](#)) show that the clay is apparently homogeneous with a typical water content, w , around 32 % and density of $19,5 \text{ kN/m}^3$. The plasticity, I_p , is assumed to be 7 % for quick clay and 14 % for sensitive non-quick clay. Grain distribution analysis show a grain fraction of 30 % clay, few present sand and the rest is silt.



Figure 2.1: Project site location

The fill was constructed simultaneously with this study. The start of construction was 26 of August 2016 and finished before 16 of April 2017. The location of the project site can be seen in figure 2.1 and the relevant field investigations in the area are shown in figure 2.2. The designed fill can be seen in figure 2.3, which show extension, pre-fabricated vertical drains (PVD) and the different sections. Section B is investigated in this study. Vertical drains are installed under almost the entire fill.



Figure 2.2: Field investigations for project site (Modified after (NGI, 2015))

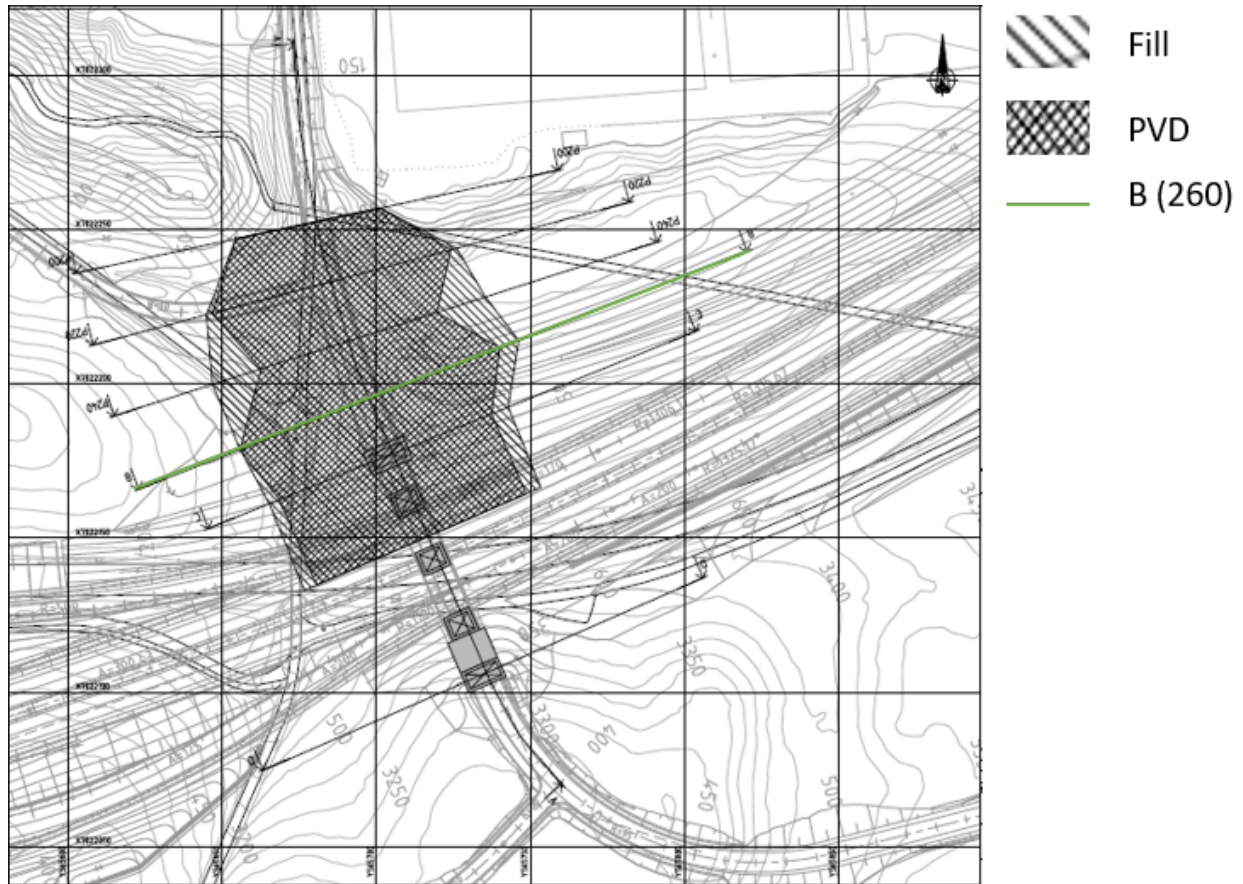


Figure 2.3: Project site with cross sections, PVD and fill extension (Modified after (NGI, 2015))

2.2 Field Measurements

The fill has been instrumented to monitor the vertical displacement and the development of excess pore pressure. The settlements beneath the fill are measured with settlement gauges, settlement plates and the pore pressure with pneumatic piezometers. The location of the field measurements can be seen in figure 2.4. The pre-fabricated vertical drains are not shown in figure 2.4 for diagrammatic clarity.

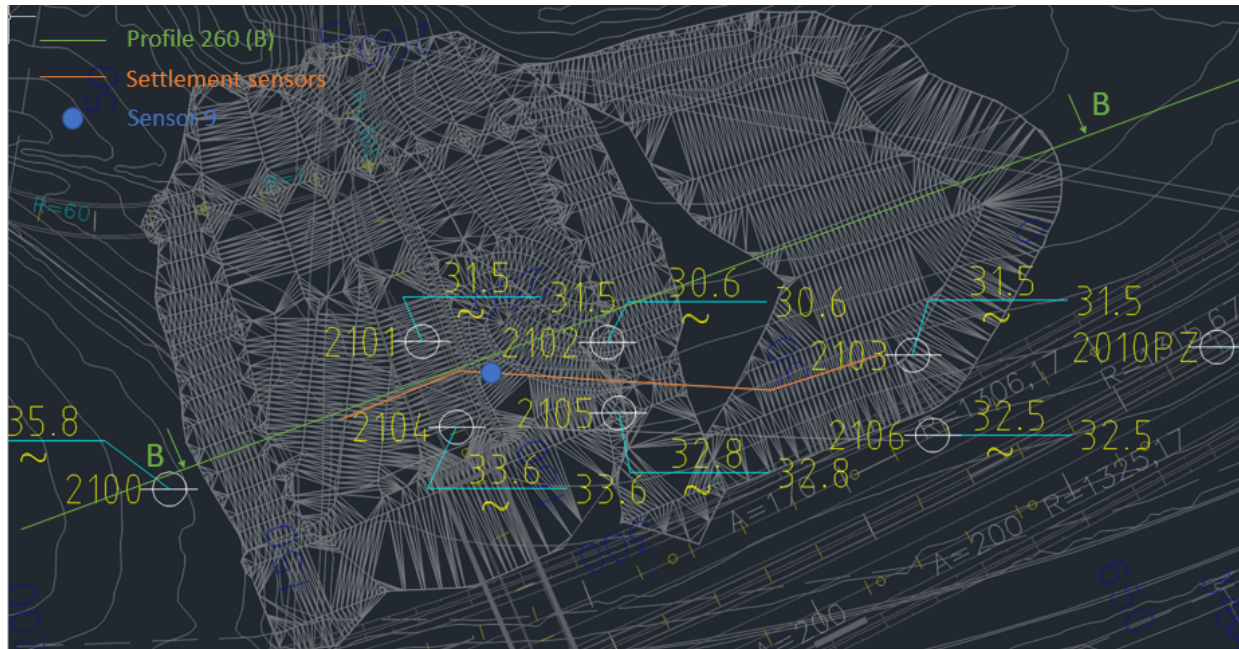


Figure 2.4: Piezometers and field settlement measurements in site area (Shaded area is fill in plane view). Sensor 9 is marked in blue (Modified after data from Statens Vegvesen)

2.3 Previous Work

As mentioned earlier in this chapter the predicted settlement for the fill has been calculated by NGI (NGI, 2015) and the predictions compared to observed settlement from field measurements are shown in figure 2.5. The calculations are based on the Janbu model for calculating settlement (NGI, 2015). Projected fill time was 4 months (120 days), but in reality it was closer to 7 months. More details about the project site and ground conditions can be found in (NGI, 2014b), (NGI, 2014a) and (NGI, 2015).

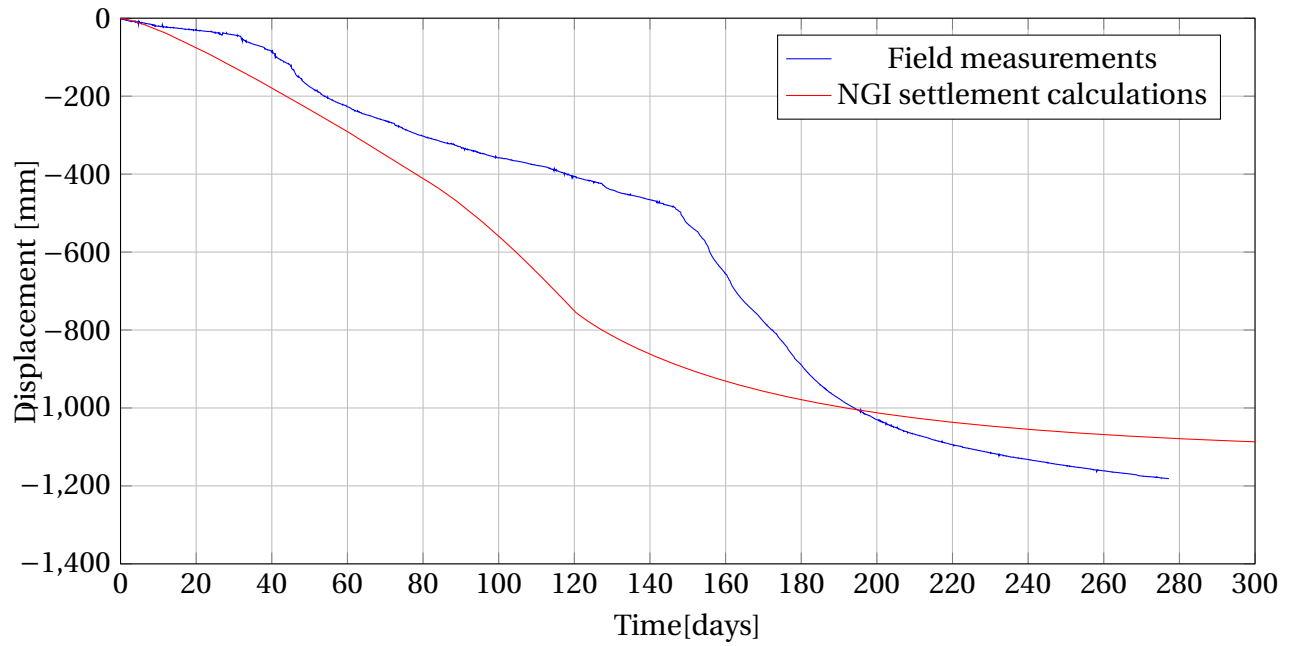


Figure 2.5: Settlement NGI

Chapter 3

Background Theory

The purpose of this chapter is to present the the main causes of settlement in soft clay that is relevant to this site. It is not the intention to give a fully description of settlement in general, but rather to explain how the different measures affect the settlement progress.

3.1 Consolidation Theory

Classical consolidation theory developed by Terzaghi (Terzaghi, 1943) states that pore fluid and the solid particles are in-compressible. This means that volume changes must be accompanied by excess pore pressure. This is a good approximation for clays, but later studies show that compression of the pore water and compression of particles is taken into account (Verruijt, 2008). Clays are highly compressible materials and deformation can be as large as several percents. By determining the consolidation of a material, one can predict the settlement that will occur with time. Settlements will decrease with time, but will never completely stop.

3.1.1 Primary Consolidation

Additional load will at first be carried by increased pore pressure, but with time the excess pore pressure will dissipate and this will lead to an increase in effective stress which causes settlement. This first loading leads to a consolidated clay and is denoted primary consolidation settlement. The ratio between settlement at time, t , and final primary settlement is defined as degree of consolidation as shown in equation 3.1:

$$U_p = \frac{\delta(t)}{\delta_p} \quad (3.1)$$

3.1.2 Secondary Consolidation

Secondary consolidation is following primary settlement and is not related to porepressure dissipation. The concept of consolidation is shown with the different stages in figure 3.1, where t_p describes the required time for primary consolidation to end. The effective stress situation is constant during secondary consolidation stage, $\frac{d\sigma'_v}{dt} = 0$, and it is controlled by the creep theory first described by Bjerrum (Bjerrum, 1967). Creep is considered as long term deformations and (Bjerrum, 1967) presented the relationship between void ratio, overburden pressure and time shown in figure 3.2. This diagram describes an equilibrium state for void ratio at different stress levels and show the time lines that corresponds to the overburden pressure. The volume change can be divided into two stages, one instant compression and one primary compression related to secondary consolidation as shown in figure 3.3. As the effective stress increases, the compression increases simultaneously. The bold line in figure 3.3 show the compression with the retardation of the clay particles taken into account. The dotted line shows the compression line in case the soil particles where not able to retard the compression. (Bjerrum, 1967) state that there is a significant difference in the age of the natural clay concerning strength and stiffness properties.

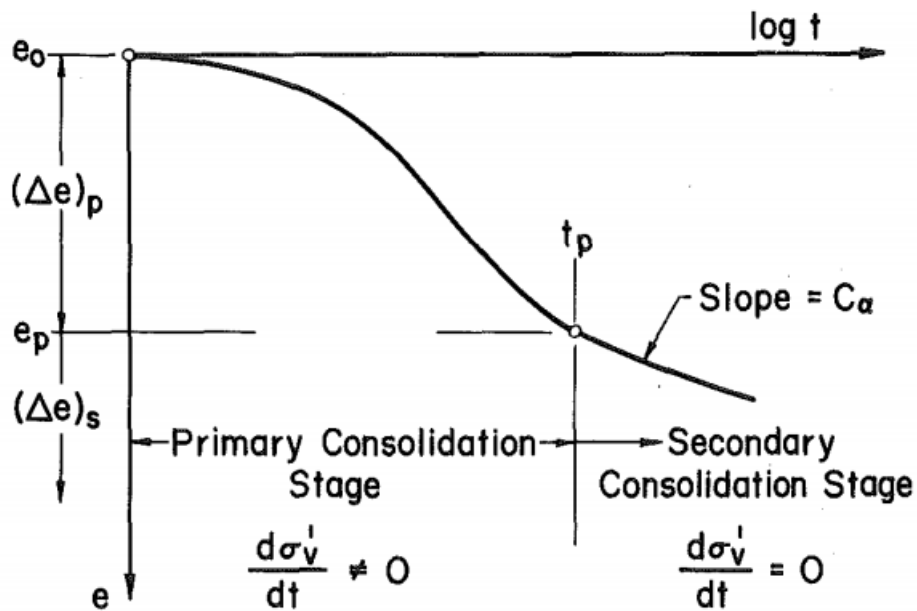


Figure 3.1: Definition of primary and secondary consolidation (After Mesri et al.).

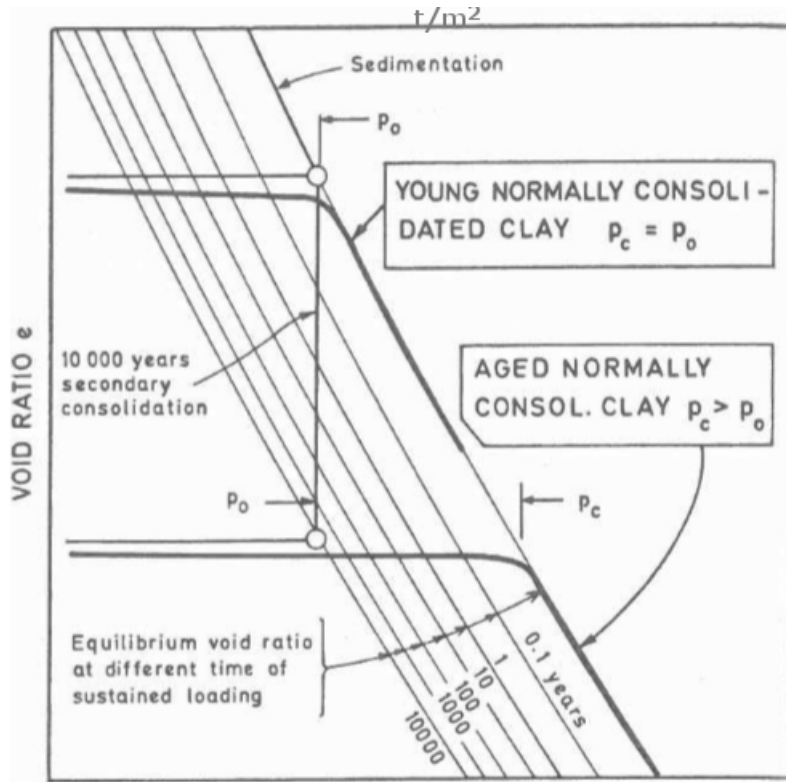


Figure 3.2: Settlement diagram (After Bjerrum (1973)).

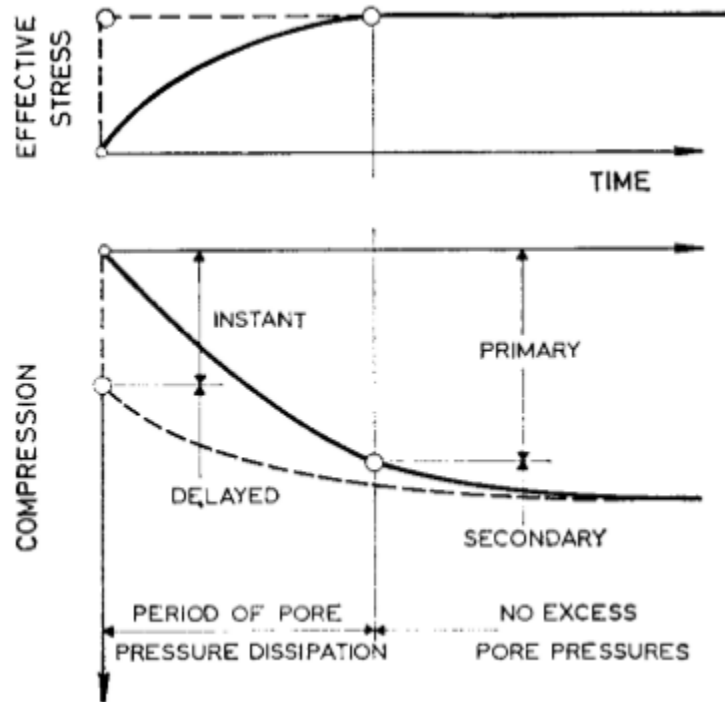


Figure 3.3: Compression (After Bjerrum (1967)).

The assumption of separating compression into primary and secondary contribution is a simplification that is not suited for describing the soil structure when it comes to effective stresses and settlement development in real cases. The excess pore pressure dissipation will depend on the thickness of the clay layer, permeability of the soil and the drainage condition. This is further described in (Bjerrum, 1967).

The creep effect will also occur during primary consolidation, but the contribution of creep strains are relatively small compared to the total strain in this stage.

3.2 Ground Improvements

Low-permeable soils, such as clays, have a long consolidation period and methods for ground improvements are used to speed up the settlement process by reducing the length of drainage paths and shortening consolidation time. The drainage path is shortened with practically all drainage happening horizontally towards the drains and vertically through the drains shown in figure 3.4.

Originally vertical drains consisted of sand drains with varying diameter. Nowadays pre-fabricated drains are preferred because of simple installation and flexibility and has become a widely used method internationally.

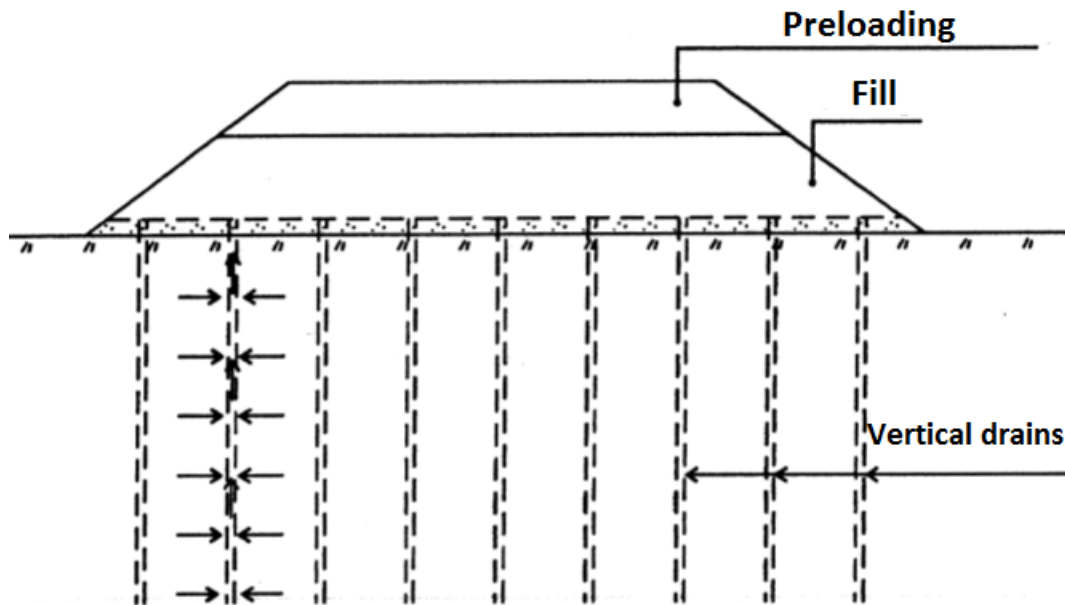


Figure 3.4: Vertical drains (Modified after [Steinar Hermann \(1996\)](#)).

3.3 Sample Disturbance

Natural soft clays are very prone to sample disturbance. Many researchers has proposed methods for correcting values derived from poor quality samples or methods for quality assessments. A method for defining pre-consolidation pressure p'_c is shown in ([Karlsrud and Hernandez-Martinez, 2013](#)). An assessment of low quality samples on plastic sensitive soft clay is shown in ([Amundsen et al., 2015](#)). The input parameters used in the soil models in the analysis are interpreted from soil samples and will have a large impact on the results. Because of this sample disturbance will be discussed in this section.

([Karlsrud and Hernandez-Martinez, 2013](#)) states that sample disturbance have a considerable effect on the mechanical properties of the sample. The stress-strain relationship and the strength of the clay are considerably affected and an example from the Onsøy site is shown in figure 3.5

where tangent modulus versus axial effective stress are compared. A large reduction in tangent modulus, M_0 , in the 54 mm piston sample is observed when loading towards the preconsolidation pressure. A higher value is also observed for the minimum tangent modulus, M_L , for the 54 mm and an increase in tangent modulus as the stress level increases into virgin consolidation.

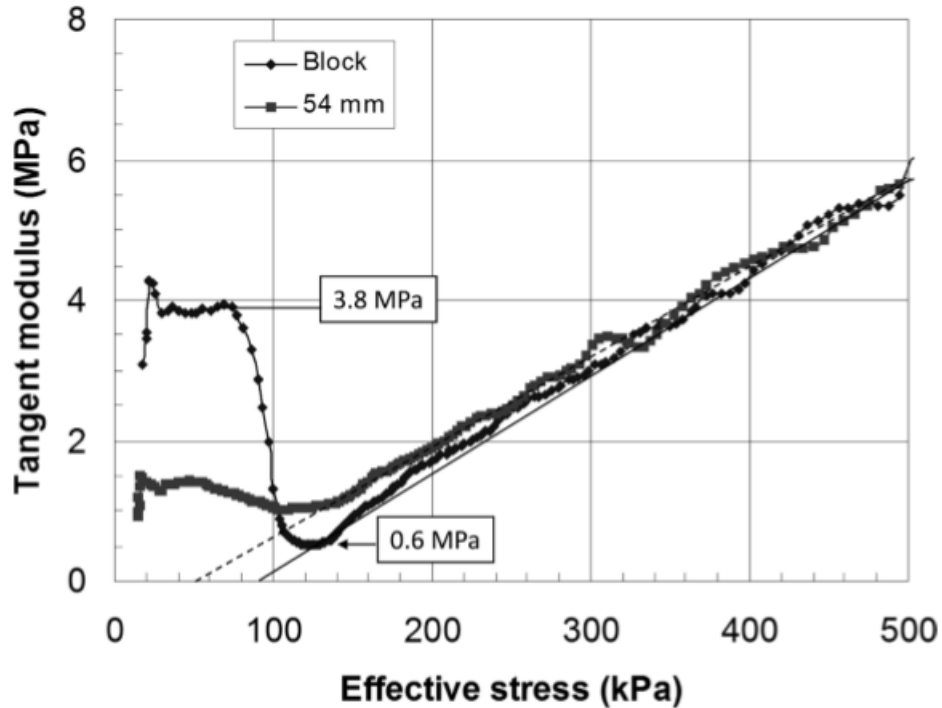


Figure 3.5: Example of oedometer test results on block sample and 54 mm sample (After [Karlsruud and Hernandez-Martinez \(2013\)](#)).

In figure 3.6 an example is presented on how to define key parameters, such as pre-consolidation pressure, p_c , and modulus values. The procedure described in ([Karlsruud and Hernandez-Martinez, 2013](#)) involves finding maximum re-loading modulus, M_o , which is the in-situ vertical effective stress when loaded from zero. From this point the modulus drops linearly to the minimum tangent modulus, M_L , with corresponding stress defined as σ'_{ML1} . For some clays the modulus is constant to stress level σ'_{ML2} before it starts to increase. The Janbu modulus number, m , is a tangent to the line towards virgin consolidation that rates increase on this line. The method for finding pre-consolidation pressure is simply the average value of the line from M_o to M_L . Normalized values for modulus relationships and p'_c are shown in ([Karlsruud and Hernandez-Martinez, 2013](#)) and included in the interpretations in ([NGI, 2015](#)).

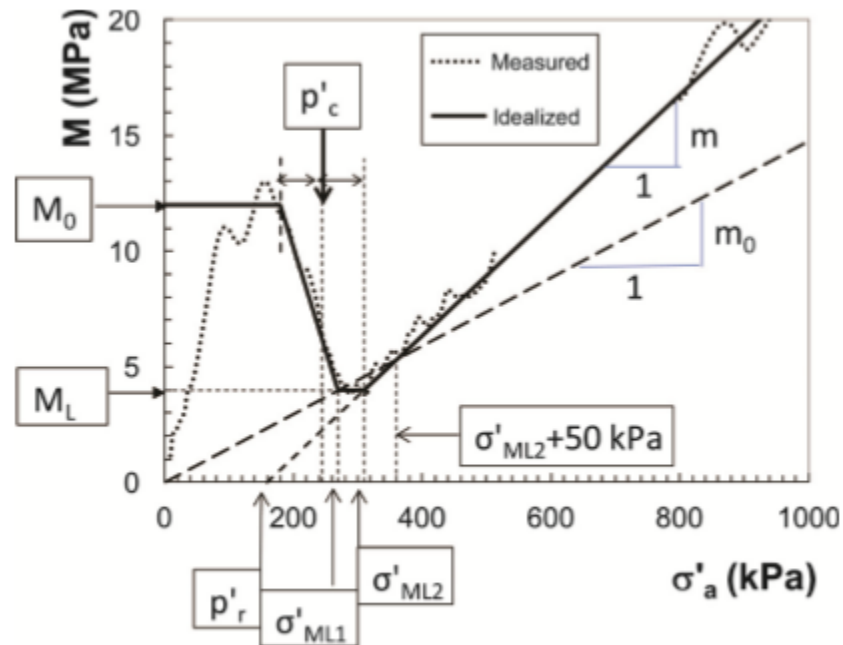


Figure 3.6: Modulus relationship from oedometer test (After [Karlsrud and Hernandez-Martinez \(2013\)](#)).

Oedometer and triaxial tests from Klett in figure 3.7 and figure 3.8 show two block samples carried out in two different laboratories, Lab 1 and Lab 2. Different handling in the labs indicate different results for the laboratory test. Lab 1 was tested with less time after opening of block. From figure 3.7 it is shown that the interpretation is easier for Lab 1 (1) than Lab 2 (2). Lab 1 tests has considerably larger M_0 than and a reduction in pre-consolidation pressure of 26-38% according to ([Amundsen et al., 2015](#)). For oedometer sample in figure 3.7 the break point of the ϵ_a vs σ'_v plot is more clear. Similar behaviour can be observed in figure 3.8 where sample from Lab 2 yields at lower effective stress. The effect of destructuration is less visible in oedometer tests than triaxial tests. The red line represents samples with no destructuration and this will be discussed later in the report.

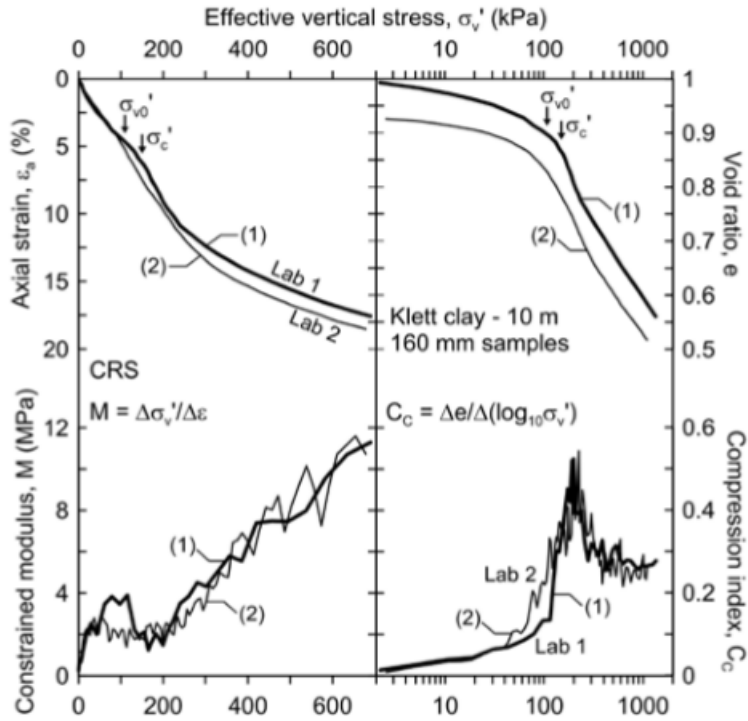


Figure 3.7: Oedometer test on block sample, Klett 10m (After Amundsen et al. (2015)).

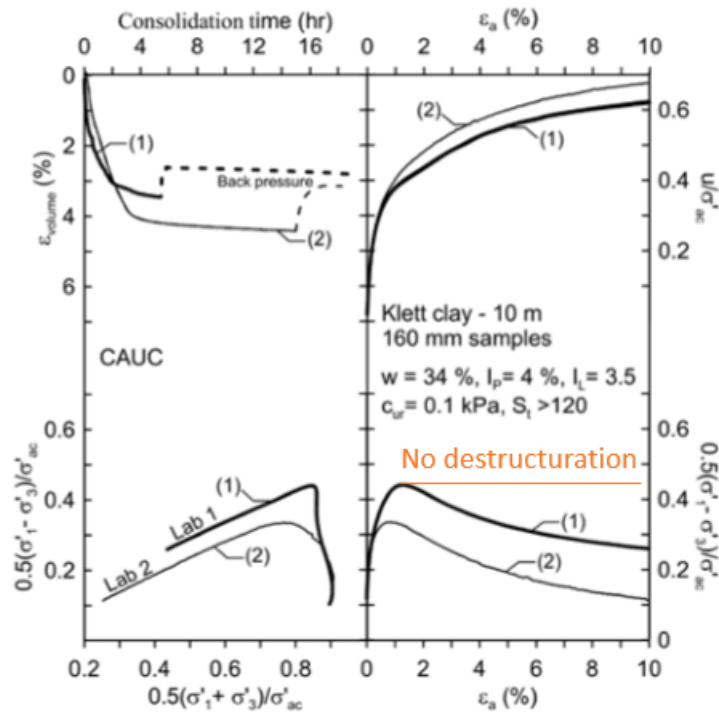


Figure 3.8: Triaxial tests on block sample, Klett 10 m. (Modified after (Amundsen et al., 2015)).

3.4 Anisotropy and Structure

Destruction of a material is gradually removal of the bondings in the soil as the strains increases. The process is driven by plastic strains. In figure 3.9 the behaviour of natural clay is shown in terms of the loading surface, p'_c and the void ratio. For elastic deformation (A-B), there is no plastic strains and consequently no destructuration. Virgin yielding starts at point B and continues to point C. From point C to D the soil is unloaded and reloaded again from D to E. The soil behaves elastically from stress path C-D-E and for further loading virgin yielding occurs (Liu and Carter, 2003). From (Leroueil et al., 1979) it is indicated that soft clays have a higher void ratio than reconstituted clays, as can also be seen on figure 3.9. It is also indicated that the compressibility is higher in soft clays than the reconstituted, but as the soil approaches the critical state line, see figure 3.10, the two samples should coincide. This is also shown in figure 4.3. The effect of destructuration generally leads to an underprediction of the vertical settlement as observed for the Murro test embankment (Karstunen et al., 2005) and the Haarajoki test embankment (Cudny and Neher, 1998).

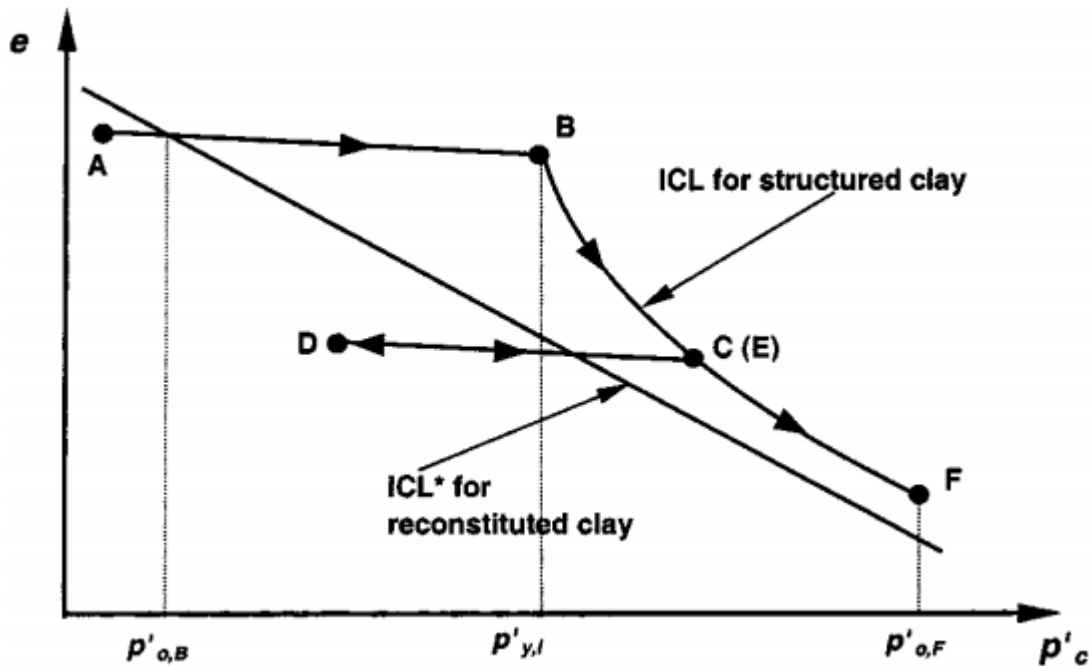


Figure 3.9: Behaviour of natural clay in $e-p'_c$ space (After Liu and Carter (2003)).

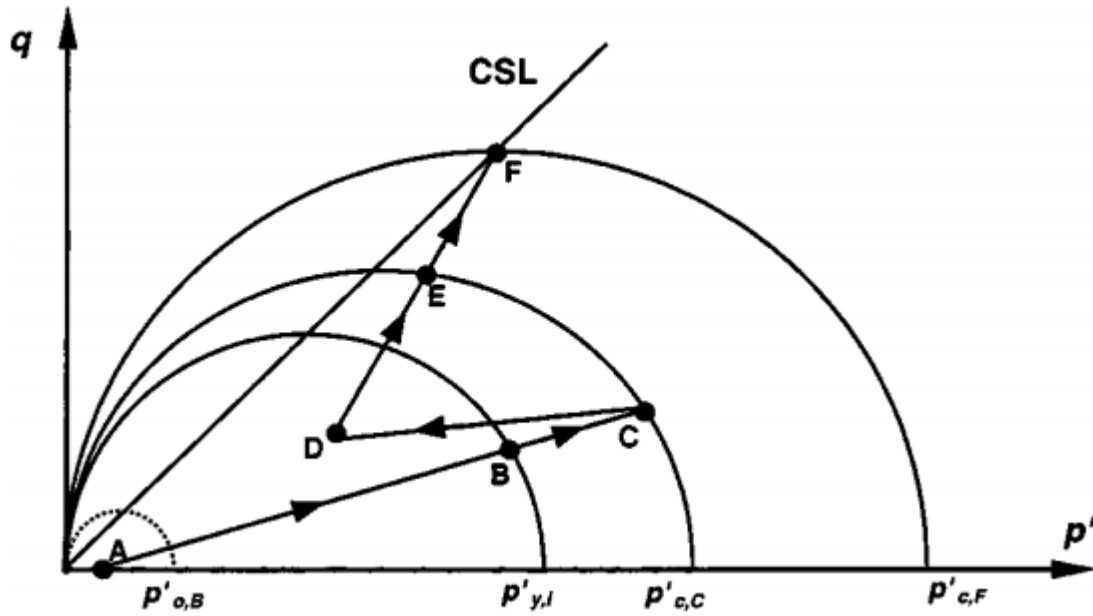


Figure 3.10: Surfaces during loading (After [Liu and Carter \(2003\)](#)).

3.5 Time Resistance Concept for Volumetric Creep

([Janbu, 1969](#)) defines time resistance as Resistance = Cause/Effect. In ([Grimstad, 2016](#)) it is shown that

$$R = \frac{dt}{de} \quad (3.2)$$

In figure 3.11 determination of the time resistance, R , and the time resistance number, r_s is shown for an idealized oedometer test ([Grimstad, 2016](#)). The end of primary consolidation phase is illustrated as the point up to "pure creep" and after this point, only creep will contribute to increased strain.

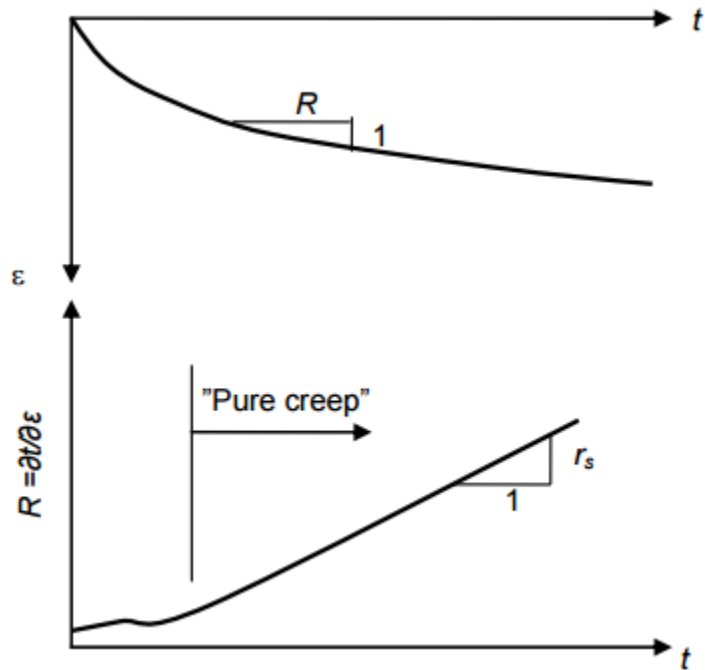


Figure 3.11: Time resistance number for oedometer tests (After [Grimstad \(2016\)](#)).

Chapter 4

Methods

The purpose of this chapter is to describe the software and the soil models used in the numerical analysis. Two different material models will be investigated in the numerical analysis and key features of each model will be explained here.

4.1 Plaxis

The fill will be modelled and analyzed in the finite element software program Plaxis 2D. The FEM theory is developed for small strain, but for large deformations Plaxis contains a feature which compensates for large strains. This feature will be used for this fill and this is later described in section [7.7](#).

4.2 Soft Soil Creep Model

The material model Soft Soil Creep is used in the analysis. This model is developed primarily for application to settlement problems of filings, embankments, foundations etc. It incorporates concepts of Modified Cam Clay models and viscoplasticity. SSC accounts for vicious effects, i.e. creep based on Janbu's time resistance concept ([Janbu, 1985](#)) and stress relaxation ([Plaxis, 2016](#)). This suits well with the purpose of this study.

The SSC model contains some limitations when it comes to prediction of the elastic range and does not show destructuration ([Mehli, 2015a](#)).

Modelling creep behavior of soft soil can give unrealistic creep deformations. Using pre-overburden pressure to control the over consolidation of soil can give large creep deformations with depth as the effective stress becomes very large compared to the POP value. The pre-overburden pressure is calculated as shown in equation 4.1. In figure 4.1 it can be seen that σ_p is kept constant, while σ'_{yy} increases with depth. For OCR, a increasing depth will not affect over-consolidation in same way. This is later described in section 7.7.

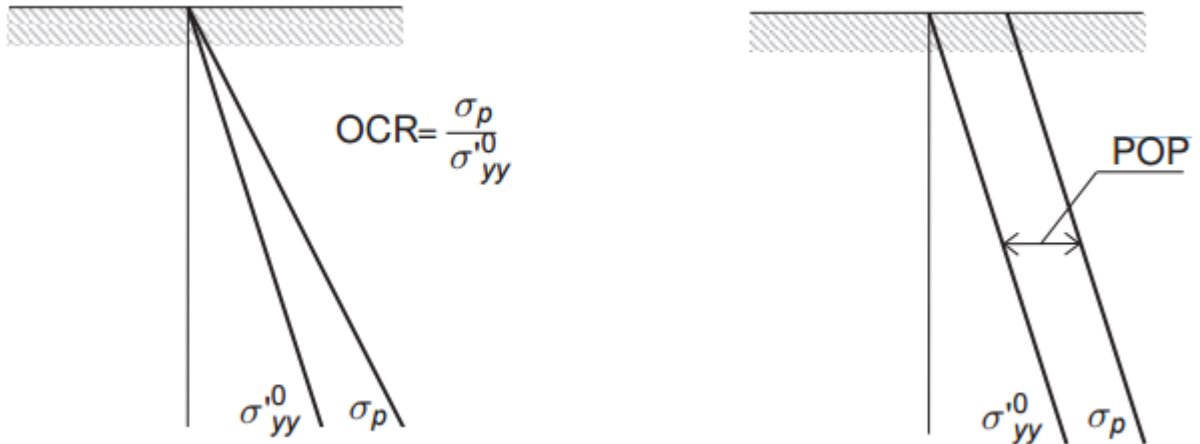


Figure 4.1: Illustration of vertical pre-consolidation stress in relation to in-situ vertical stress (After [Plaxis \(2016\)](#)).

$$POP = \sigma_p - \sigma'_{yy} \quad (4.1)$$

4.3 User Defined - Unified Enhanced Soft Clay Creep Model

The Unified Enhanced Soft Clay Creep model was developed under the framework of the CREEP project. Much of the development in the model has basis in the S-CLAY1S line of models ([Grimstad, 2016](#)). The S-CLAY1S models are used in many other studies of embankment and fills such as ([Mesri et al.](#)), ([Indraratna et al., 1994](#)), ([Cudny and Neher, 1998](#)) and ([Karstunen et al., 2005](#)). The S-CLAY1S models includes features that accounts for plastic anisotropy and anisotropy combined with destructuration, respectively. The Unified Enhanced Soft Clay Creep model is a synthesis of these models into a single model ([Grimstad, 2016](#)). For this study the model has been modified to induce POP instead of the standard OCR as control parameter for over-consolidation.

The destructuration rule is given by:

$$\frac{d\chi}{d\lambda} = -\chi * a_v * \sqrt{\left(\frac{\partial Q}{\partial p'}\right)^2 + \omega^2 * \frac{2}{3} * \left(\frac{\partial Q}{\partial \sigma_d}\right) * \frac{\partial Q}{\partial \sigma_d}} \quad (4.2)$$

where a_v is a destruction parameter, χ is a variable that introduces the effect of structure to the model and ω gives the relative portion of destruction coming from shearing [Grimstad \(2016\)](#).

4.3.1 Rotational Parameter β_{0NC}

The model parameter β is a steady state value obtained in a K_{0NC} condition. In order to compare the boundary value problem to the SSC model, a low β_{0NC} is used. A low β_{0NC} leads to low anisotropy.

4.3.2 Rotational Parameter μ

The parameter, μ , determines how fast the surfaces rotates. There is no easy way to derive a correct value for μ and the only solution would be to conduct model simulations with different values and then compare values to best fit ([Wheeler et al., 2003](#)). For this study a recommended value from ([Zentar and Koskinen](#)) will be used.

4.3.3 Destructuraion Parameter χ

The amount of particle bonding is described with a variable χ ([Karstunen and Koskinen, 2008](#)). This parameter changes due to destructuration as seen in figure 4.2 and 4.3 and will eventually become zero.

For this study the amount of structure will be determined/tested partly through IL oedometer tests, tri-axial and through model simulations with comparing the inclination of the settlement curve to measured settlement.

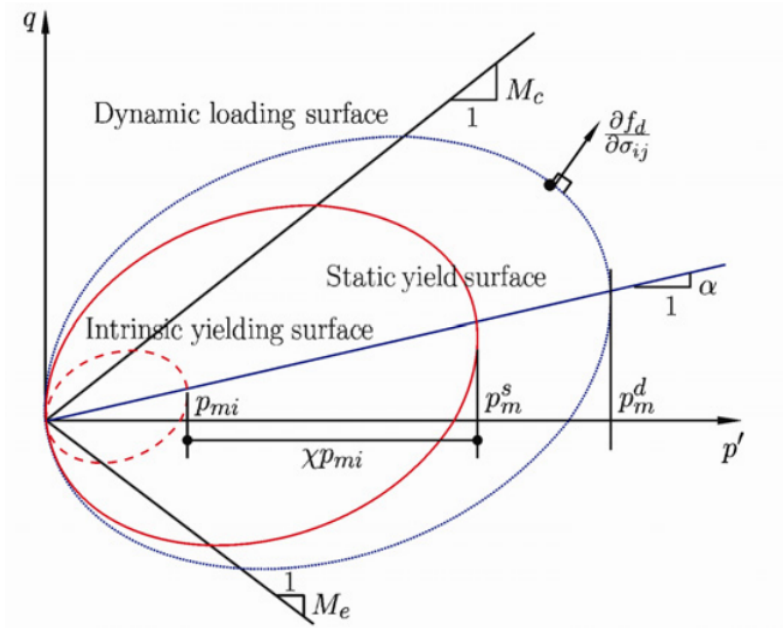


Figure 4.2: Surface definitions in p' - q plot (Karstunen and Koskinen (2008)).

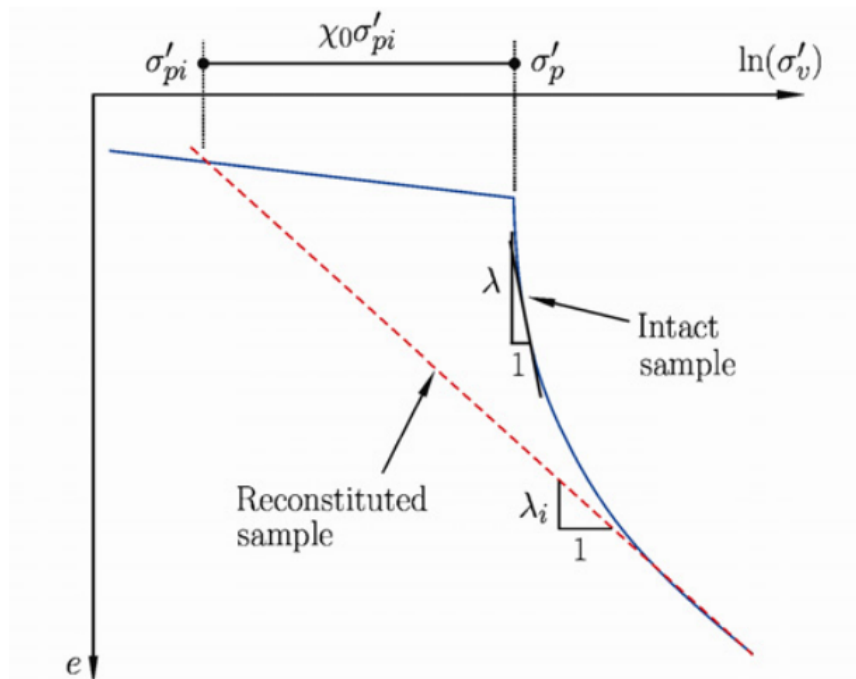


Figure 4.3: One-dimensional behaviour of intact and reconstituted samples of soft sensitive clays(Karstunen and Koskinen (2008)).

There are several ways of finding χ and (Grimstad and Degago) present a method involving time

resistance number found in an IL oedometer test:

$$\chi_0 = \frac{r_{si} - r_{smin}}{r_{smin}} \quad (4.3)$$

where r_{si} is insitric time resistance number and r_{smin} is the minimum measured time resistance number. Figure 4.4 show the principle for sample 2010 at depth 9.40 m. and will give a value of:

$$\chi_0 = \frac{1300 - 300}{300} = 3.33 \quad (4.4)$$

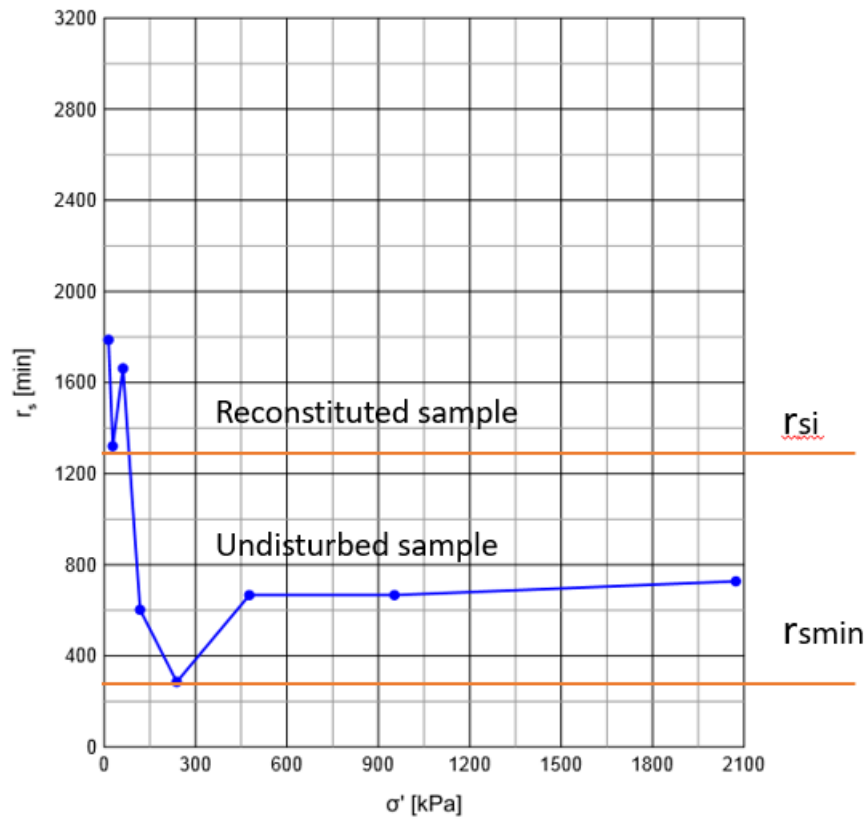


Figure 4.4: Concept for finding χ for sample 2010 at depth 9.40 meter.

4.3.4 Destructuration Parameter a_v

The rate of destruction is controlled by the parameter a_v and this will be determined through calibration in Soil Test in Plaxis. Values for a_v will be chosen and tri-axial simulations will be verified to fit with laboratory results.

4.3.5 Destructuration Parameter ω

The destructuration parameter ω describes the relative portion of destruction coming from plastic shear strains. This parameter is found through Soil Test in Plaxis and calibration to fit with laboratory tests.

4.3.6 Compression Parameter g^*

The parameters κ^* and g^* are related to volumetric and deviatoric stiffness ([Plaxis, 2016](#)). The relationship is given by:

$$\frac{\kappa^*}{g^*} = \frac{3(1-2\nu)}{2(1+\nu)} \quad (4.5)$$

$\nu = 0.15$ gives:

$$\frac{g^*}{\kappa^*} = 1.095 \quad (4.6)$$

This shows that g^* and κ^* should be in the same range.

Chapter 5

Soil Parameters

The purpose of this chapter is to present the input parameters which have been utilized in the numerical simulation. Soil samples relevant for the site have been interpreted through previous work and calibrated through back-calculation procedure to obtain similar results as in laboratory and field.

5.1 General

The procedure for finding input parameters for the material models are standard test practice.

1. Previous work discussed in ([NGI, 2015](#))
2. Interpret soil samples.
3. Simulate the laboratory tests in numerical software and back calculate to adjust parameters to best fit with laboratory and field measurements.

Table 5.1: Input parameters for Soft Clay Creep model and the Unified Enhanced Soft Clay Creep model

Type	Test type	Parameter	Unit	Physical meaning
Settlement	Index test	e_0	-	Initial void ratio
	1-D Compression test (Tri-axial, IL oedometer or CRS)	λ^*	-	Modified compression index
	1-D Compression test (Tri-axial, IL oedometer or CRS)	κ^*	-	Modified swelling index
	1-D Reconstituted compression (IL oedometer)	μ^*	-	Modified creep index
	1-D Compression test (Tri-axial, IL oedometer or CRS)	p_c	kPa	Pre-consolidation pressure
	1-D Reconstituted compression (IL oedometer)	r_{si}	-	Intrinsic creep number
	K0-oedometer	ν_{ur}	-	Poisson ratio
Destructuration	Tri-axial	ϕ_{cs}	°	Frictional angle critical state
	Tri-axial	K_0^{NC}	-	Normal consolidated region
	Tri-axial	X_0	-	Initial value of structure
	Tri-axial	ϕ_p	-	Frictional angles
	Tri-axial	g^*	-	Compressibility parameter
	Tri-axial	a_v	-	Rate of destructuarion
	Tri-axial	ω	-	Destructuration contr.
	1-D Compression test (Tri-axial, IL oedometer or CRS)	POP	kPa	Pre overburden pressure
	Tria-axial	μ	-	Rotation of surfaces
	Tri-axial	β_{K0NC}	-	Initial rotation ref. surface
	-	τ	day(s)	Reference time
	1-D Compression test (Tri-axial, IL oedometer or CRS)	OCR_{max}	-	Limit for creep induced OCR

The input parameters for the settlement analysis in the SSC model will be determined through interpreted laboratory data. The parameters linked with the Unified Enhanced Soft Clay Creep model will be partly interpreted by experimental data, but recommended values will also be used to simplify the process. The recommended values will be chosen from literature and in

consultation with Ph.D Candidate Jon A. Rønningen at NTNU. The main objective of the implementation of the user defined model is to investigate the effects from destructuration in the plastic range as described in section 4.3.

5.2 Permeability Parameters

Plaxis distinguishes between horizontal, k_x , and vertical, k_y , permeability. The change of permeability, c_k , is an advanced feature used in consolidation analysis. The permeability will change according to equation 5.1:

$$\log\left(\frac{k}{k_0}\right) = \frac{\Delta e}{c_k} \quad (5.1)$$

where Δe is the change in void ratio, k is the permeability in the calculation and k_0 is the input parameter of the permeability (k_x and k_y). A more thorough investigation of the c_k parameter could be done for each sample, but for this study the change of permeability is assumed to be $c_k=0,5 \cdot e_0$ (Tavenas et al., 1983).

For the project site on Klett permeability has been interpreted in (NGI, 2014b) and average values are listed in table 5.2.

Table 5.2: Assumed permeability values based on oedometer tests

k_0	k_0	β_k
$2 \cdot 10^{-9} \text{ m/s}$	0,063 m/year	5,0

The volumetric strain is described by the parameter β_k and is further described by the expression in equation 5.2.

$$\log k_i = \log k_0 - \beta_k \cdot \epsilon_a \quad (5.2)$$

In a standard CRS test pore water dissipation is associated with vertical permeability, k_x , due to the limitations of test procedure. This means that permeability in natural soft clays are expected to be higher in the horizontal than the vertical direction. (Indraratna et al., 1994) and (Mehli, 2015b) operate with values for k_x with a magnitude of $(1,5-2) \cdot k_y$. The same assumption is made

in this study as a basis for the permeability conditions.

5.2.1 Numerical Modelling of Prefabricated Vertical Drains

The classical way of calculating consolidation of soils improved by vertical drains as presented by (Barron, 1900) and later improved by Hansbo (Hansbo, 1981) must be converted into 2-D numerical procedures. There are several studies on how well the matching schemes from radial flow to equivalent two dimensional flow agree. A transformation procedure and verification study in Plaxis 2-D is shown by (Lin et al., 2000) and by (Indraratna and Redana, 2000).

A conversion from radial flow in the actual condition to the equivalent (2-D) plane strain flow is required to correctly model prefabricated vertical drains under fillings and embankments. See appendix B.1 for matching procedure.

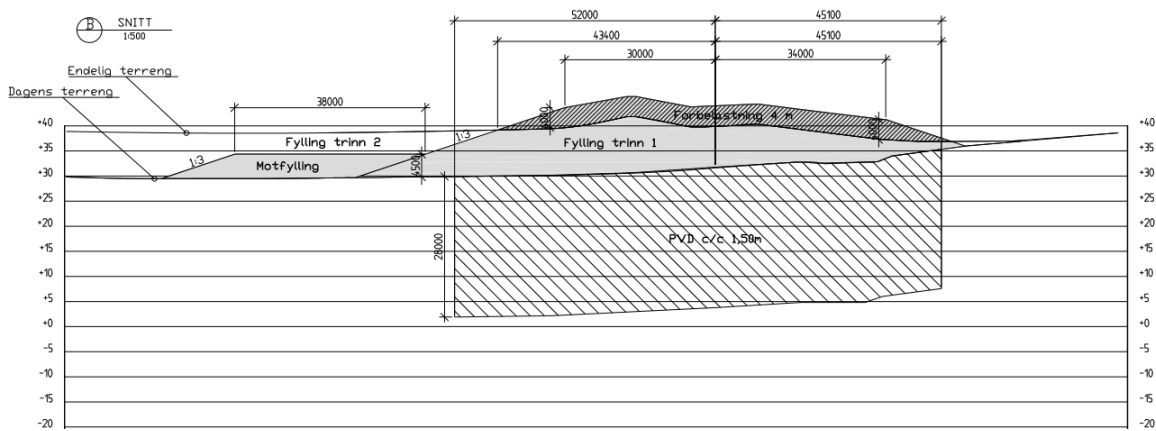


Figure 5.1: Cross section through embankment with vertical drains (After NGI (2015)).

- Drain pattern: triangular
- Length: 28 m
- Drain spacing: 1,50 m
- Cross section: 100 mm x 5 mm
- Equivalent diameter: 100 mm

The permeability parameters used in the analysis are listed in table 5.3

Table 5.3: Permeability 2D plane strain

Material	k_x (m/day)	k'_x (m/day)	k_y 8.64E-4(m/day)
Reconstituted clay	1.728E-4	2.29E-4	8.64E-4
Quick clay	3.456E-4	4.59E-4	1.728E-4
Soft clay	3.456E-4	4.59E-4	1.728E-4

5.3 Compressibility Parameters λ^* , κ^* and $r_{si}(\mu^*)$

The modulus numbers from CRS and IL oedometer tests are interpreted in (NGI, 2015) and (NGI, 2014b) and used as a basis for the evaluation of the compressibility parameters in the 2-D model. The oedometer samples has been reevaluated and new modified modulus number has been interpreted based on the method presented in (Karlsrud and Hernandez-Martinez, 2013). Reinterpreted parameters are listed in table 5.4 and the interpretation to determine the values may be seen in appendix D.1.

The secant modulus is determined as shown in figure 5.2. Regarding low quality samples from the site area, the destructuration can play a significant role in determining the modulus numbers. It is shown in figure 5.3 that the inclination is steeper for larger effective stresses than for lower stress states. The modulus number $m = 23.5$ for effective stress towards normal consolidation up to 1200 kPa, but for effective stress up to 500 kPa a line can be drawn giving $m_{nc} = 14.3$. m_{oc} is interpreted to be 105 for samle 1210 at depth 9.40 meter.

$$m_{nc/oc} = \frac{\Delta M}{\Delta \sigma'} \quad (5.3)$$

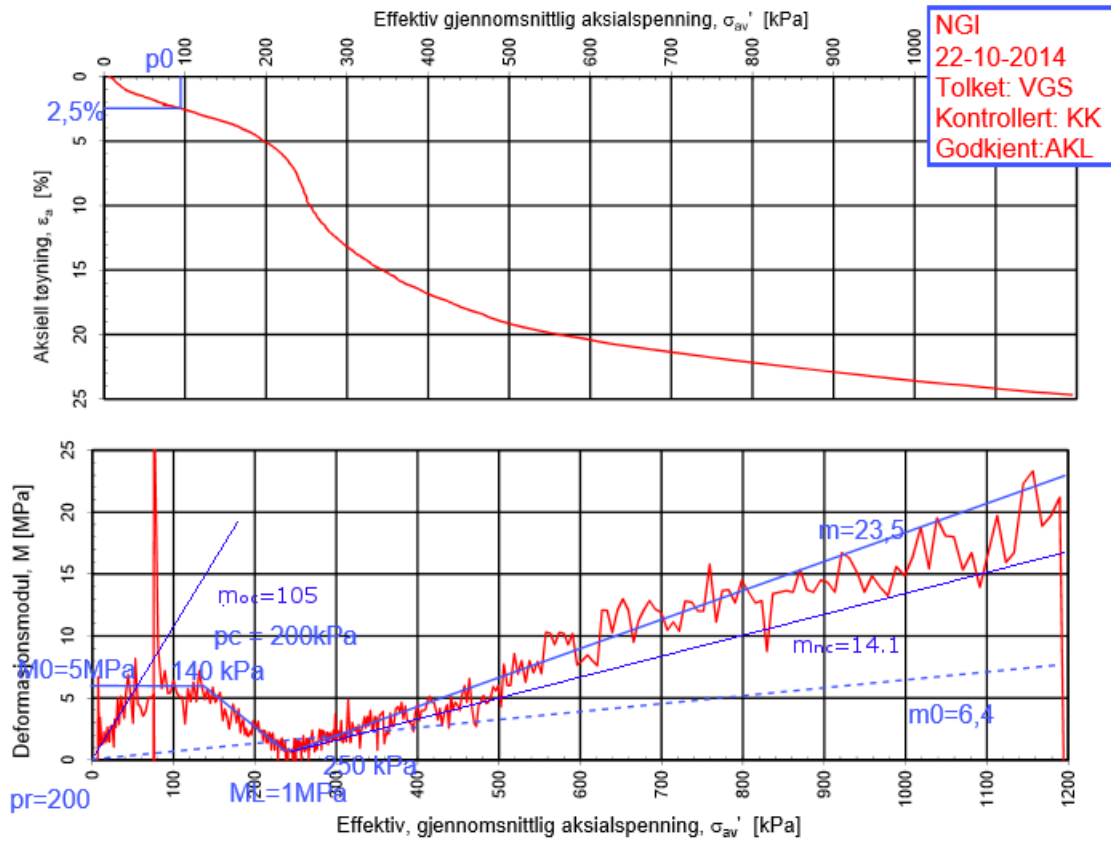


Figure 5.2: CRS oedometer test 1210 at depth 9.40 meter (Modified after NGI (2015)).

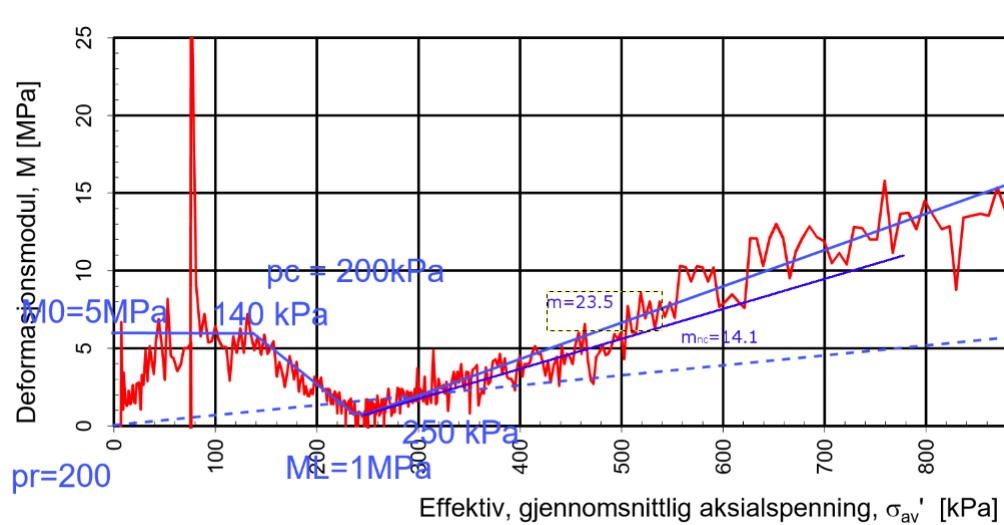


Figure 5.3: CRS oedometer test 1210 at depth 9.40 meter zoomed in (Modified after NGI (2015)).

This procedure has been done for oedometer tests of good enough quality. The sample quality is shown in (NGI, 2014b) and an evaluation based on methods for sample quality determination

used in (Karlsrud and Hernandez-Martinez, 2013) and (Amundsen et al., 2015) has been used to choose laboratory tests. The interpreted values for chosen tests are listed in figure 5.4

Table 5.4: Interpreted modulus numbers and pre-consolidation pressure

Borehole	Depth	m_{nc}	m_{oc}	p_c
1210	4.45	17.3	-	200
1210	9.40	23.5	110	200
1502	14.91	14.8	110	210
1502	18.67	14.3	84	250
1504	10.35	12.3	-	115
1505	13.55	22.5	-	-
1510	18.73	14.1	55	250
2015	9.40	-	76	260
2058	11.36	21.8	94.3	290
2059	9.50	-	50	240

The compressibility parameters (λ^* and κ^*) alongside the creep parameter (μ^*) is found from reinterpreted laboratory data and from normalized values (Karlsrud and Hernandez-Martinez, 2013) and adjusted to make best fit with measured settlement.

$$\lambda^* = \frac{\lambda}{1+e} = \frac{1}{m_{nc}} \quad (5.4)$$

$$\kappa^* = \frac{\kappa}{1+e} = \frac{1}{m_{oc}} \quad (5.5)$$

$$\mu^* = \frac{1}{r_s} \quad (5.6)$$

where m_{nc} is the secant modulus in the normally consolidated range and m_{oc} is the secant modulus in the over consolidated range, see figure 3.6. The creep number, r_s , is determined from IL oedometer tests and can be expressed as:

$$r_s = \frac{\Delta R}{\Delta t} \quad (5.7)$$

(NGI, 2015) and (NGI, 2014b) show that r_s is in the range of 300-700 for the site area and with a normalized value of $r_s = 510$ as input parameter. This value has been used as the input parameter for the creep index. The available data from the IL oedometer tests can not be

reevaluated appropriately through field measurement since the construction of the fill just finished and the values are therefore not adjusted.

Final input parameters for SSC are displayed in table 5.5. The fill (external loading) consists of reconstituted clay with an average weight of $19,5 \text{ kN/m}^3$ with sand layers. See (NGI, 2015) and (NGI, 2014a) for more information about fill material.

Table 5.5: Input parameters

Material	γ (kN/m^3)	λ^* (-)	κ^* (-)	μ^* (-)	POP (kPa)
Dry crust	19.5	0.0435	0.022	(-)	200
Reconstituted clay	19.5	0.0435	0.022	1.96E-3	200
Quick clay	19.5	0.0769	0.028	1.96E-3	200
Soft clay	19.5	0.0769	0.028	1.96E-3	200

5.4 Initial Stress

The pre-overburden pressure (POP) is defined as:

$$POP = \sigma'_c - \sigma'_v \quad (5.8)$$

An anticipated initial stress distribution with depth for profile 260 is shown in figure 5.4. The POP is used as initial stress both for the SSC and the Unified Enhanced Soft Clay Creep model. The initial horizontal stress is determined automatically for the SSC, but for the user defined model a value must be determined. As starting point for this study K_0^{NC} was set to:

$$K_0^{NC} = 1 - \sin(\phi) \quad (5.9)$$

Trendlines shown in (NGI, 2014b) gives $a = 2$ and $\phi = 31^\circ$. This gives $K_0^{NC} = 0.49$. Poisson ratio, $\nu_{ur} = 0.15$ is used as a recommended value (Nordal, 2016)

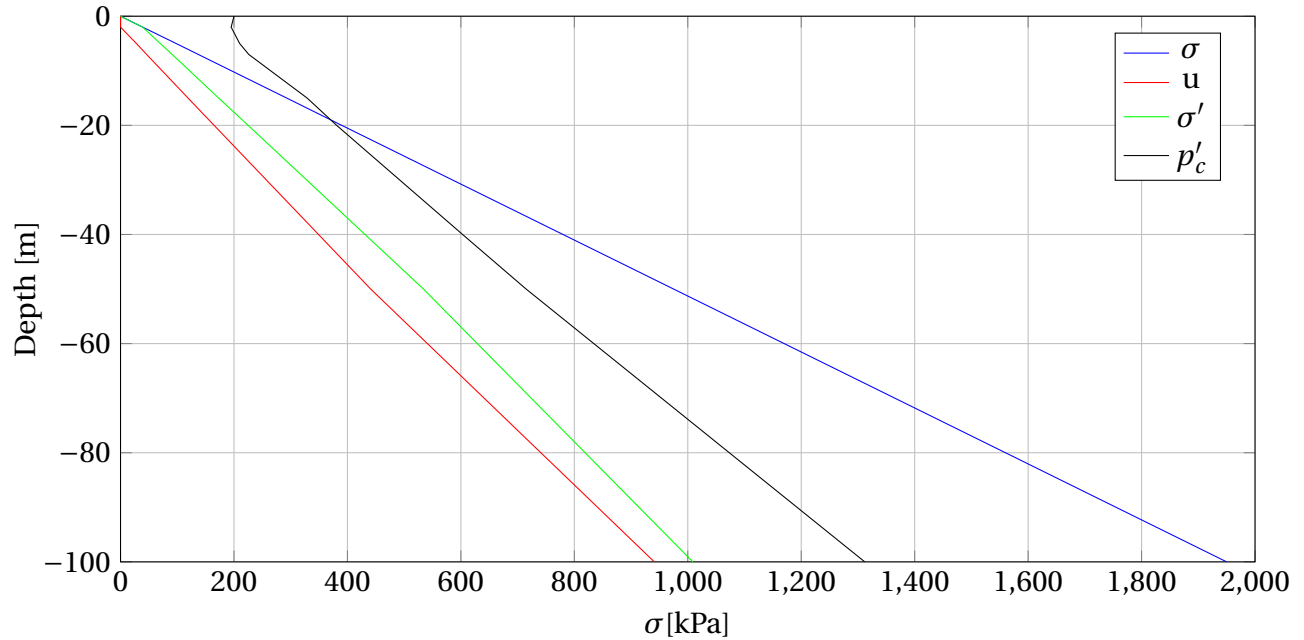


Figure 5.4: Stress and pore pressure distribution in depth for profile 260 (Modified after [NGI \(2015\)](#))

5.5 Strength Parameters

The strength parameters for the SSC model is taken from ([NGI, 2015](#)) and necessary input in Plaxis. The strength parameters related to the USDM model are based on back calculations of interpreted samples in order to calibrate parameters, see section 5.6. The frictional angle at critical state, ϕ_{cs} , is interpreted through Soil Test in section 5.6.

5.6 Back Calculation

Back calculations of CRS(C) tests has been done through soil test and curve fitting. The sample quality have affected interpretability. Soil Test has been used as a basis to calibrate input parameters alongside the mentioned procedure in section 3.3

The limitations for the SSC model regarding destructuration, as mentioned in section 4.2, is tested through the implementation of the USDM model. The performance analysis presented in Chapter 7 focuses on back calculating observed settlement through field measurements. The destructuration will be studied through calibration of input parameters from tri-axial tests against laboratory tests and field measurements.

Sample 2010 at depth 9.40 meter is studied in detail and data is shown in table 5.6. The same input parameters regarding λ^* and κ^* have been used for both models in the Soil Test option in Plaxis. The USDM has been calibrated to obtain similar results as laboratory tests and the calibrated parameters can be seen in table 5.7. More verification against laboratory tests can be seen in appendix C.

Table 5.6: Sample 2010 depth 9.40 m. tri-axial data

Sample nr.	Test size	Type	Depth	w_i	I_p	p'_0	σ'_{ac}	σ'_{rc}	K'_0
[-]	[mm]	[-]	[m]	[%]	[%]	[%]	[kPa]	[kPa]	[-]
2010	72	CAUA	9.40	33.0	6.0	119.0	119.0	71.0	0.6

Table 5.7: Calibrated parameters USDM

Parameters	
ϕ_{cs}	31°
ϕ_p	18°
λ^*	0.0769
K_0^{nc}	0.530
r_{si}	510
x_0	5.0
κ^*	0.0280
g^*	0.0280
a_v	25.00
ω	0.25
POP	119
μ	100.00
β_{k0nc}	0.100
τ	1.00
OCR_{max}	1.500

It can be seen in figures 5.5 to 5.8 that the Unified Enhanced Soft Clay Creep Model is superior to the Soft Soil Creep Model in terms of reproducing soil behaviour observed in laboratory tests. SSC is not able to show destructuration and cannot predict soil behaviour correctly as the strain increases. USDM show good agreement with laboratory test for destructuration. The excess pore pressure is closer to laboratory test for USDM, but both models underestimate

pore pressure development. For USDM 10 % of the excess pore pressure is not captured, while for SSC it is 30 %. USDM is able to capture the effective stress path, but yields too low. The same is observed for SSC, but SSC simulates less of the horizontal response.

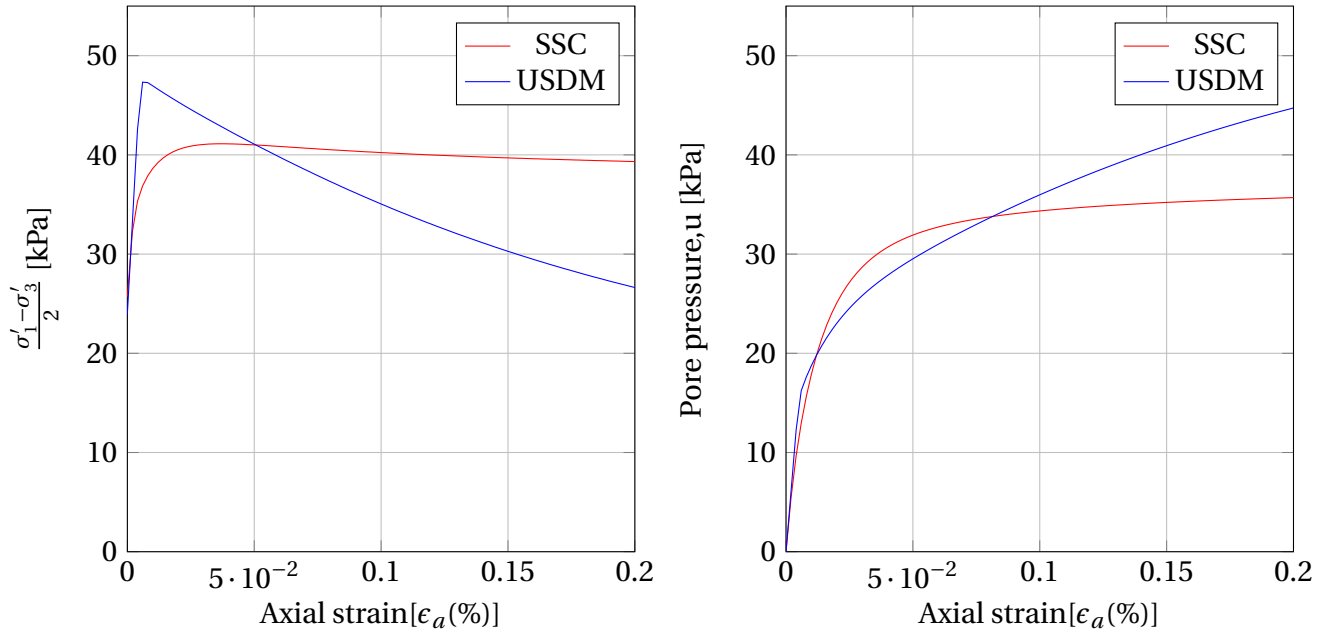


Figure 5.5: Stress-strain relationship and pore pressure development for SSC and USDM

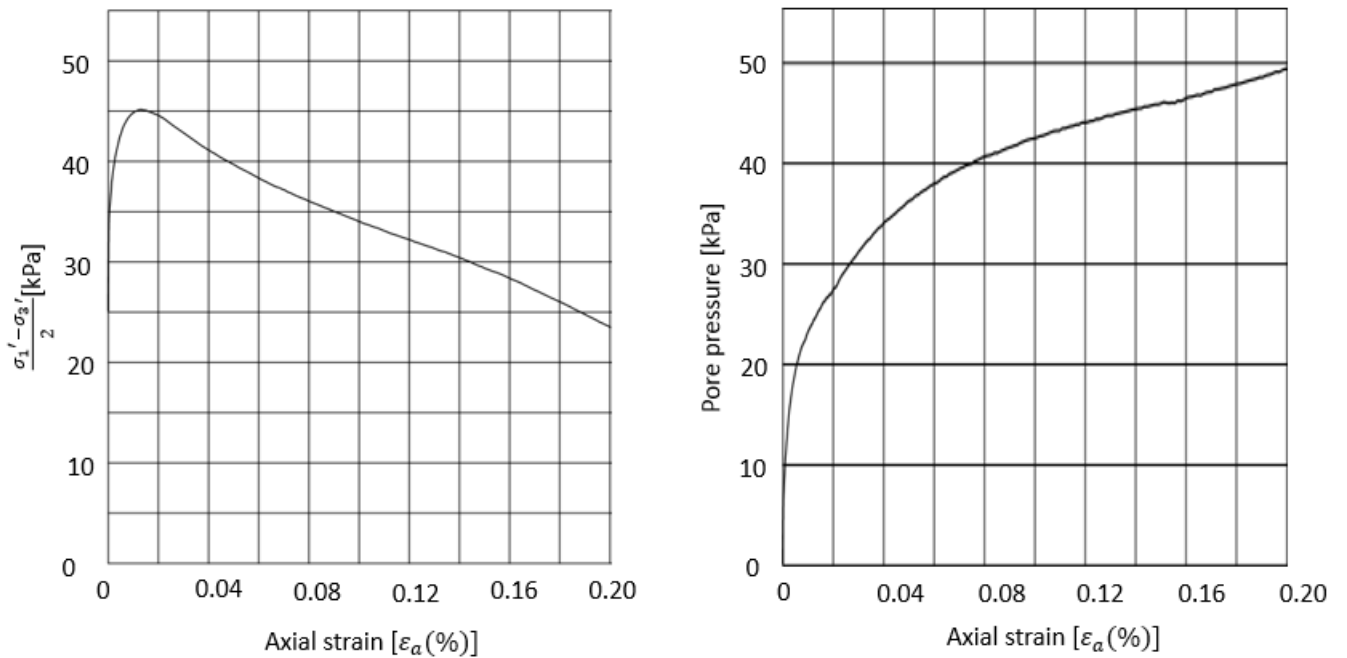


Figure 5.6: Stress-strain relationship and pore pressure development from lab tests (Modified after [NGI \(2014a\)](#))

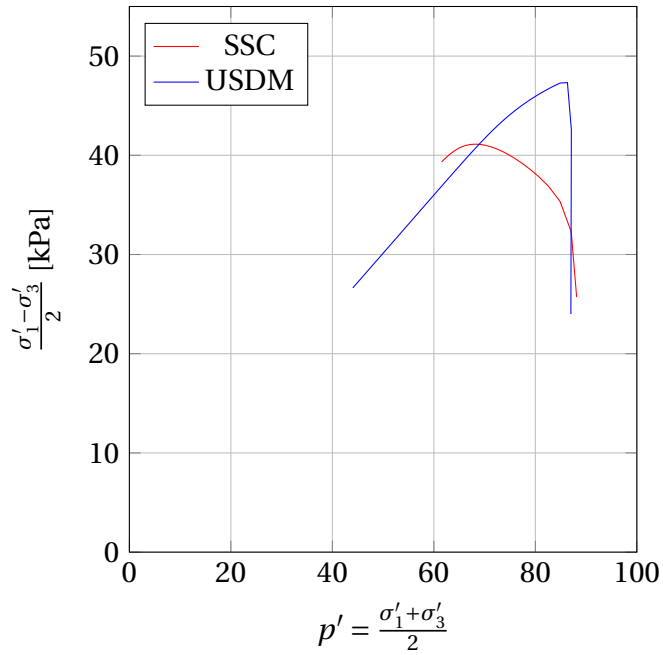


Figure 5.7: Effective stress path SSC and USDM

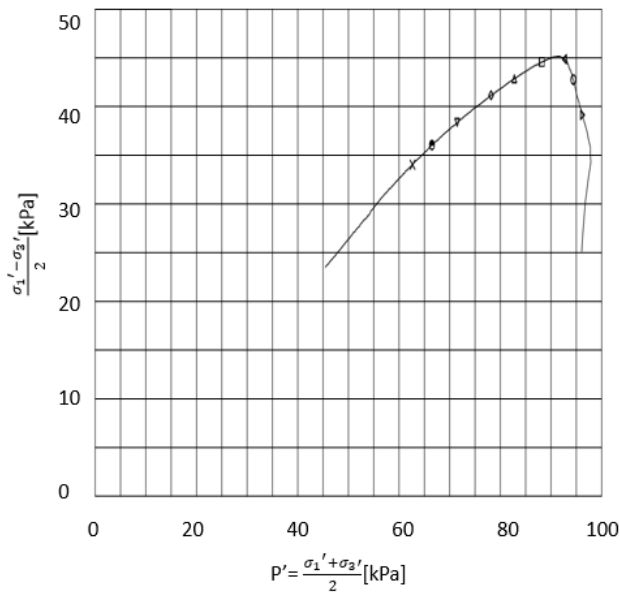


Figure 5.8: Effective stress path lab (Modified after NGI (2014a))

5.7 USDM Input

The calibrated input parameters found from section 5.6 and appendix C and modified in section 7.2 and 7.3 for the USDM are displayed in table 5.8.

Compression index, λ^* and swelling index, κ^* , are the same as showed in section 5.3. For the USDM model with increased initial value for structure in section 7.2 and 7.3 the x_0 is changed to 5 for both soft clay and reconstituted clay. The upper crust is modelled with the same parameters as for the SS model.

Table 5.8: Calibrated input parameters USDM

Parameters	Soft clay	Reconstituted clay
ϕ_{cs}	31°	31°
ϕ_p	22°	22°
K_0^{NC}	0.53	0.53
r_{si}	510	510
x_0	4	3
g^*	0.028	0.022
a_v	25	25
ω	0.25	0.25
μ	40	40
β_{k0nc}	0.25	0.25
τ	1.00	1.00
OCR_{max}	1.500	1.500

Oedometer simulation has been tested in Plaxis Soil Test to investigate the effect of destructuration on parameters from table 5.8. The only changed parameter is amount of structure, χ . More destructuration leads to a steeper curve after p'_c , shown in 5.9, and more vertical strain.

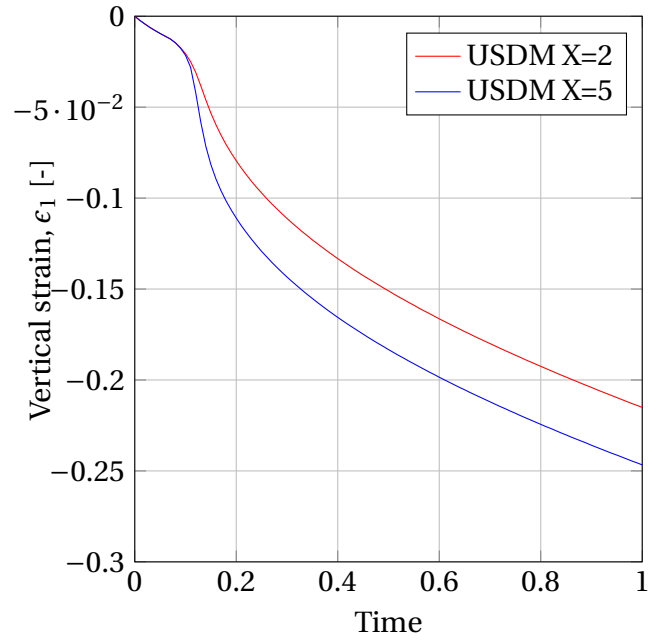


Figure 5.9: Destructuration oedometer

Chapter 6

Plaxis 2-D Model

The purpose of this chapter is to explain how the 2-D model is built up. Geometry and load history (construction) of the fill has been modelled realistically and are presented in this chapter.

6.1 Geometry

The terrain and fill has been modelled as described in (NGI, 2015) section B, profile 260. The model height, not included height of fill, is 190 meter and the width is 212 meter. The fill itself is 122 meter wide and approximately 15 meter at highest point, see figure 6.1. Figure 5.1 show the cross section, which have been used as input for the model in Plaxis. The phreatic line is placed 2 meters below ground level for the entire model based on in situ tests (NGI, 2015). The boundaries are free and the flow conditions are seepage for outer boundaries.

Vertical drains are modelled beneath fill, as shown in figure 5.1. They are 28 meters long, drain behaviour is normal and head is set to same level as ground water. Soil permeability for the affected layers have been modelled according to appendix C. The description of each layer is shown in figure 6.2.

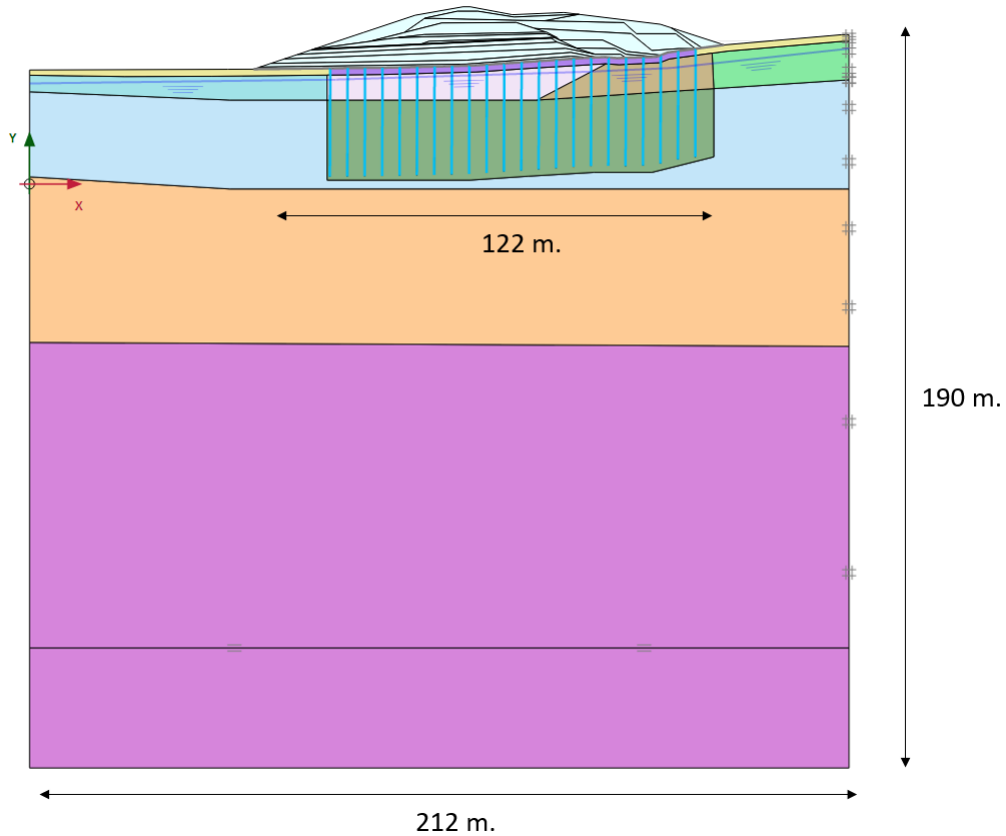


Figure 6.1: Geometry plaxis model



Figure 6.2: Layer description

6.2 Mesh

The mesh used in the analysis is medium with 4129 15-noded elements, see figure 6.3. Areas considered as important for output results have refined mesh. This is in particular areas beneath the highest point of the constructed fill below fill, shown in figure 6.4.

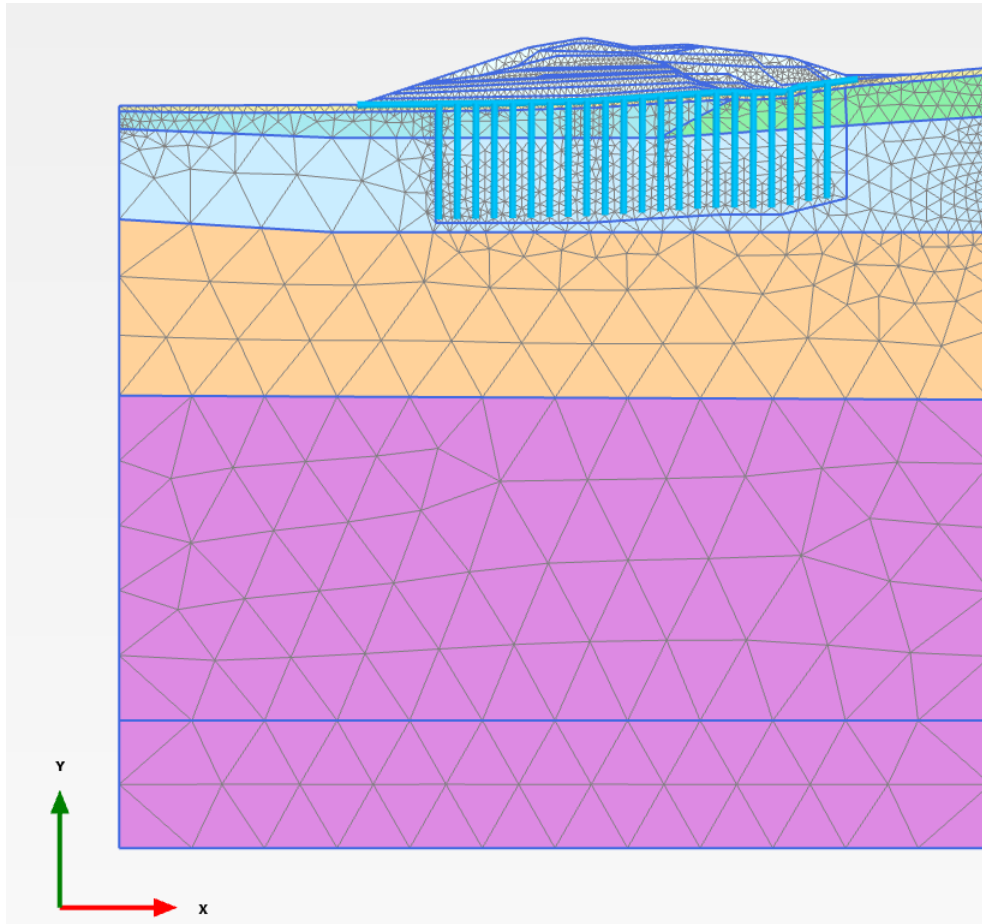


Figure 6.3: Mesh

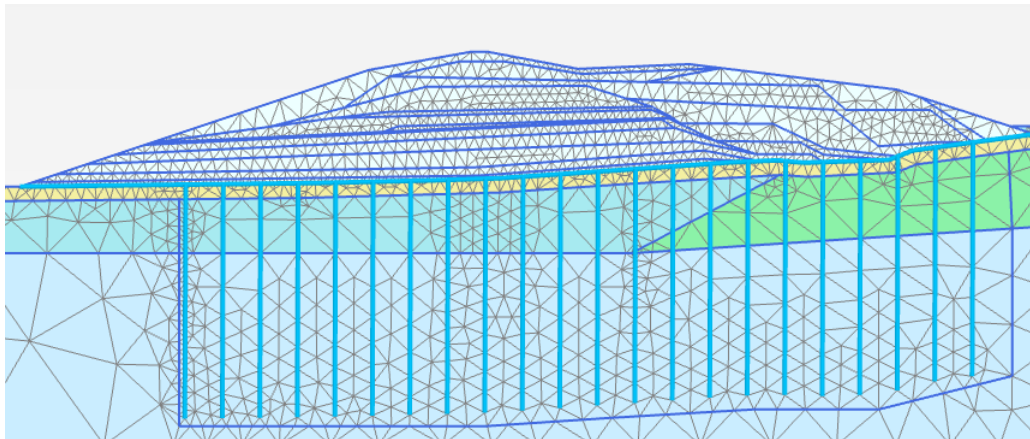


Figure 6.4: Refined mesh areas

Significant deformations will occur during the simulation and both analysis with and without updated mesh and water pressure have been tested. This is described later in Chapter 7.

6.3 Loading

The loading of the fill is divided into phases as shown in table 6.1 and each phase has the same general options showed in table 6.2. Measured height, from laser measurements, and date for each layer is shown in appendix D and figure 6.5. A realistic load simulation has been created through this data. Each fill layer is applied with the given time interval. The last measured height is done after end of construction and the time interval could deviate from the applied time.

Due to lack of load measurements for phase 1-4 drone photos has been used to recreate load application, see appendix D. The first measured height was performed at 25.10.2016, almost 2 months after start of construction.

A compressed load situation, later described in section 7.4, is shown in table 6.3.

Table 6.1: Construction history of fill in staged construction

Phase	Description	Time interval [days]	End time [days]
0	Initial phase	0	0
1	Fill part 1.1	15	15
2	Fill part 1.2	10	25
3	Fill part 1.3	15	40
4	Fill part 1.4	16	56
5	Fill part 2	16	72
6	Fill part 3	10	82
7	Fill part 4	11	93
8	Fill part 5	34	127
9	Fill part 6	12	139
10	Fill part 7	8	147
11	Fill part 8	8	155
12	Fill part 9	11	166
13	Fill part 10	4	170
14	Fill part 11	13	183
15	Fill part 12	22	205
16	Consolidation 1 year	240	360
17	Unloading	120	480
18	Consolidation	5000	5480

Table 6.2: Phase options

Phase options	
Calculation type	Consolidation
Loading type	Staged construction
Pore pressure calculation	Steady state groundwater flow

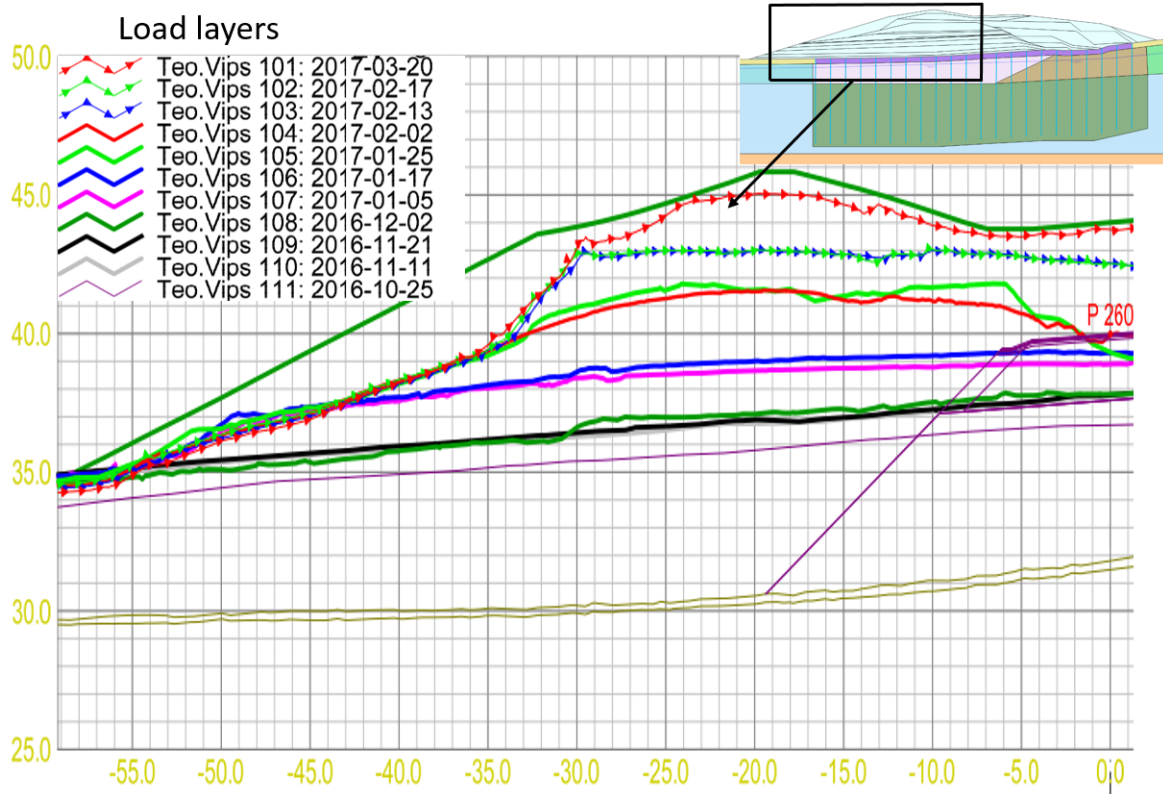


Figure 6.5: Loading

Table 6.3: Compressed loading phases in staged construction

Phase	Description [mm]	Time interval [days]	End time [days]
12	Fill part 9	10 (11)	165 (166)
13	Fill part 10	4 (4)	169 (170)
14	Fill part 11	7 (13)	176 (183)
15	Fill part 12	12 (22)	188 (205)

Chapter 7

Numerical Analysis

The purpose of this chapter is to present and discuss the result from the numerical analysis. The observed settlement from field measurements is compared to calculated settlement for the two respective material models. The development of pore pressure is compared with piezometers for comparison of excess pore pressure. After first prediction modifications has been made to obtain more similar results between field measurement and the numerical analysis

7.1 Simplifications and Assumptions

Certain simplifications has been made in the analysis. The soil properties in the dry crust has been given the same parameters as the reconstituted clay. No data for the over consolidated dry crust was available and assumptions were therefore made. Input parameters with higher stiffness for the OC top crust was analyzed, but this analysis showed that the top crust characteristics was not of big importance and the assumption of same behavior as reconstituted clay was kept. The layers in the 2D-Model are based on interpreted data from (NGI, 2014a) and (NGI, 2015).

7.2 Settlement

The settlement is monitored with a settlement gauge and settlement plates as described in section 2.2. The vertical displacement below the highest point of the fill is analyzed in this chapter and the location for output points can be see section 7.7. For the main part of this chapter the settlement is analyzed for 400 days which include loading (ca. 200) days and

consolidation phase (until unloading of preloading). An unloading after 300 days is included as part of objective to remove preloading as soon as excess pore pressure has dissipated, see Chapter 1.

The field measurements are plotted with and without correction for settlement plates in figure 7.1 and show an increase of around 50 mm at 275 days. The corrected displacement will be used for comparison with the numerical analysis and will only be referred to as field measurements.

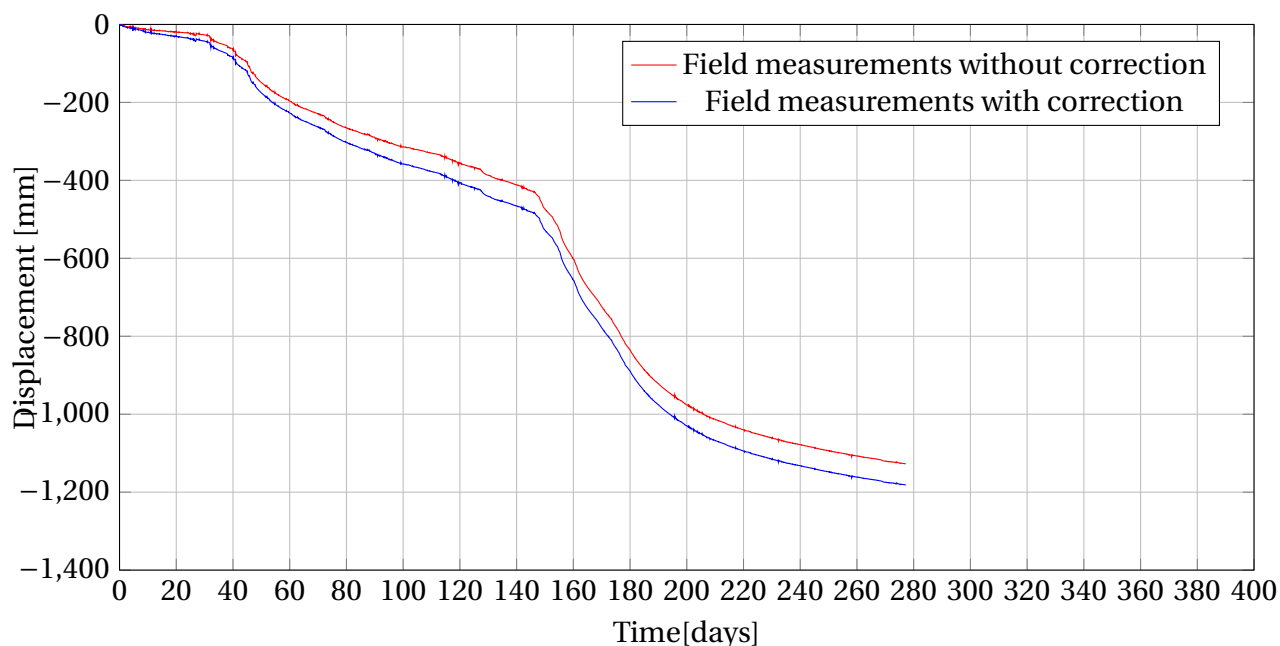


Figure 7.1: Settlement with and without correction for settlement plates

The load history for the fill is shown in figure 7.2 and is based on measured heights from the cross section of interest, described in section 6.3. The load application is described as linear up to 6 meters after around 45 days. No measured values before this makes the curve linear, but a recreation of loading has been created through drone photos showed in Appendix D. The measured values for figure 7.2 are not at the highest point of the fill, but the inclination of the graph is assumed to be the same. However, since the height is 12 meter compared to 15 meter at the highest point it is believed that the end time can be different for the point under investigation. Note that this load history is based on construction history in table 6.1. The load intensity increases from 150 days and at this point the pre-consolidation stress is exceeded as seen in figure 7.3. This encounter leads to a steeper settlement curve at 150 days and this will be described further in 7.4.

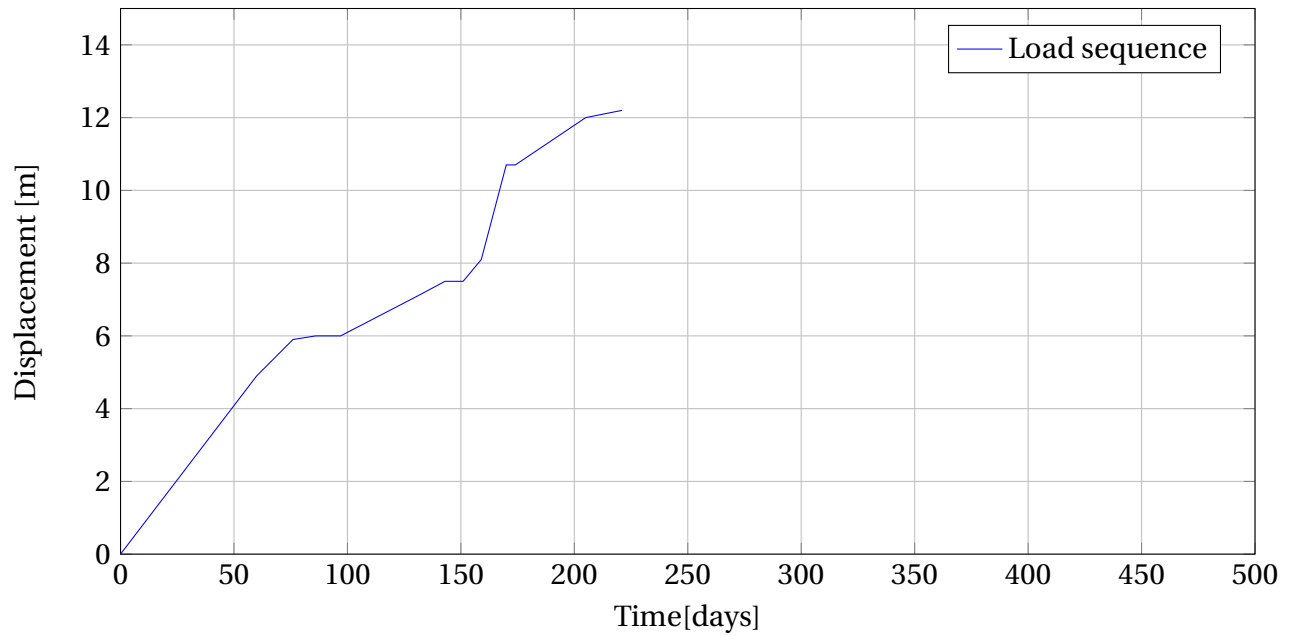


Figure 7.2: Load sequence

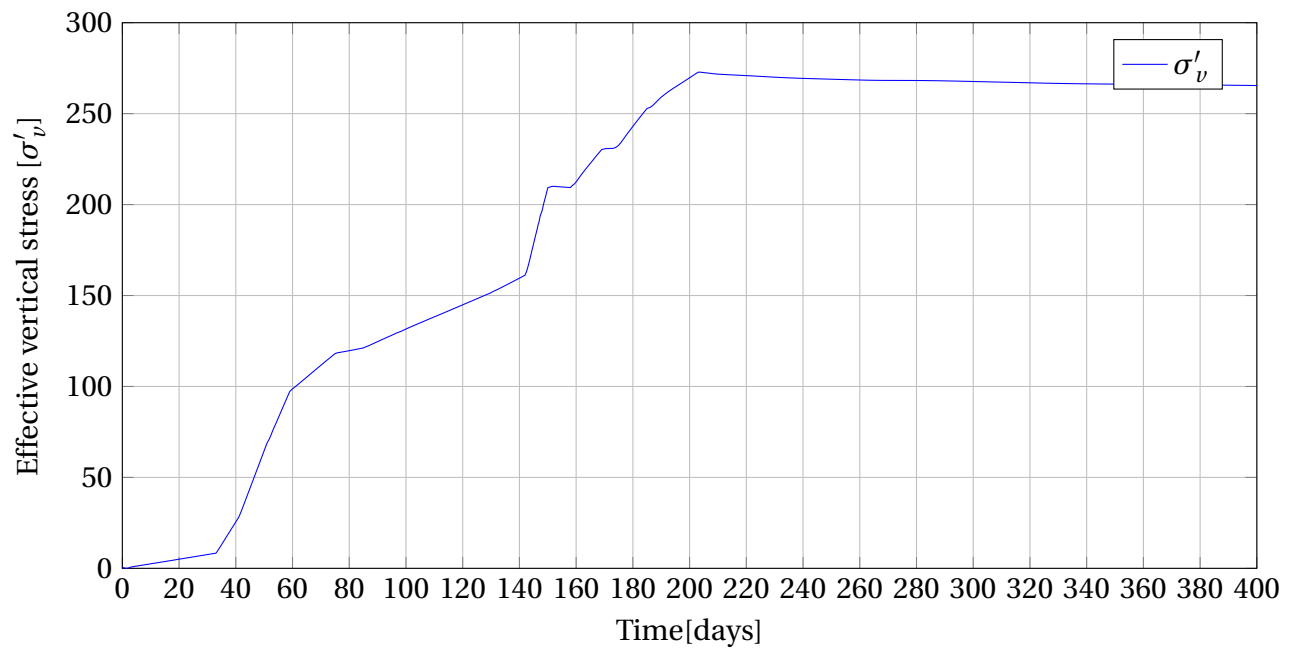


Figure 7.3: Effective stress development

The performance of the fill has been analyzed through a series of settlement analysis and the results are shown in figure 7.5. The calculated vertical displacement was first analyzed and compared to field measurements without correction for displacement from settlement plates and is shown in figure 7.4. The two material models utilized in the numerical analysis has been

compared to field measurements in figure 7.5. Both the Soft Soil Creep model and the Unified Enhanced Soft Clay Creep model show similar results as the field measurements. The SSC show a small overestimation before reaching pre-consolidation pressure while the USDM underestimates the settlement before p'_c . After around 150 days the vertical displacement coincide for the two models, but both under predicts the settlement after passing pre-consolidation pressure.

The USDM with slightly adjusted parameters for structure and destructuration is plotted in figure 7.6. This adjustments are made on basis of the calibrated tri-axial tests in 5.6. Calibration showed that destructuration parameter, χ was most likely between 4 and 5 for soft clay and a very good fit with SSC is obtained.

Both the SSC model and the USDM have good fit with field measurements, but struggle to recreate settlement after pre-consolidation stress is exceeded.

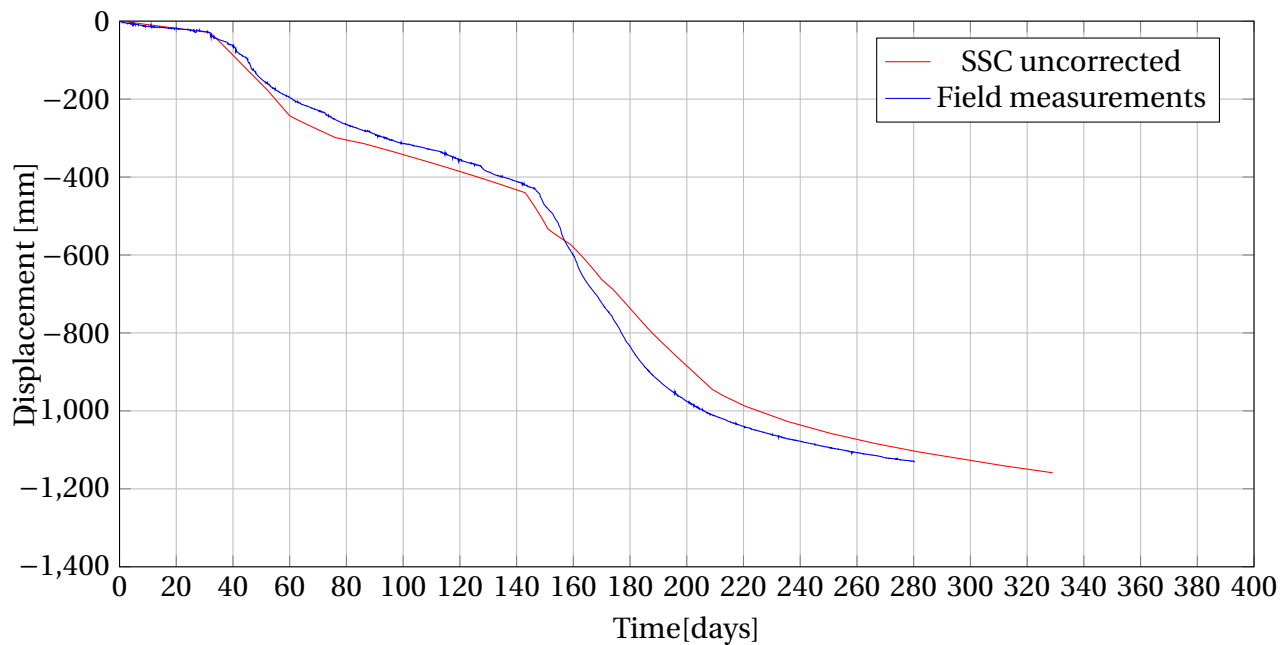


Figure 7.4: Settlement with and without correction for settlement plates

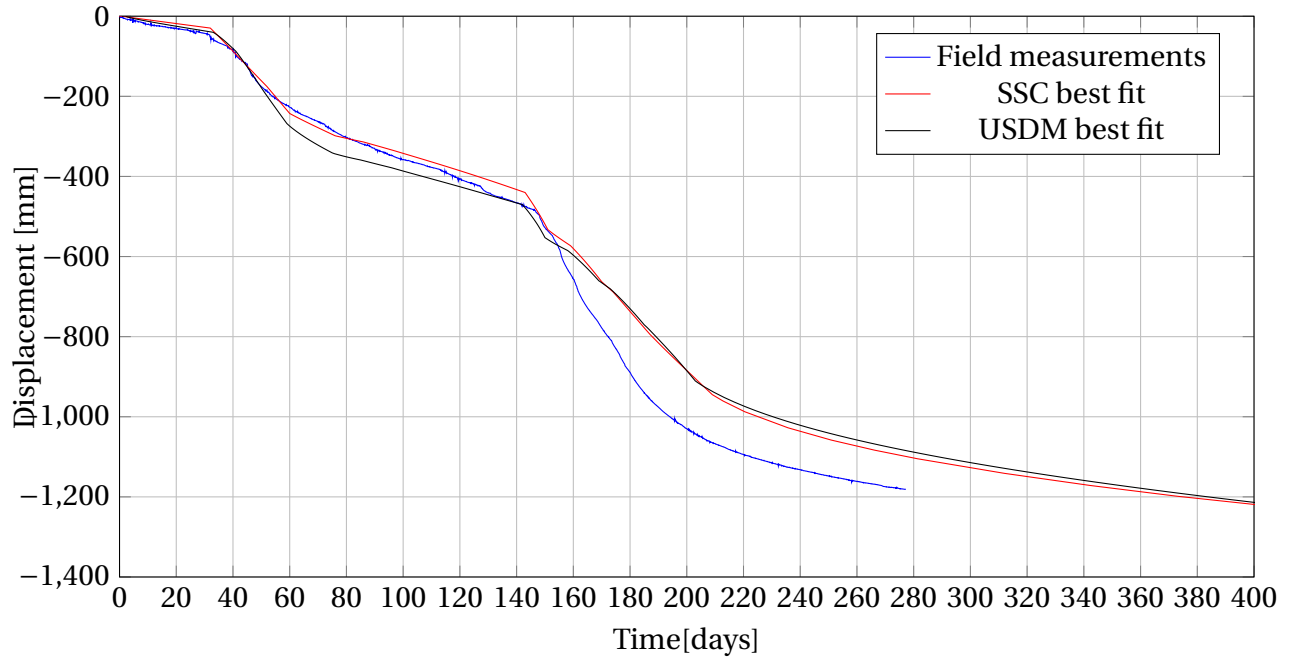


Figure 7.5: Settlement

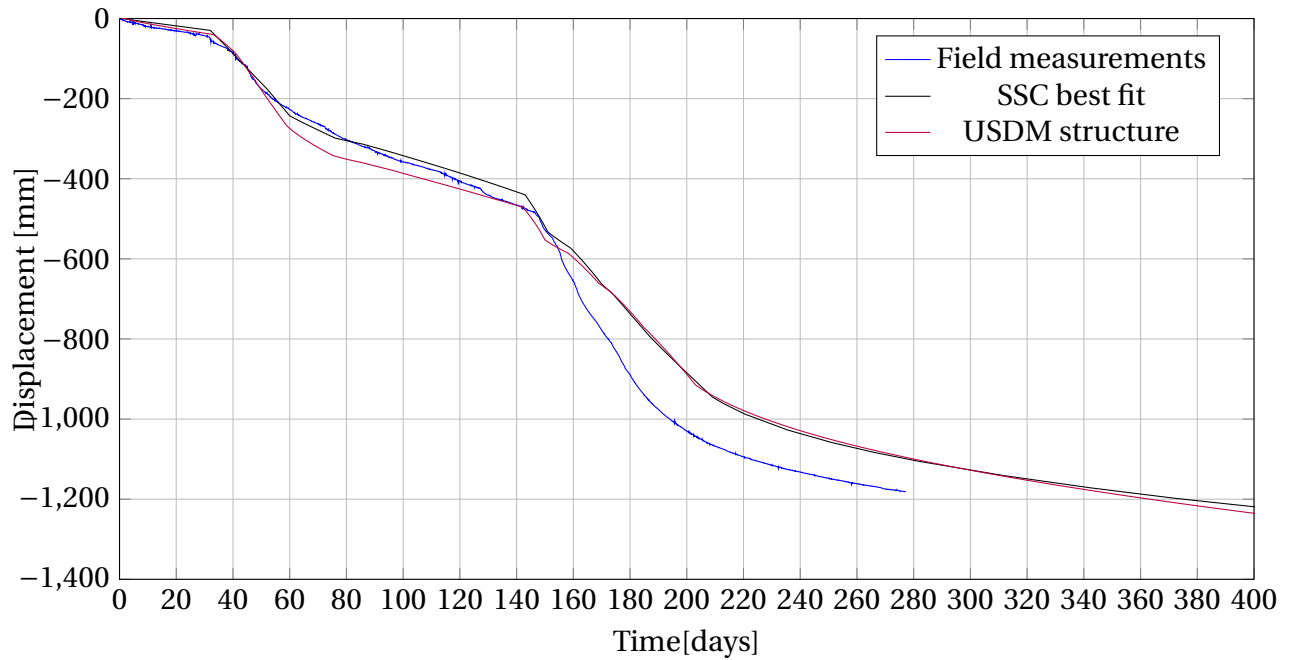


Figure 7.6: Settlement

The surface settlement is plotted for the SSC model with drains and without drains compared to field measurements in figure 7.7. The effect of pre-fabricated drains speed up the settlement process considerably and the vertical displacement can be observed to be almost doubled at

250 days after introducing PVD as ground improvements.

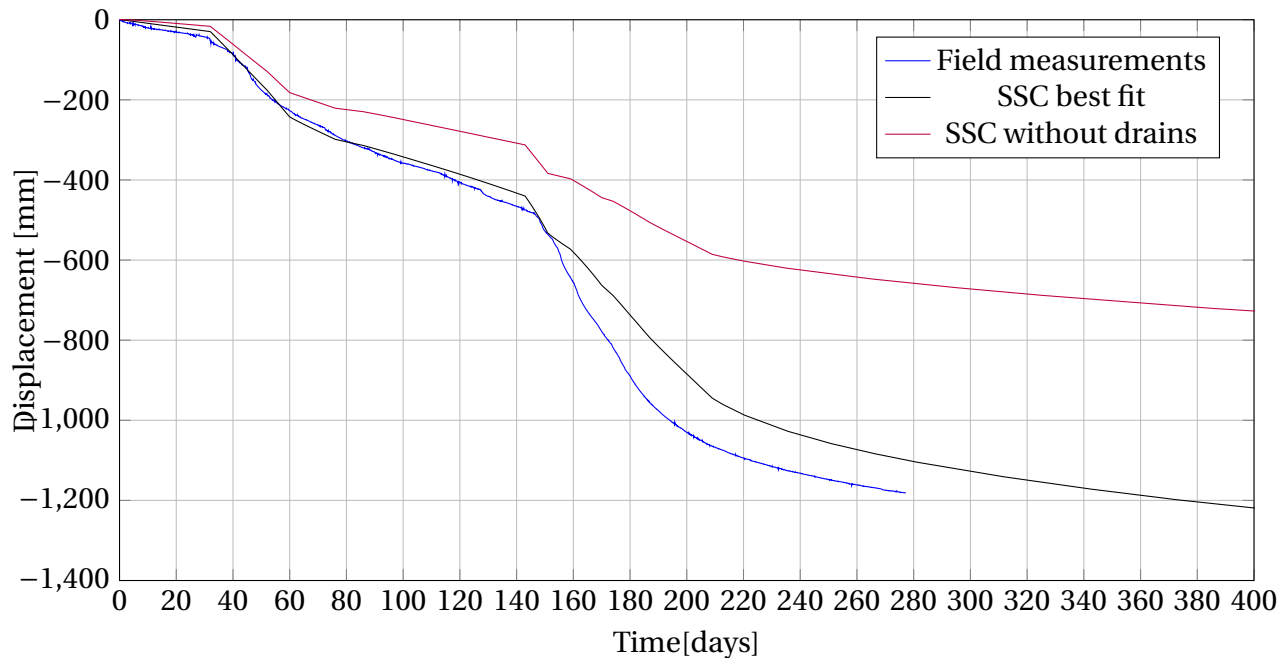


Figure 7.7: Settlement compared with no ground improvements

7.3 Pore Pressures Beneath Fill

The time-dependent pore pressure variations are monitored by pneumatic piezometers, described in section 2.2. These instruments can be placed within or outside the influence zone of the triangular grid pattern (PVD with 1.5 m spacing) and closer location to vertical drain equals less variations in excess pore pressure. In the 2D-analysis the computed pore pressure will be at the corresponding depth as piezometers, but the location will not be exact. This may affect the output results in regard of magnitude of the excess pore pressure and stress points close to boundary show less variations and stress points further away will show more.

The pore pressure from the numerical analysis is compared to values from piezometer 2101 5 meter below ground surface and 2102 and 2105, 12 meter below ground surface, see figure 2.4. In figure 7.8 pore pressure development for SSC, USDM and piezometer 2102 is compared. The general trends between finite element results and field data agree well and this corresponds to section 5.6, illustrated by figure 5.5 and 5.6. However, the magnitude of the excess pore pressure deviates significantly from 145 days to around 185 days, which corresponds to the breakpoint of the settlement curve around 150 days shown in figure 7.5. This is discussed in

section 7.4. Both SSC and USDM predicts lower values than field measurements. The USDM is superior the SSC in prediction of excess pore pressure and is chosen for further investigations.

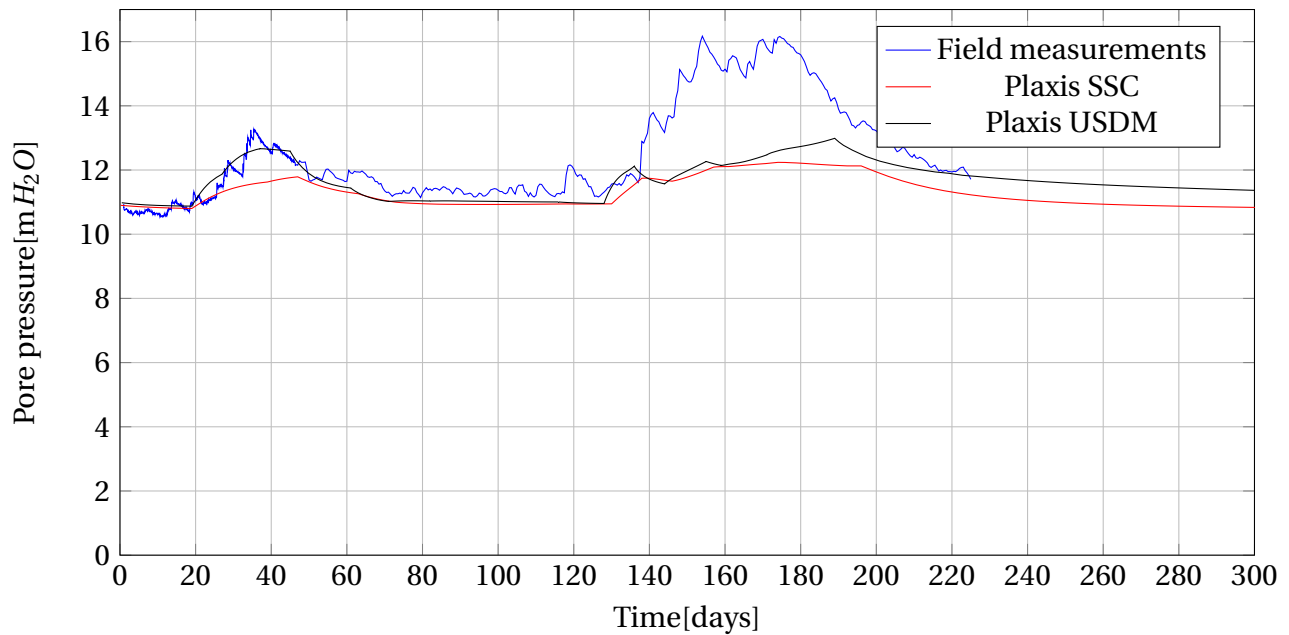


Figure 7.8: Pore pressure development 2102 12m.

Two points (K and L in section 7.7) have been analyzed and figure 7.9 and figure 7.10 show results for USDM compared to piezometer 2105. In Figure 7.9 the observed peak after ca. 155 days for field measurements and almost 190 days for USDM can indicate difference in loading. Figure 7.10 show better correspondence between peaks and appear approximately at the same time. This agrees well with the load situation since the loading (reached highest point) ended after 160 days for point L, see figure 7.25 and D. The point L is at a lower point and the fill finished earlier at this point than for point K, which is under the highest point of the fill.

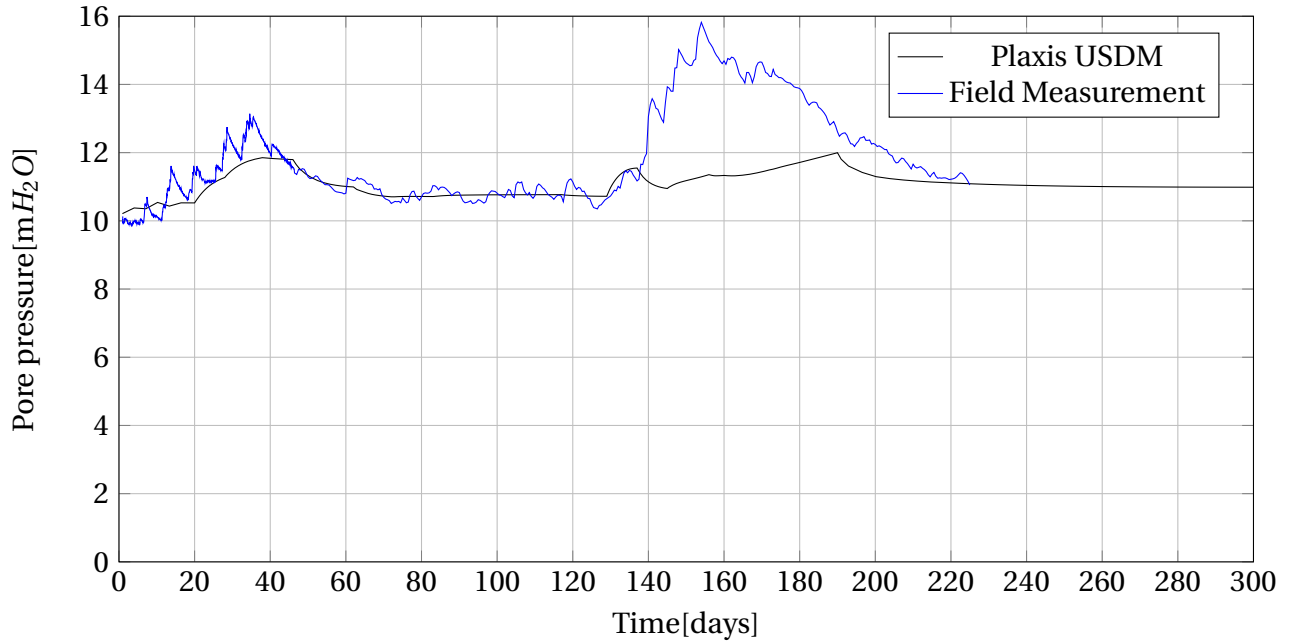


Figure 7.9: Pore pressure development 2105 12 m. depth

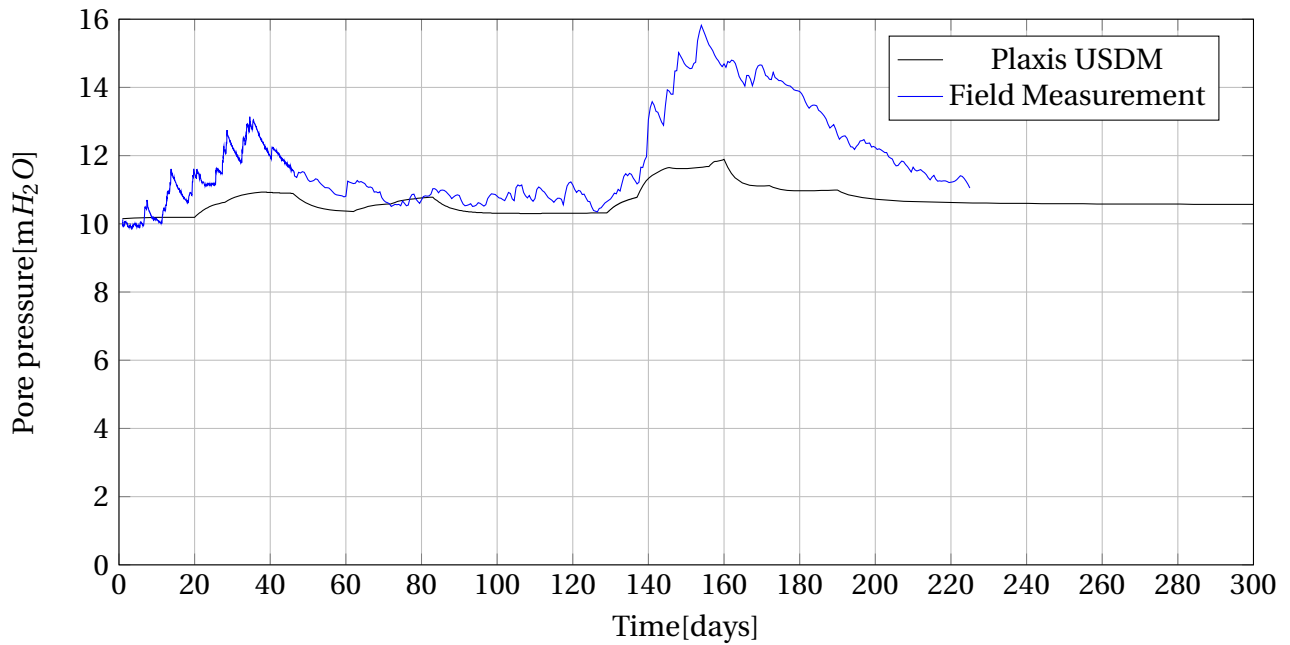


Figure 7.10: Pore pressure development 2105 12 m. depth

Pore pressure development for 2101 5 meter below ground surface compared to USDM is shown in figure 7.11. The trendline is similar for both cases, but with over 50 % lower estimation for the numerical analysis. As mentioned earlier in this chapter the PVD can be placed inside or outside the influence zone. Small jumps in pore pressure development is

observed for the field measurements in figure 7.11 and it can be caused by positioning close to vertical drain boundaries. The same thing is observed for Plaxis, but the lower values are obtained as shown. The matching scheme from axisymmetric to plane strain can give different values for excess pore pressure around drain boundaries.

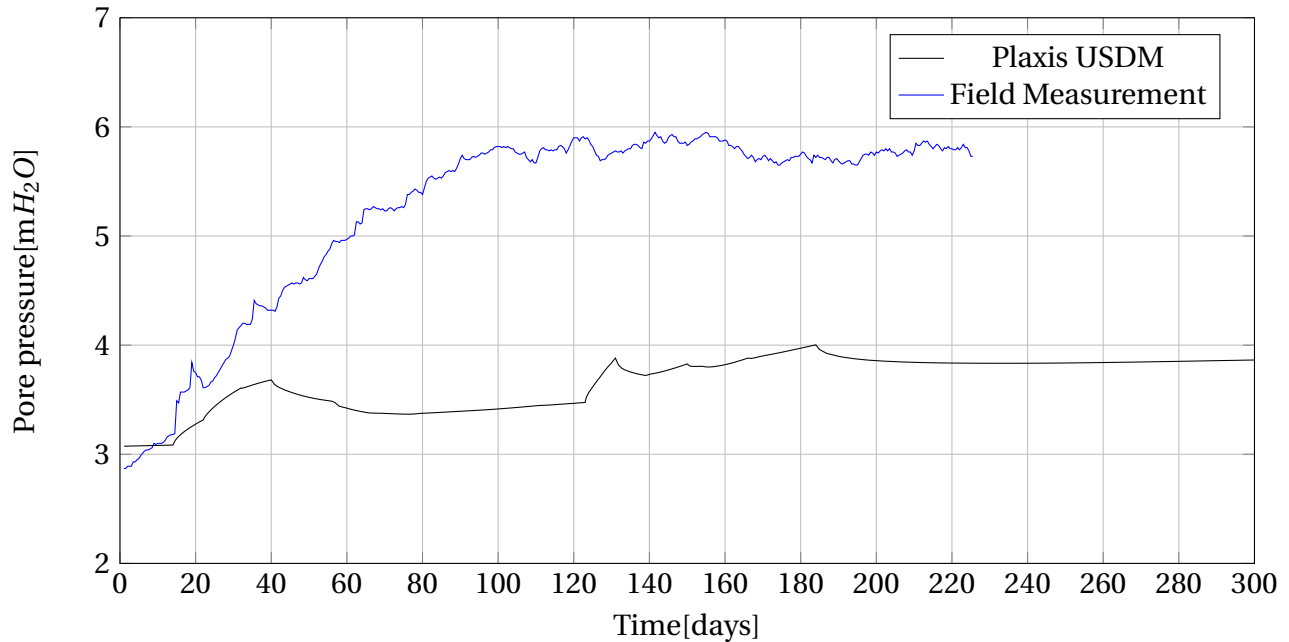


Figure 7.11: Pore pressure development 2101 5 m. depth

In figure 7.12, a case without vertical drains is analyzed and the excess pore pressure dissipation is significantly increased when introducing ground improvement methods such as PVD. The excess pore pressure for the 2D model with drains is showed in 7.13 and without drains for figure 7.14. A comparison of excess pore pressure can be seen in figure 7.15.

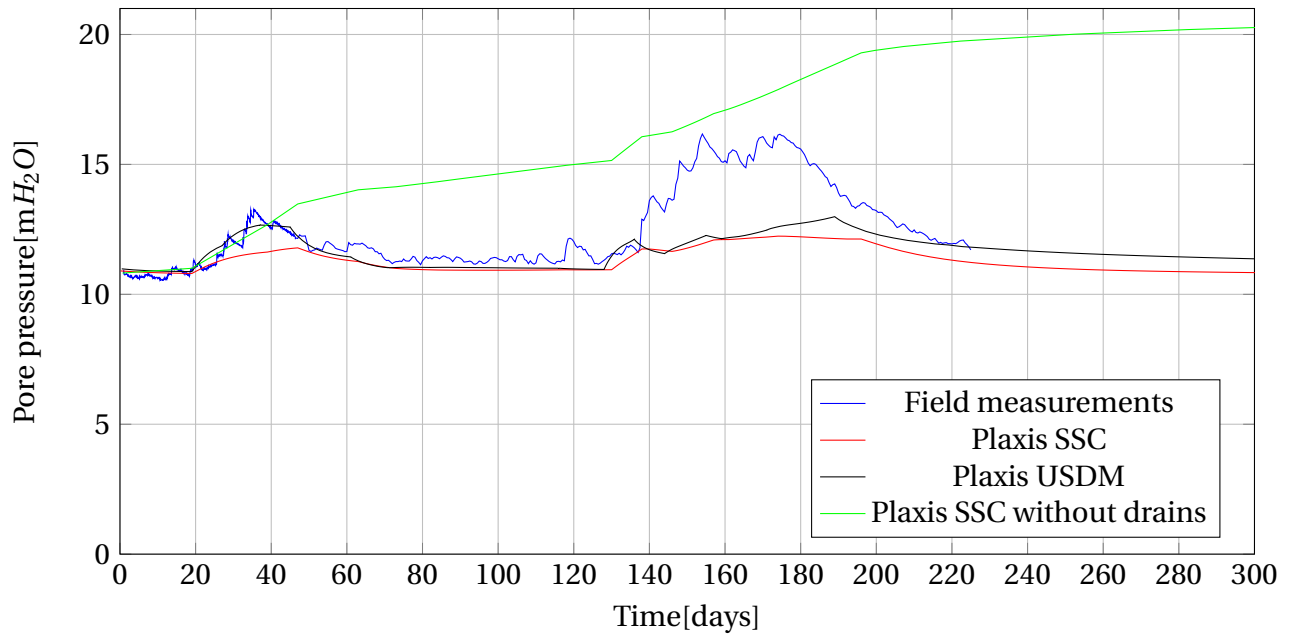


Figure 7.12: Pore pressure development 2102 12m.

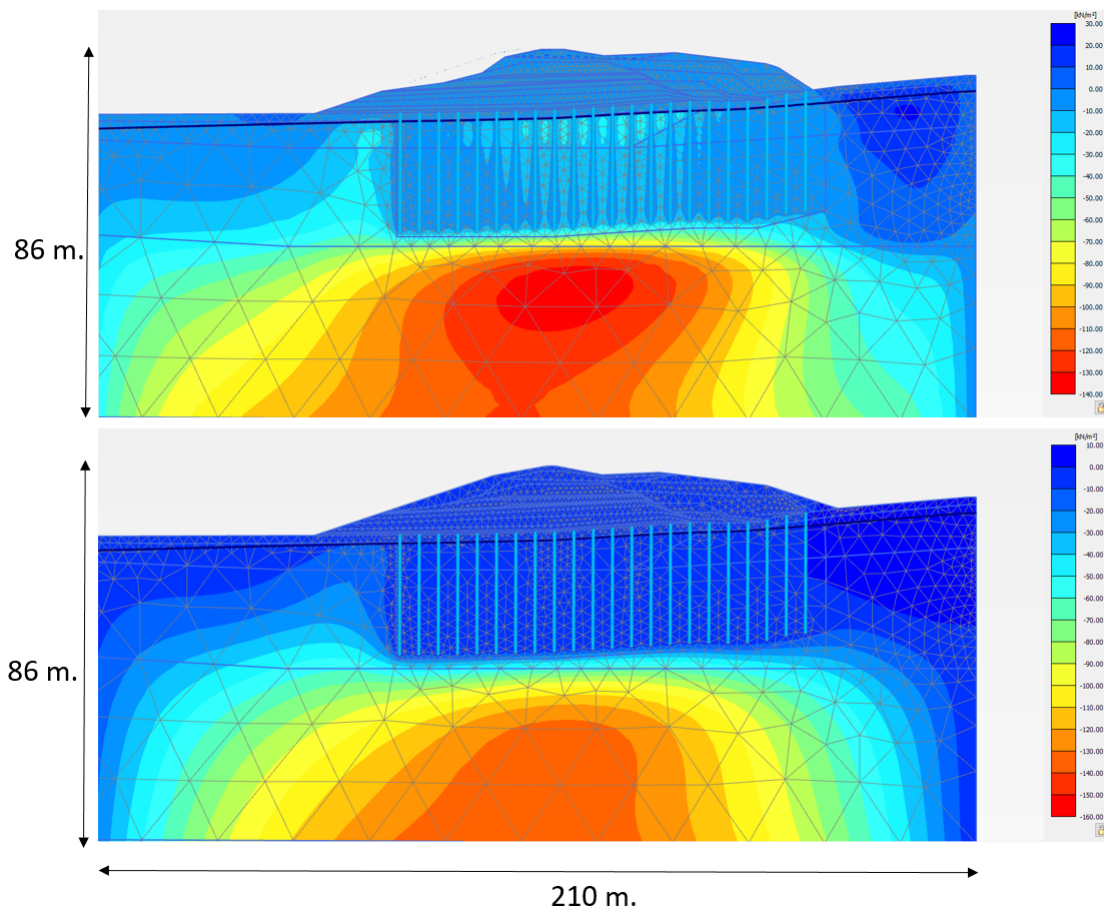


Figure 7.13: Excess pore pressure at 183 days (Fill part 11) and 400 days (Consolidation 1 year)

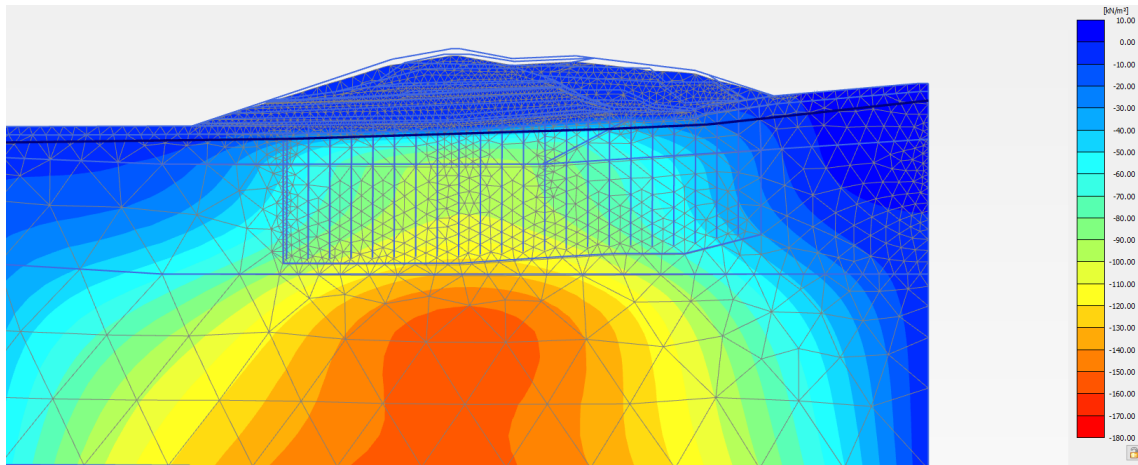


Figure 7.14: Excess pore pressure at 183 days 400 days (Consolidation 1 year) for SSC without drains

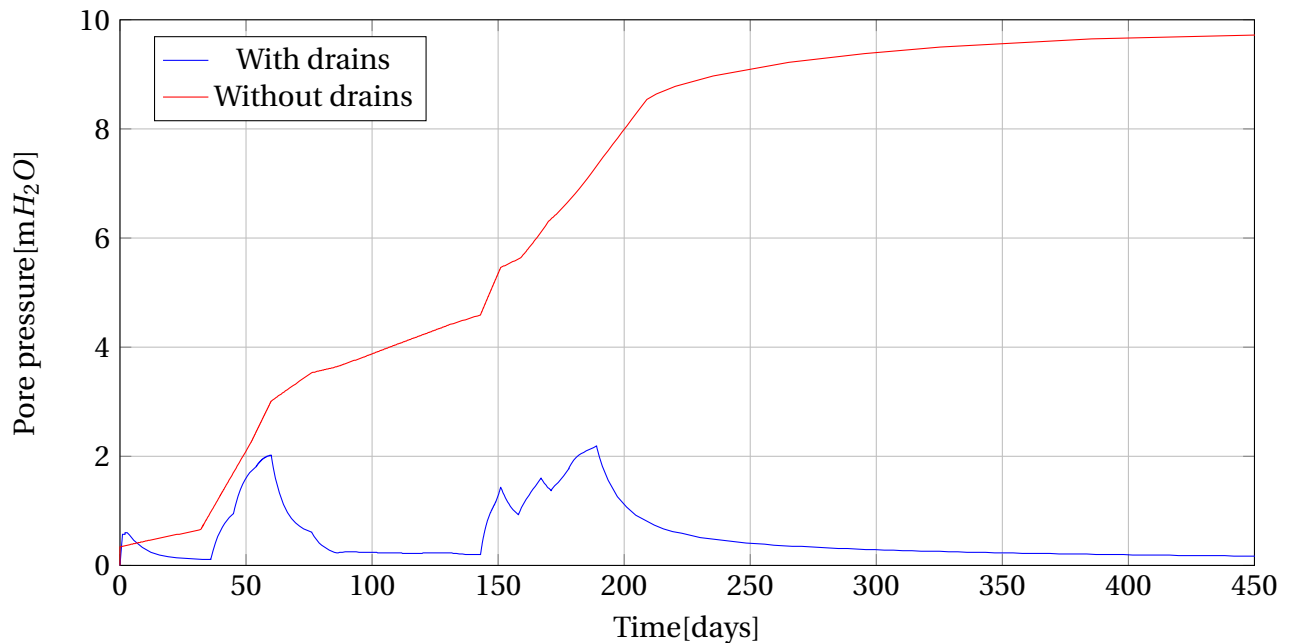


Figure 7.15: Excess pore pressure with and without vertical drains for compressed loading

7.4 Modifications

The settlement with a compressed load situation as described in section 6.3 may be seen in figure 7.16. The gap between observed settlement and measured settlement after around 145 days in combination with pore pressure deviations presented in section 7.2 and 7.3 gave basis for investigations of a more compressed load situation. The settlements after modifications

agrees very well with field measurements, but still an underestimation of settlement before p'_c and an overestimation after passing p'_c can be observed. Note that the declination from 145 days and 155 days is identical to field measurements.

The pore pressure is simultaneously analyzed and compared with settlement for the modified load case and may be seen in figure 7.17. A better fit between field measurement and calculated pore pressure development is obtained, but as mentioned in section 7.3 the location is not exact. In figure 2.4 it can be seen that piezometer 2105 is located some distance away from investigated point.

One important observation is made at the end around 280 days. The SSC model settlement curve has a steeper declination than the field measurements. At this point structure is decisive for the continuing development, along with creep. A modification which could obtain better fit for long time is presented in figure 7.18. Note that only the parameter X has been changed and other parameters must be changed as well to obtain better fit, like for example the rate of destructuration, a_v . For "USD structure" in figure 7.18 creep has not been modified, but the contribution from creep could be too high.

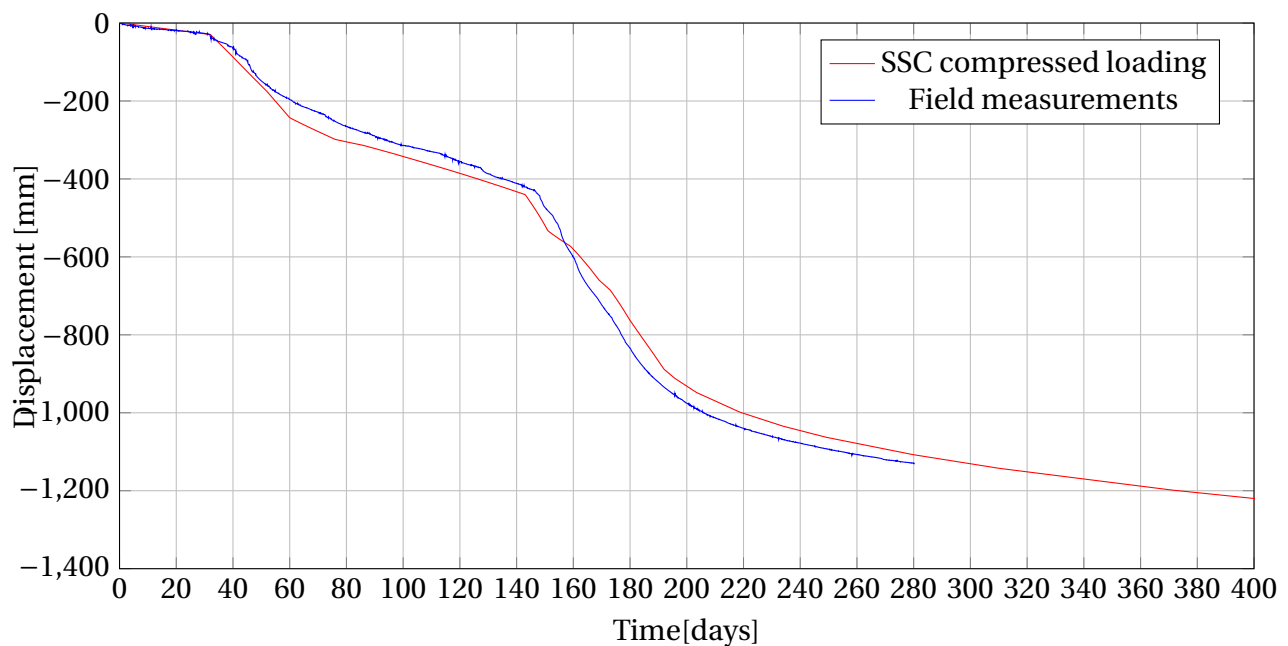


Figure 7.16: Settlement compressed loading

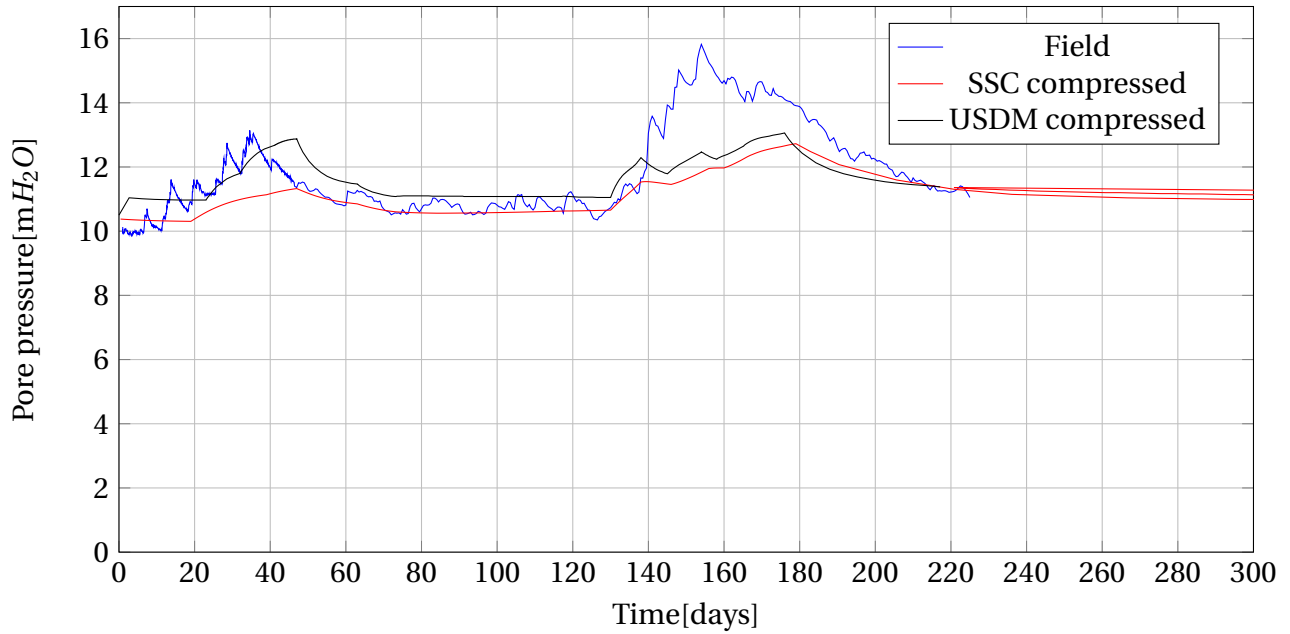


Figure 7.17: Pore pressure development 2101 5 m. with compressed loading

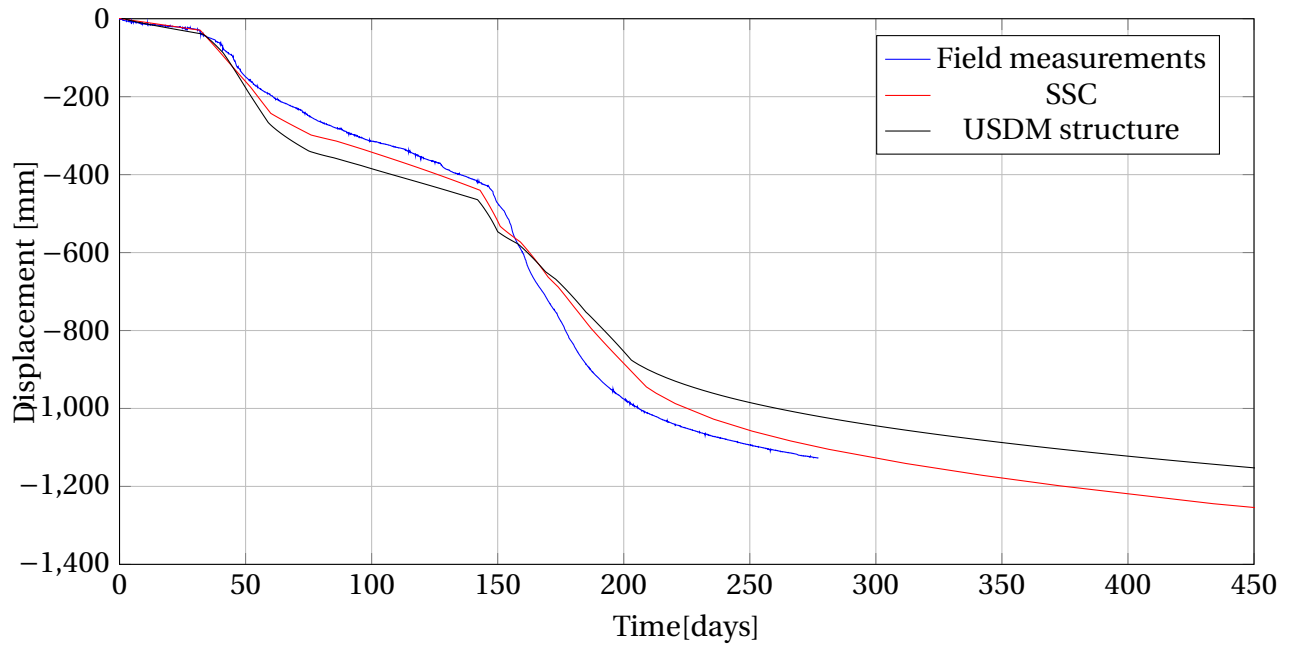


Figure 7.18: Settlement modified structure

7.5 Unloading

Unloading of the preloading is determined by excess pore pressure dissipation and variation over time shown in figure 7.15 and section 7.3 indicate that the preloading can be removed after

300 days with close to full dissipation of excess pore pressure at this point. In figure 7.19 the preloading is removed after 300 days and pore pressure development is showed in figure 7.20

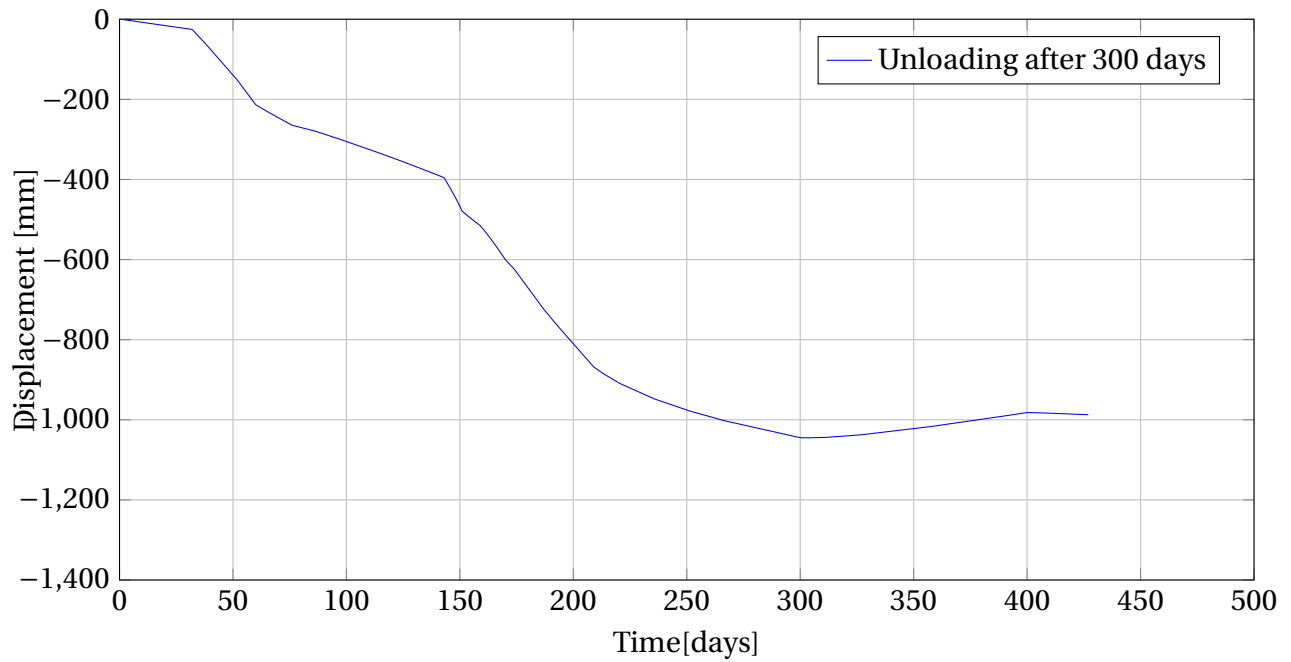


Figure 7.19: Settlement for unloading preloading after 300 days

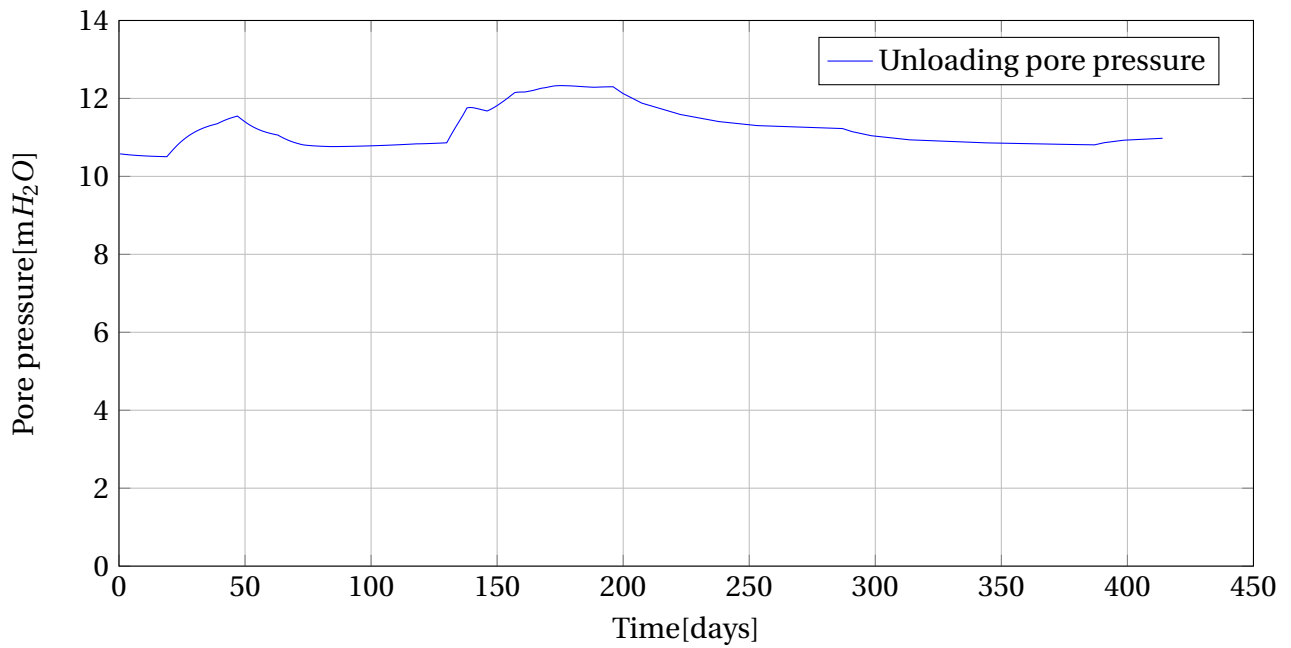


Figure 7.20: Pore pressure unloading after 300 days

7.6 State Parameters

The recovery of X over time was investigated to achieve a better prediction of settlement with time. The effect of structure is plotted vs. field measurement and SSC model, and can be seen in figure 7.6 and 7.18.

The development of structure is shown in figure 7.21 and 7.22. The initial value of X is set to 5 and decreases with time, towards zero. After fill part 11 the structure is destroyed in the upper layer, the reconstituted clay, and partly in the soft clay. After the consolidation phase the structure is much more destroyed due to creep strains. For the dry crust, Soft Soil model is utilized and hence will not have any state parameters such as X .

It can be seen that this feature in the USDM gives extra parameters to control structure over time. For this study the observed settlement from field have recently finished loading and creep strain development is still in early phase.

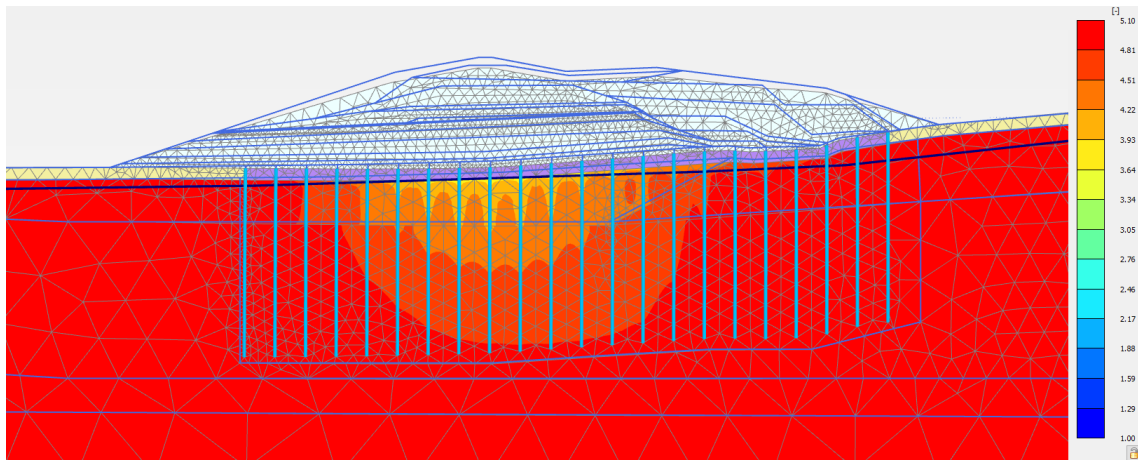


Figure 7.21: Destruction of structure after phase 11

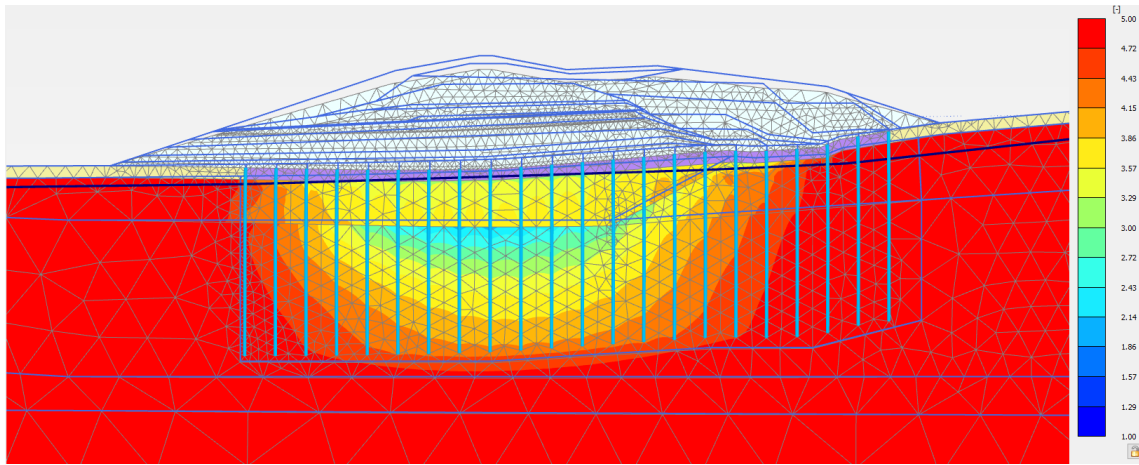


Figure 7.22: Destruction of structure after consolidation phase

7.7 Mesh Analysis

The mesh utilized in the analysis was normal mesh with refined mesh for areas important for output results, see section 6.2. For each phase, mesh and water pressure was updated. To investigate the sensitivity of the mesh, both coarser and finer mesh was compared along with updated mesh and not updated mesh. Very small difference was observed with normal mesh and very fine mesh, see figure 7.23.

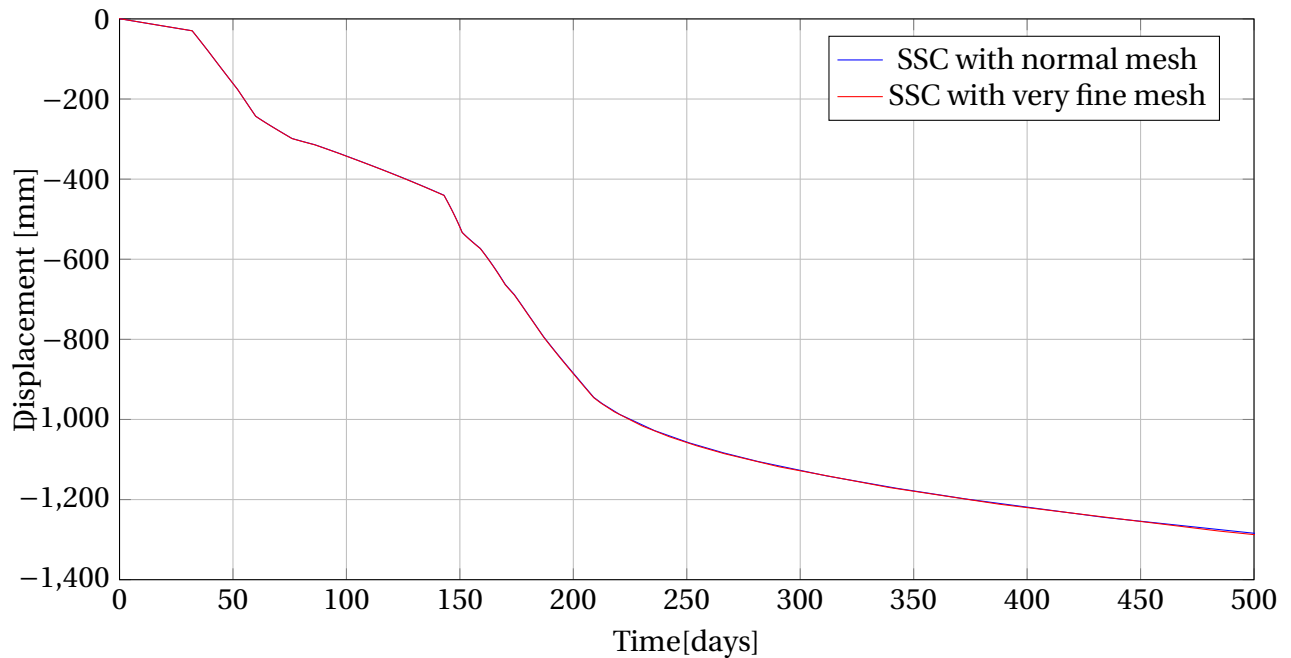


Figure 7.23: SSC with normal and very fine mesh

As described in section 4.2 models with large depth can give unrealistic creep deformations using POP to control over-consolidation ratio. For this mesh this was solved by using OCR, not POP, for layers below vertical drains. POP was used for top layers, while OCR for two bottom layers. The creep deformation was tested on the model by running simulation with no load over 5 years. Deformations of a few millimeters verified the model for the time of interest, but for a model only using POP as control for the over-consolidation resulted in unrealistic creep deformation over long time. OCR was used on basis of this verification.

$$POP = \sigma_p - \sigma'_{yy} \quad (7.1)$$

For this fill large deformation occur and for verification of the analysis an updated mesh and water pressure is compared to not updating. As a result of buoyancy forces the effective weight of the soil that settles below the water level will change. This leads to a reduction of the effective overburden in time. In figure 7.24 it is shown that the vertical deformation are less when the updated mesh and updated water pressure are used. This is caused by including second order deformation and updated water pressure results in smaller effective stress (Plaxis, 2017). A more realistic deformation is achieved, even though the difference is small.

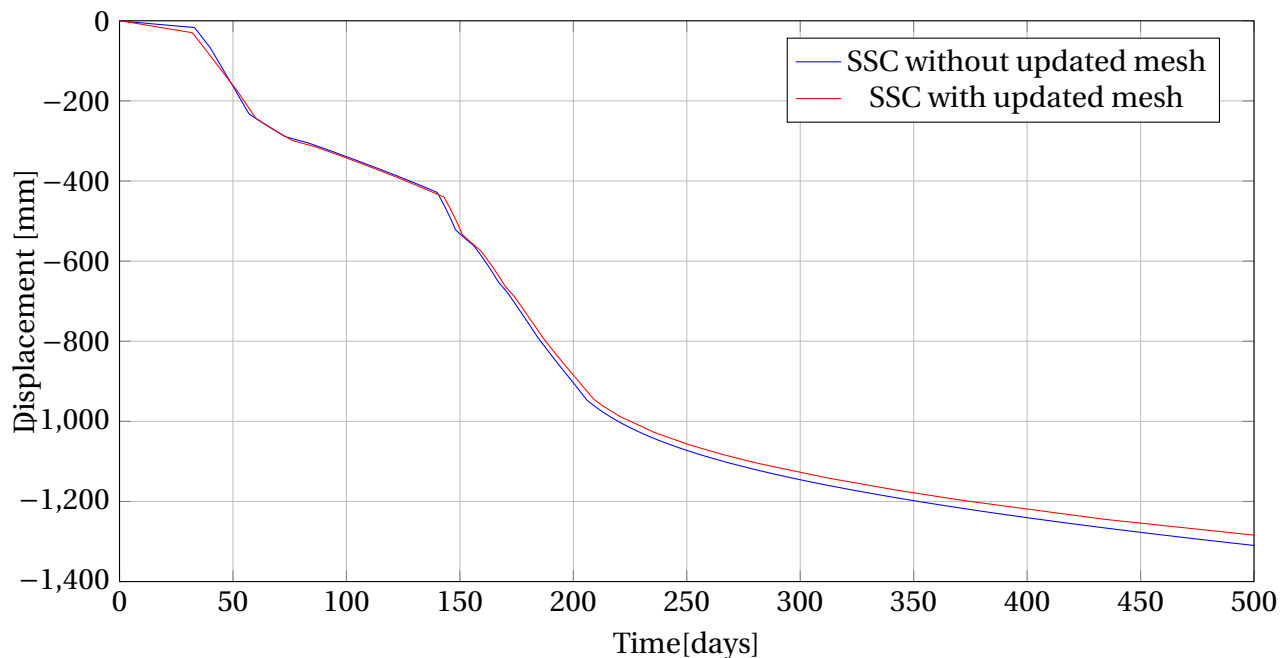


Figure 7.24: SSC with updated mesh and water pressure

The output nodes and stress points are illustrated in figure 7.25.

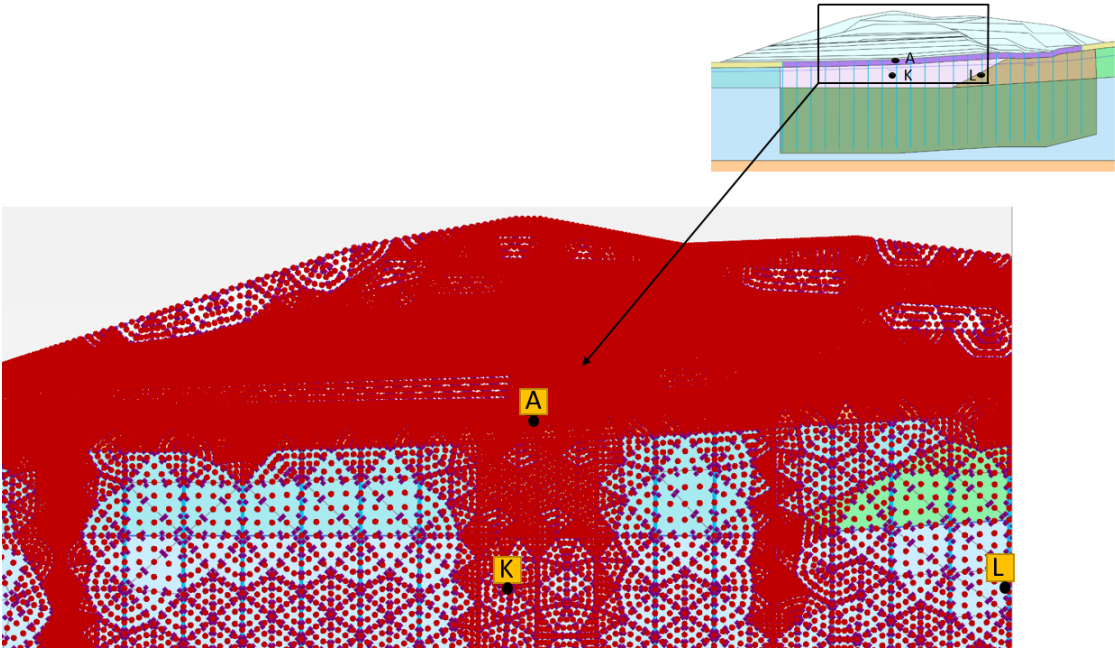


Figure 7.25: Stress point and node for output results

Chapter 8

Summary and Recommendations for Further Work

8.1 Summary and Conclusions

The performance of an instrumented fill constructed on a soft soil foundation stabilized with vertical drains was analyzed in this study. Data from the project site has been collected, evaluated through background theory and resolved in input parameters for the material models. The settlement and pore pressure development was analyzed in the finite element software Plaxis 2D, where a plane strain model with exact geometry and load application was modelled.

In this study assessed values from soil samples have been adjusted to fit with the observed settlement. The Soft Soil Creep model was used as basis for this study, but the soil model contains some limitations regarding over prediction of the elastic range of soil behaviour. The model does not take into account the effect of destructuration and an investigation with an advanced material model, the Unified Enchanted Soft Clay Creep model, was introduced.

The pore pressure development from the numerical analysis was compared to field measurements in section 7.3 and later modified in section 7.4 to obtain better fit. Improved results were achieved with almost identical pore pressure trend.

The settlements of the stabilized clay subjected to loading from the constructed fill can be predicted reliably with the two models used in the numerical analysis. First predictions deviated from field measurements in section 7.2 and modifications were made in section 7.4.

Soil parameters were re-evaluated and calibrated. After modifications an approximately identical settlement was achieved. This study show that for this fill, the deviations are probably not related to destructuration, but loading intensity. It is too early to draw conclusions on how destructuration affects settlement development for this fill.

This study indicates that removal of preloading can be done after 300 days justified by excess pore pressure dissipation in 7.3. Most primary settlement is completed at this time and close to all excess pore pressure has dissipated.

The reliability of the predictions can be increased by investigating more samples and comparing it to field measurement. A better fit between field measurement and the user defined model could probably be achieved with further investigations on input parameters.

8.2 Discussion

The pore pressure development over time for the numerical analysis deviates from field measurements in regard of magnitude of excess pore pressure after approximately 150 days. This can partly be explained by the reduced capability to predict excess pore pressure for the two material models used in the analysis as explained in section 5.6. However, the difference in magnitude are considerable and an explanation could be that the load intensity increases more than modelled in this period. This theory is based on last height measurement of fill being done after finishing construction and on the very steep incline in the load graph, seen in figure 7.2. The pore pressure curve for field measurements presented in figure 7.8 implies that the peak is almost 20 days earlier than for Plaxis. This substantiates the theory of more intense loading. The theory is tested in section 7.4 and with a compressed loading after 150 days the pore pressure show better agreement between field measurements and Plaxis results.

Another explanation for pore pressure deviations could be that the piezometers are pushed down as the load from the fill is applied. However, the deviations are bigger than expected, especially for 2101 at 5 m. depth. The transformation from axisymmetric to plane strain is also questionable in reasons for direct comparison between calculated and observed pore pressure. The small internal variations of excess pore pressure compared to other piezometers are probably related to distance from drain boundaries. It is assumed that 2101 at 5 m. depth is close to the drain boundary.

The settlement from the numerical analysis agrees with the settlement from field

measurements, but deviates after passing 150 days in line with the pore pressure development. Settlement is overestimated in parts where applied stress is lower than pre-consolidation pressure and underestimated when stress is higher than pre-consolidation pressure. The Unified Enhanced Soft Clay Creep model was implemented to investigate the effect of destructuration. The USDm show no clear signs of improvement in matching the settlement from field measurement, but from section 7.2 it can be seen that USDm can be used to match the settlement curve over time, i.e. creep settlement. Important observations are made in section 7.2 and 7.4 regarding the continuing settlement development. The settlement curve indicates that calculated settlement are expected to exceed observed settlement before end of consolidation stage. This can be adjusted with r_{si} for both models and with parameters such as structure and for instance the limits for allowable creep, OCR_{max} , for USDm model. Field measurement settlements are still monitored and the consolidation phase along with creep settlement could be back-calculated through continuing data. It may also be a conservative approach for the determination of the creep factor and further observations could review this.

A difference in behaviour for the two material models can be observed in the elastic range in 7.2. An explanation could be stress development for the two models. Figure 8.2 show an oedometer simulation for SSC and USDm with same stiffness paramters. A increasing difference with increasing mean effective stress, p' , can be observed. This is caused by cohesion, shown in figure 8.1 and equation 8.1. The important part is how in situ stress is predicted.

$$K_{ur} = \frac{E_{ur}}{3(1-2\nu_{ur})} = \frac{p' + c \cdot \cot\phi}{\kappa^*} \quad (8.1)$$

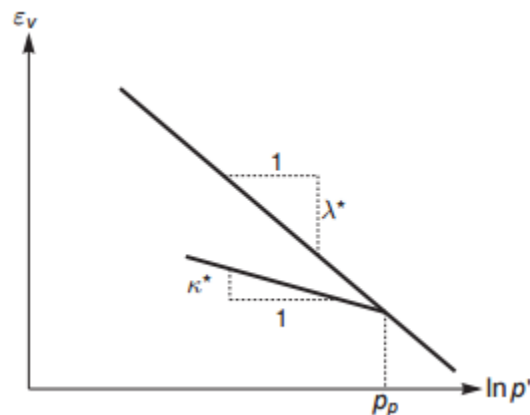


Figure 8.1: Relation between volumetric strain and mean stress (After (Plaxis, 2016))

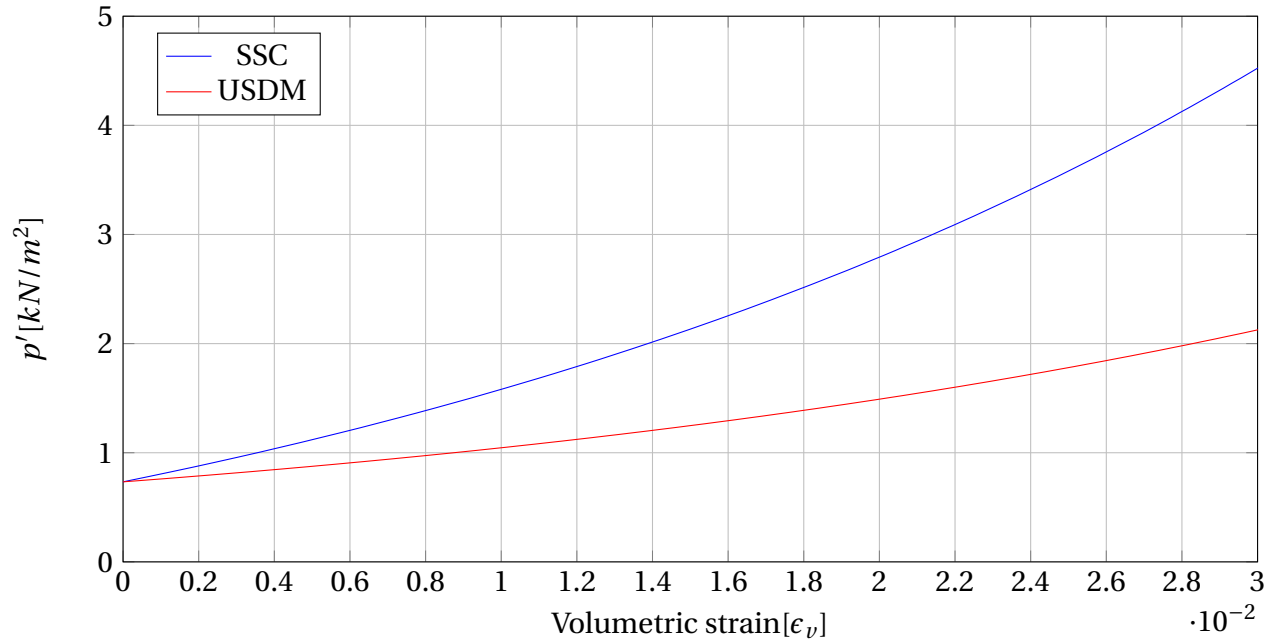


Figure 8.2: Elastic stress development for oedometer simulation in Soil Test

The simplifications for soil parameters in the 2D Model could cause a different behaviour of the soil than the model gives. Based on the variations in sample quality, good parameters for more detailed layers is difficult to find and error sources are considered to have a considerable impact on parameters. Based on this and on the results from the numerical analysis, the simplifications are sufficient for this study.

8.3 Recommendations for Further Work

The construction of the embankment finished shortly before the end of this study and further comparison of settlement and pore pressure over time would be of great interest. It is recommended to keep investigating the performance of the fill for both material models used in this analysis and especially the Unified Enhanced Soft Clay Creep model since it includes structure. A more detailed evaluation of input parameters for the USDM should also be done simultaneously to improve the performance. The study of the destructuration is also limited to a certain amount of soil samples. A closer look at anisotropy should also be done, as Norwegian clays are highly anisotropic.

The simplifications of soil properties regarding input parameters made in this study show no limitations of the ability to obtain a good match between calculated and observed field measurements. However, there are uncertainties involved and a more detailed research is

recommended. A model with OCR instead of POP controlling the over-consolidation could be interesting to investigate, especially for the creep phase as mentioned in section 4.2.

The recommendations is classified as:

- New pore pressure measurements from piezometers supplied by Statens Vegvesen was measured at the same time as this report is due and this results should be compared with the pore pressure from Plaxis to study the effect of the vertical drain in consolidation. There is not time to include measurement in the report, but one plot is made. Figure 8.3 show the new measurement compared to USDM compressed loading.
- A more detailed evaluation of input parameters for USDM would improve model.
- The designed lay time for the fill before unloading is one year after start of construction. A further monitoring and comparison of field measurements against numerical analysis will give valuable results especially in terms of consolidation and creep.

Data for the last pore pressure measurement became available at the end of this study. This is compared with the results from USDM compressed loading and show that the excess pore pressure is close to fully dissipated. This agrees well with the findings in this study. Further investigations are recommended.

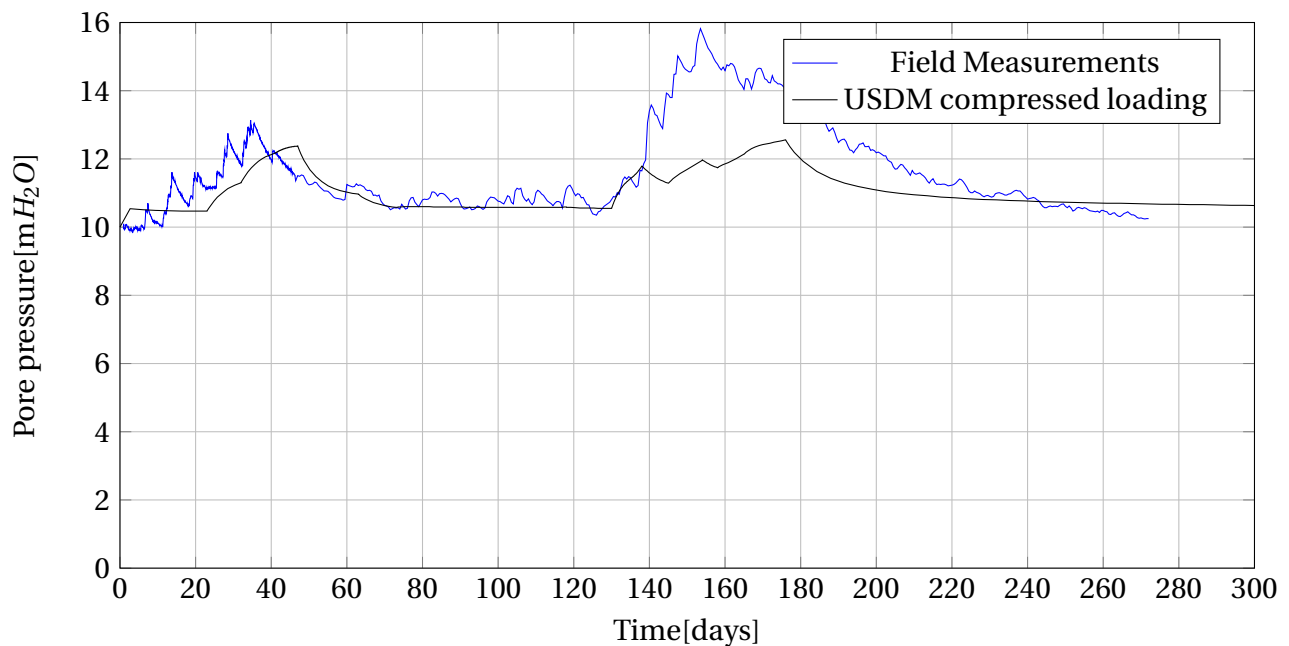


Figure 8.3: Pore pressure development 2105 12m.

Appendix A

Acronyms

SSC Soft Soil Creep Model

SSC Soft Soil Model

USDM User Defined Soil Model

FEM Finite Element Method

FEA Finite Element Analysis

NGI Norwegian Geotechnical Institute

2D Two Dimensional

PVD Pre-fabricated Vertical Drains

NGU Geological Survey of Norway

CRS Constant Rate of Strain

IL Incremental Loading

POP Pre-overburden Pressure

OCR Over Consolidation Ratio

CAUA Undrained Compression Test

Appendix B

Permeability

This appendix will show calculations for the matching scheme for the transformation of vertical drains from axisymmetric to 2-D plane strain.

B.1 Vertical Drains Calculations

([Barron, 1948](#)) developed the horizontal consolidation under ideal conditions using axisymmetric cell model

$$U_h = 1 - \exp\left(-\frac{8T_h}{\mu}\right) \quad (\text{B.1})$$

The degree of consolidation from [Vegdirektoratet \(2014\)](#):

$$U_h = 1 - \exp\left(-\frac{8 * C_h * t}{D^2 * F_{(n)}}\right) \quad (\text{B.2})$$

The degree of consolidation over time is shown in figure [B.1](#)

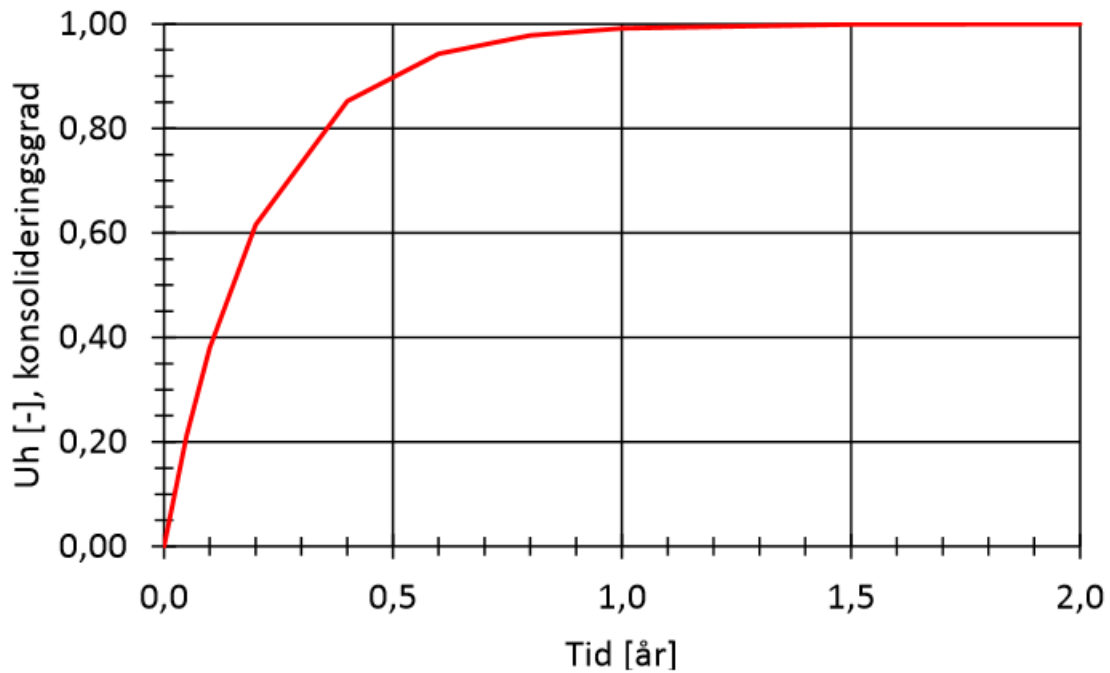


Figure B.1: Degree of consolidation over time (After [NGI \(2015\)](#)).

The U_h after 0,5 years is $U_h = 0,9$. Primary consolidation is $t_p = 0,5$ years for $c/c = 1,5$ m. ([NGI, 2015](#)).

The conversion for vertical drains from axisymmetric to 2-D plane strain model is calculated according to ([Indraratna and Redana, 2000](#)) and ([of Civil Engineering Researche and Codes](#)). The principle for conversion is displayed in figure [B.3](#).

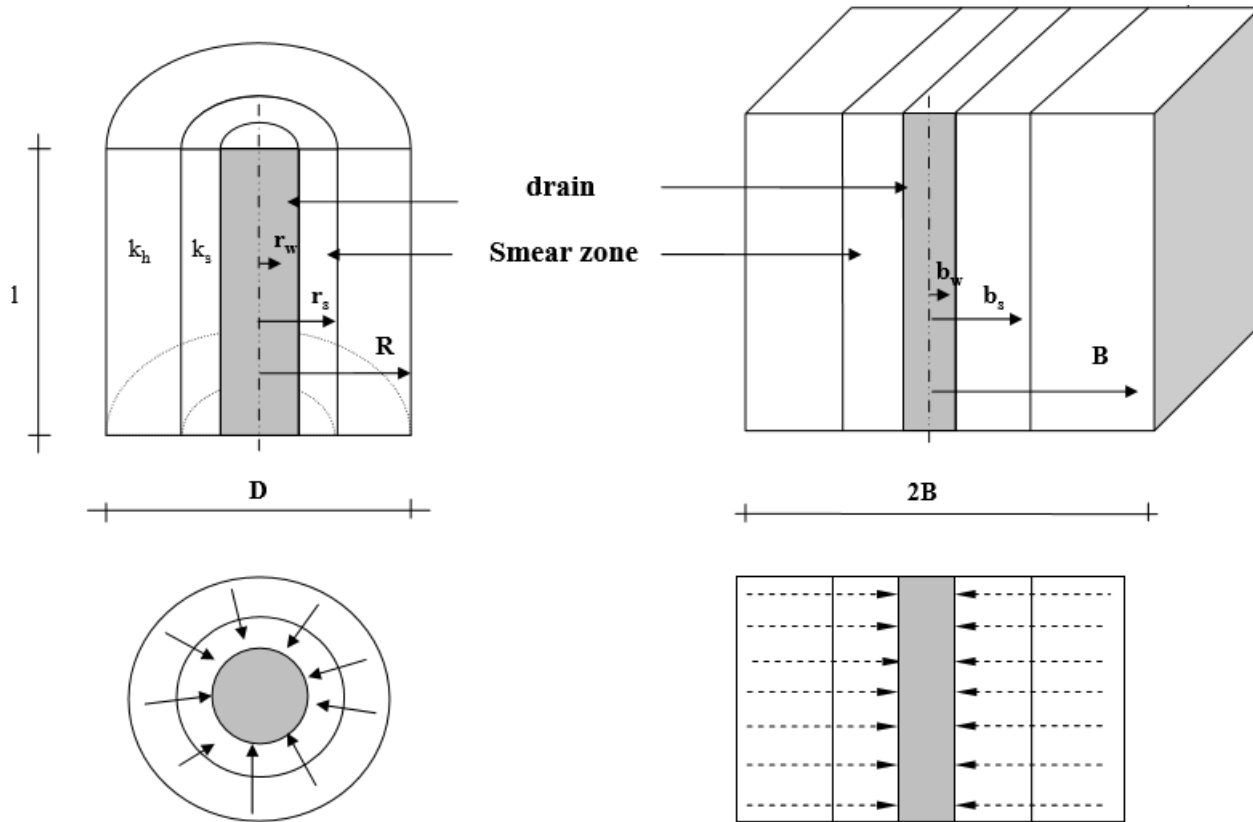


Figure B.2: Conversion of axi-symmetric radial flow to 2-D plane strain flow (After [Lin et al. \(2000\)](#)).

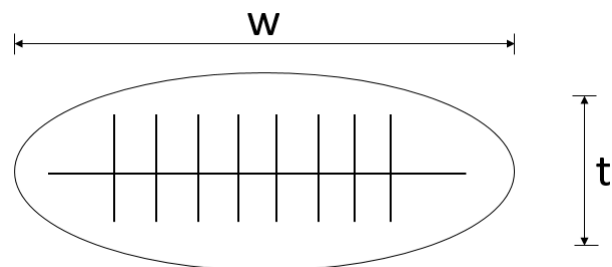


Figure B.3: Pre-fabricated vertical drains (PVD)

There are two important factors in the analysis when modelling vertical drains, which are smear effect and well resistance. The effect of well resistance can be ignored in the design according to ([Indraratna and Redana, 2000](#)). The disturbance of the soil around the drain has a significant effect in prediction of settlement of embankments with vertical drains ([Indraratna and Sathanathan, 2003](#)).

$$k'_h = \alpha * \frac{B^2}{\mu * (2R)^2} \cdot k_h \quad (\text{B.3})$$

$$\alpha = 3.24 \cdot \frac{\ln(1-U) + 0.21}{\ln(1-U)} \quad (\text{B.4})$$

$$\mu = \frac{n^2}{n^2 - 1} \cdot \left(\ln(n) - \frac{3}{4} + \frac{1}{n^2} \left(1 - \frac{1}{4n^2} \right) \right) \quad (\text{B.5})$$

$$R = \frac{s}{2 \cdot 1.05}$$

$$d = \frac{2(w + t)}{\pi}$$

$$n = \frac{D}{d}$$

k'_h / k'_x = Horizontal coefficient of permeability in smear zone

k_h / k_x = Horizontal coefficient of permeability

α = Geometric parameter representing smear in plane strain.

R = Radius of axisymmetric unit cell. See figure B.3.

r = Radius, see figure B.3.

r_s = Radius of smear zone. See figure B.3

r_w = Radius of vertical drain. See figure B.3

k_s = Smear zone permeability. See B.3.

U = Degree of consolidation

D = Diameter of axisymmetric cell (2R). See figure B.3

d = Equivalent drain diameter

B = Half of horizontal distance between drains in the 2D plane strain model. See figure B.3

L = Length of vertical drains.

s = Spacing between drains.

w = With of drain. See figure B.2.

t = Thickness of drain. See figure B.2.

Values for the PVD are from (NGI, 2015)

L = 28 m

s = 1.5 m

w = 150 mm

$t = 5 \text{ mm}$

$B = 2.25 \text{ m}$ (Spacing of 4.5 meter in 2D plane strain model)

$U = 90 \%$

Table B.1: Permeability 2D plane strain

Material	$k_x(m/day)$	$k'_x(m/day)$	$k_y(m/day)$
Reconstituted clay	1.728E-4	2.29E-4	8.64E-4
Quick clay	3.456E-4	4.59E-4	1.728E-4
Soft clay	3.456E-4	4.59E-4	1.728E-4

Appendix C

Methods

This appendix will show the method, described in section [3.3](#), for interpreting input parameters used in the numerical analysis.

C.1 Interpreted Oedometer Tests

A selection of samples presented in section [5.3](#) are shown here.

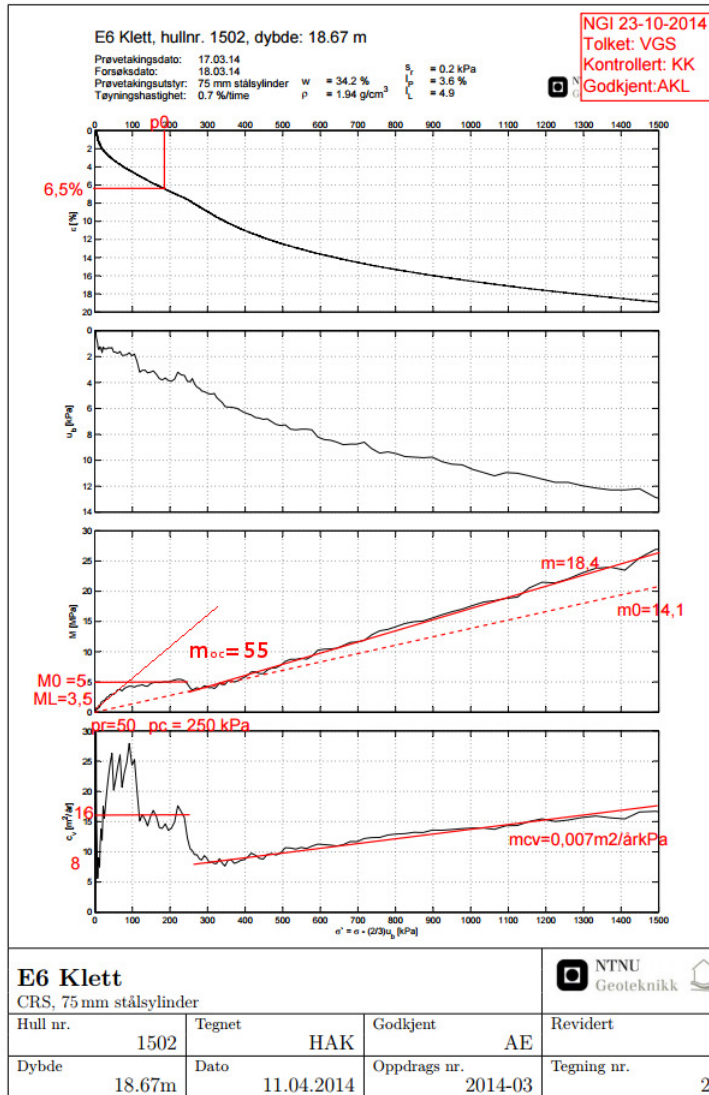


Figure C.1: Interpreted oedometer 1510 18.67 m. depth. (Modified after NGI (2015)).

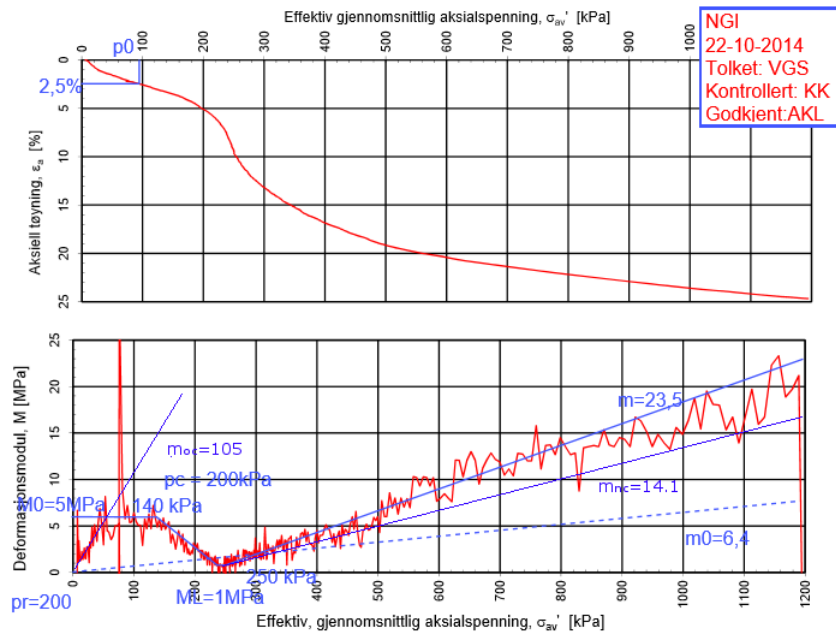


Figure C.2: Interpreted oedometer 1210 9.40 m. depth (Modified after NGI (2015)).

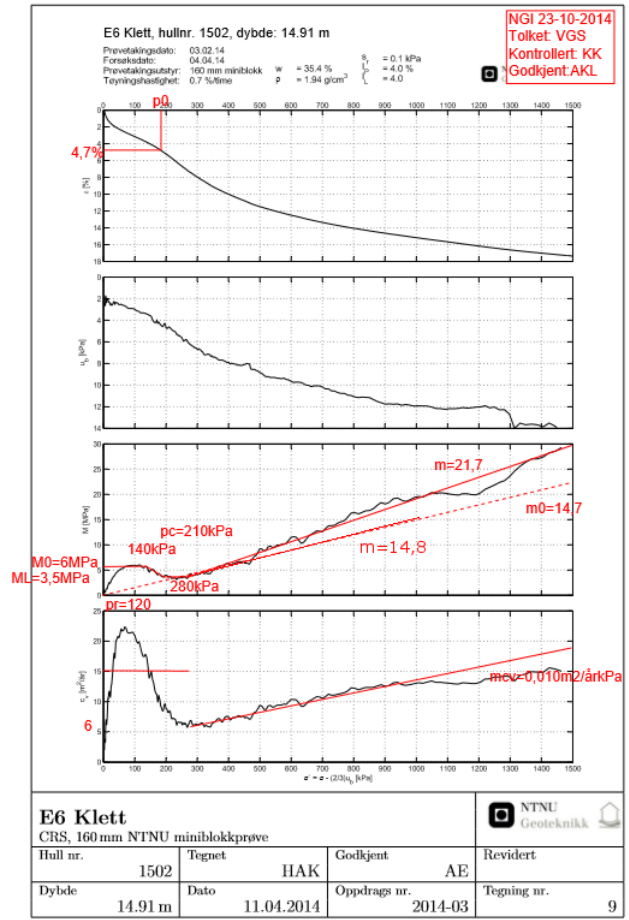


Figure C.3: Interpreted oedometer 1502 14.91 m. depth (Modified after NGI (2015)).

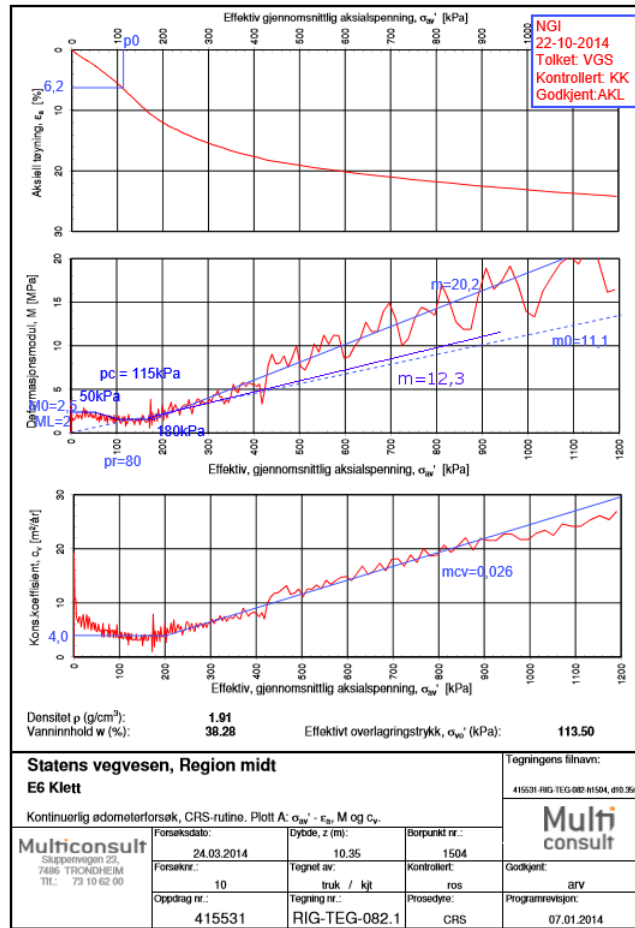


Figure C.4: Interpreted oedometer 1504 10.35 m. depth (Modified after NGI (2015)).

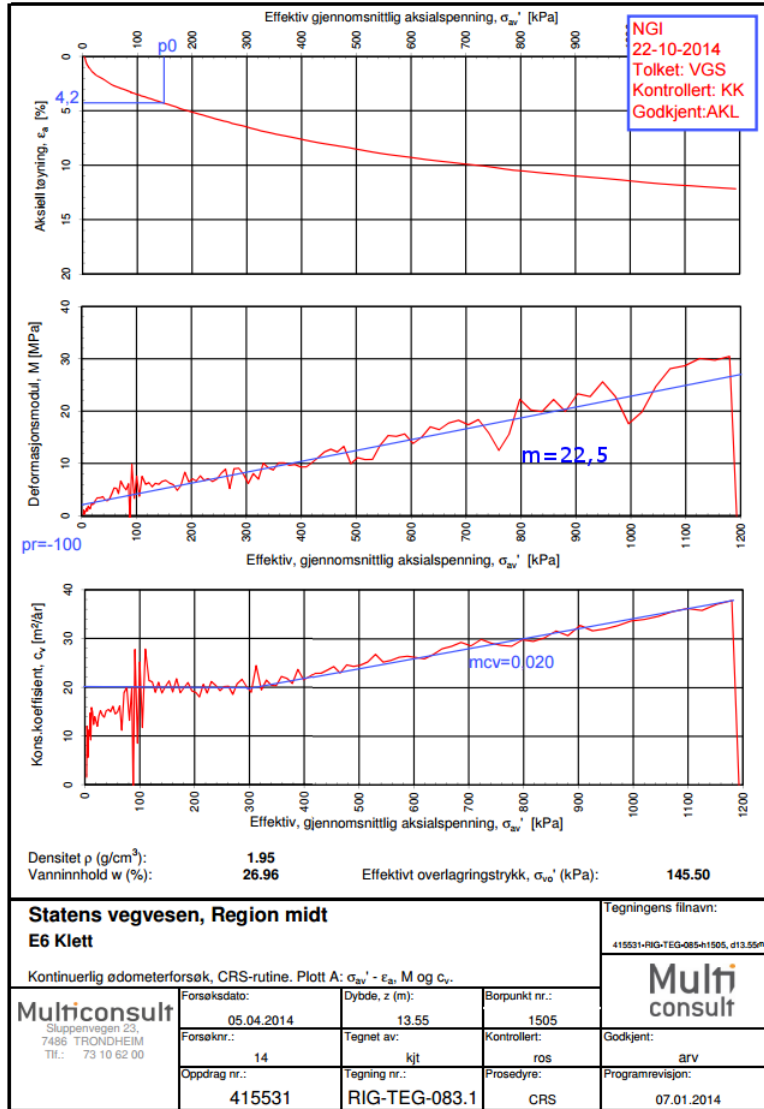


Figure C.5: Interpreted oedometer 1505 13.55 m. depth (Modified after NGI (2015)).

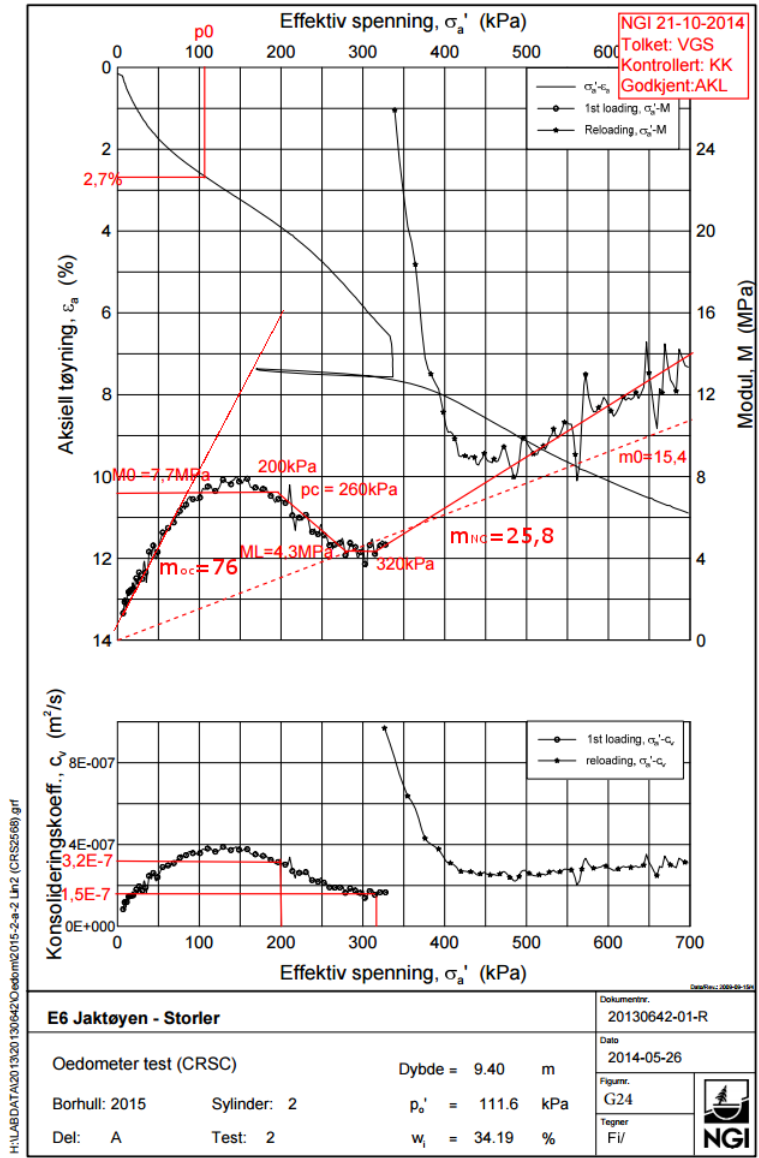


Figure C.6: Interpreted oedometer 2015 9.40 m. depth (Modified after NGI (2015)).

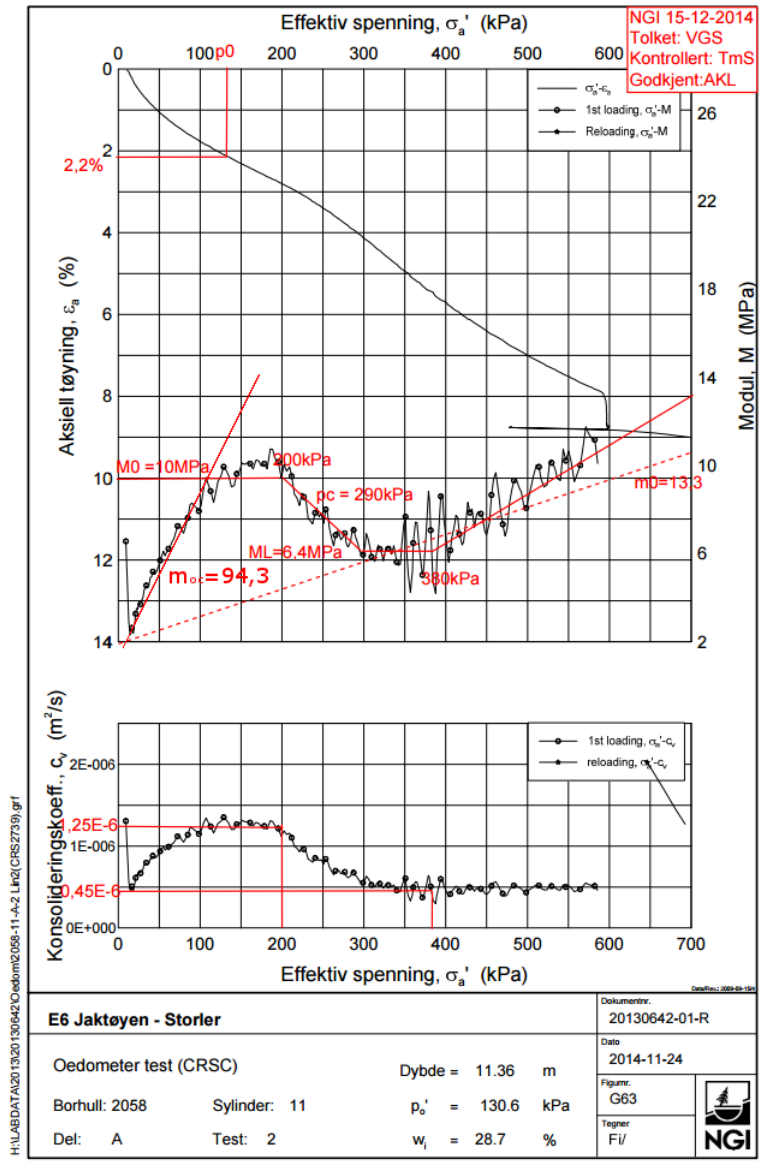


Figure C.7: Interpreted oedometer 2058 11.36 m. depth (Modified after NGI (2015)).

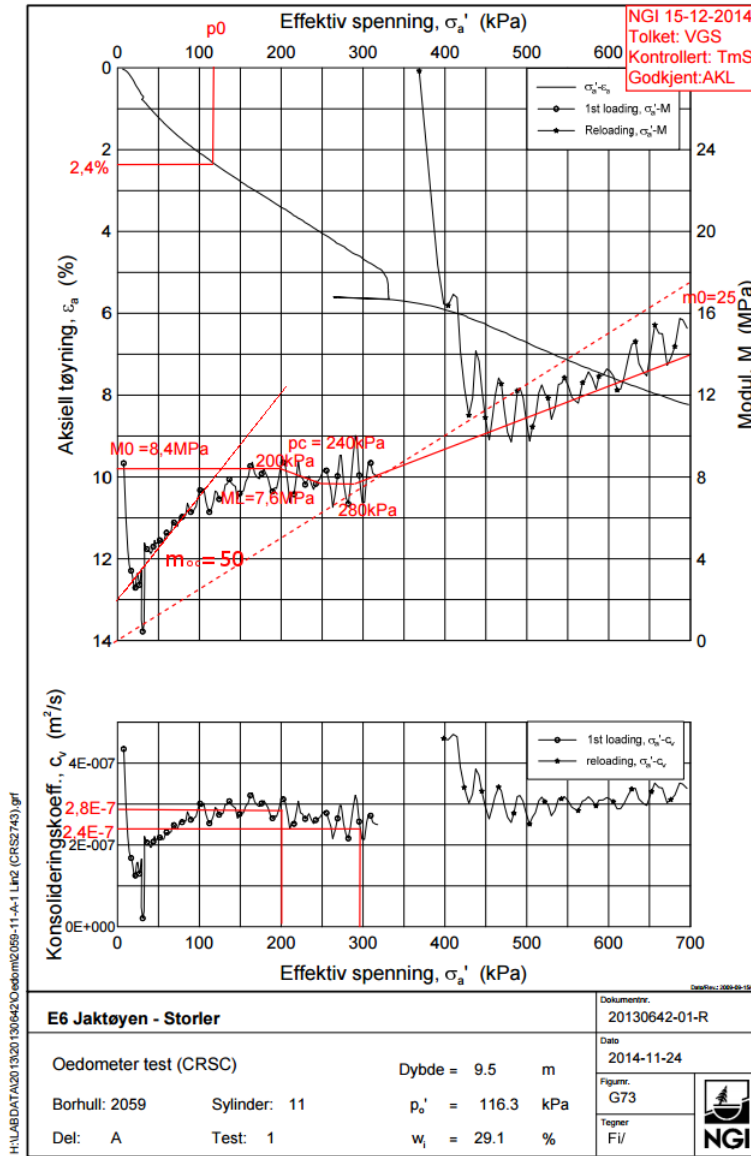


Figure C.8: Interpreted oedometer 2059 9.5 m. depth (Modified after NGI (2015)).

C.2 Tri-axial Tests

This section will show tri-axial tests explained in section 5.6. Table C.1 show input from (NGI, 2015) to the verification performed in Soil Test in Plaxis against laboratory tests. SSC and USDm are verified against block sample 1502 at depth 9.99 m. and 14.91 m. and 72 mm sample 2015 at 16.40 m. and 9.55 m. below ground surface. Figure C.9 to C.16 show same results as in section 5.6.

Table C.1: Input data for calibration

Sample nr.	Diameter [mm]	Type	Depth [mm]	w_i [%]	I_p [%]	p'_{0v}	σ'_1	σ'_3	K'_0
1502	Block	CAUA	9.99	31.0	4.0	114.0	110.0	88.0	0.80
1502	Block	CAUA	14.91	33.0	4.0	166.0	160.0	128.4	0.80
2015	72	CAUA	9.55	31.0	9.0	109.0	112.8	67.7	0.60
2015	72	CAUA	16.40	32.0	13.0	187.0	190.7	114.5	0.60

C.2.1 Block Sample 1502 at Depth 14.91 m. and 9.99 m.

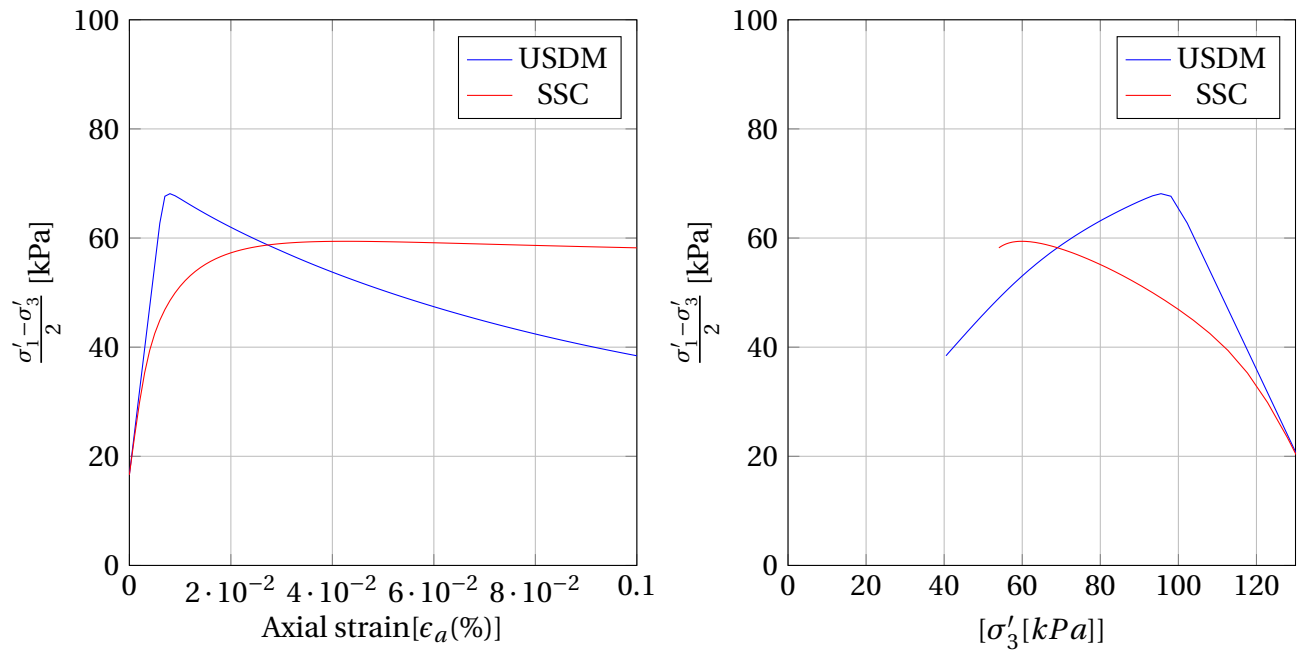


Figure C.9: Stress-strain relationship and stress diagram for SSC and USDM sample 1502 14.91 m. in Soil Test

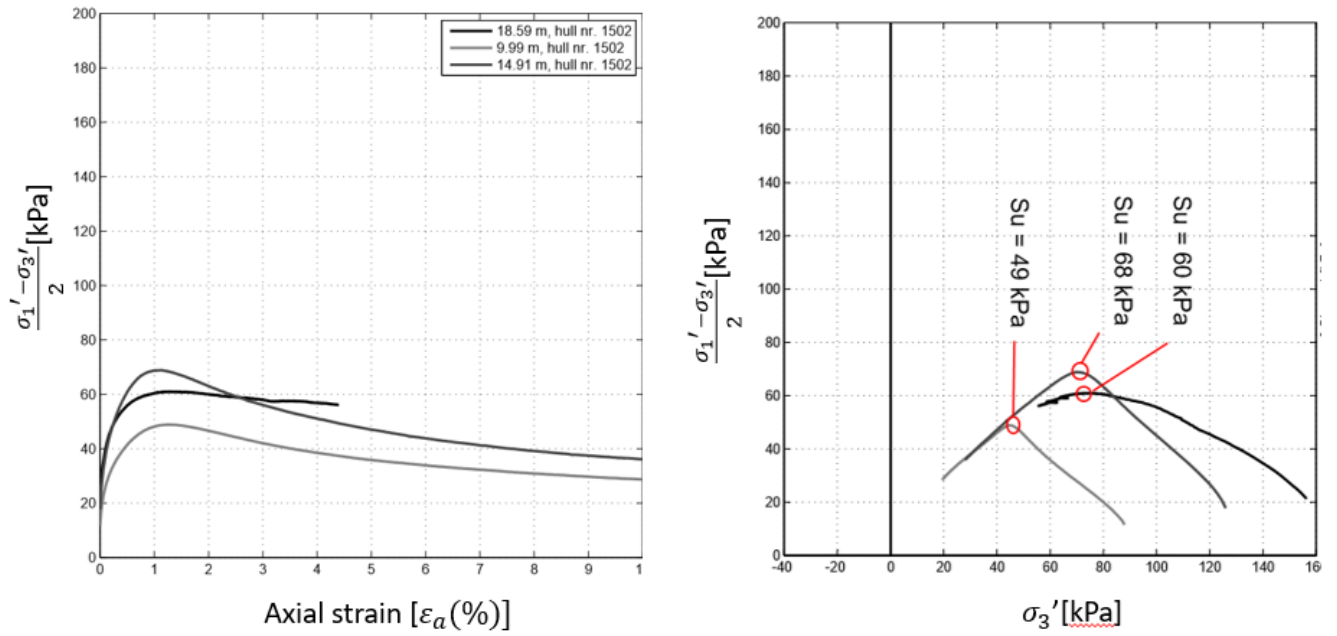


Figure C.10: Stress strain relationship and stress diagram laboratory tests sample 1502 (Modified after [NGI \(2015\)](#))

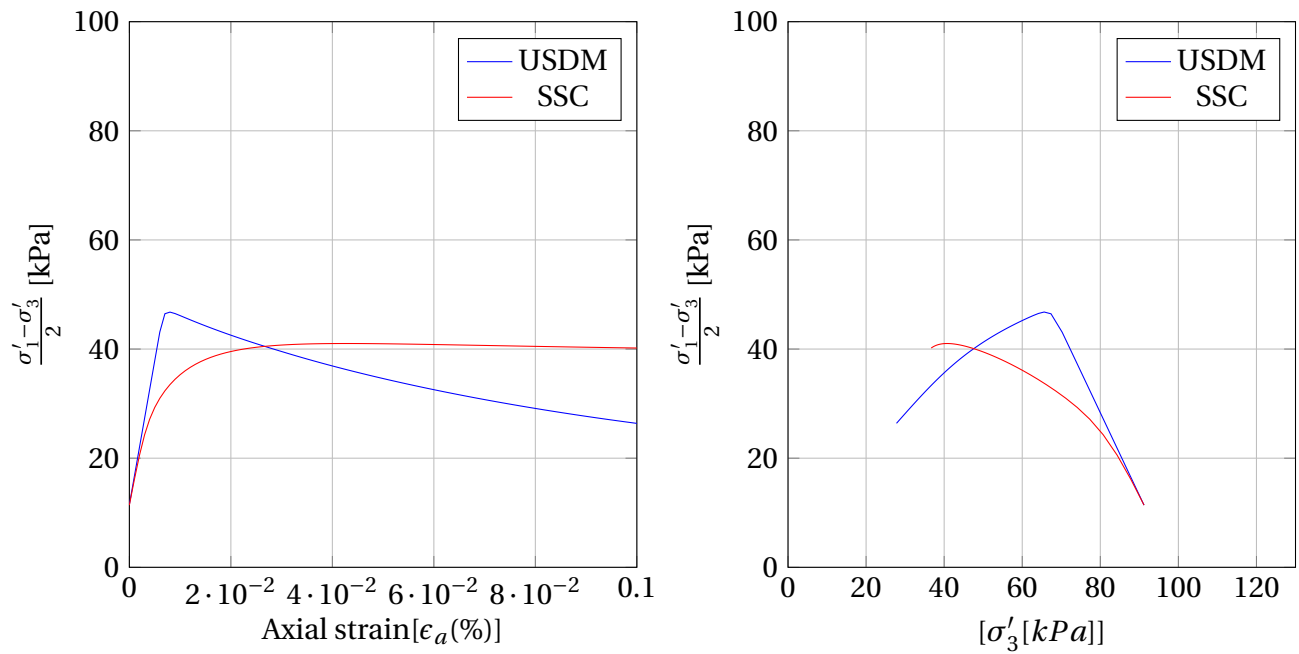


Figure C.11: Stress-strain relationship and stress diagram for SSC and USDM sample 1502 9.99 m. in Soil Test

Table C.2: Calibrated input parameters USDM

Parameters	14.91 m.	9.99 m.
ϕ_{cs}	31°	31°
ϕ_p	18°	18°
K_0^{NC}	0.53	0.53
r_{si}	510	510
x_0	5	4
POP	166	114
g^*	0.028	0.028
a_v	30	30
ω	0.4	0.4
μ	40	40
β_{k0nc}	0.1	0.1
τ	1.00	1.00
OCR_{max}	1.500	1.500

C.2.2 72mm Sample 2015 at Depth 16.40 m.

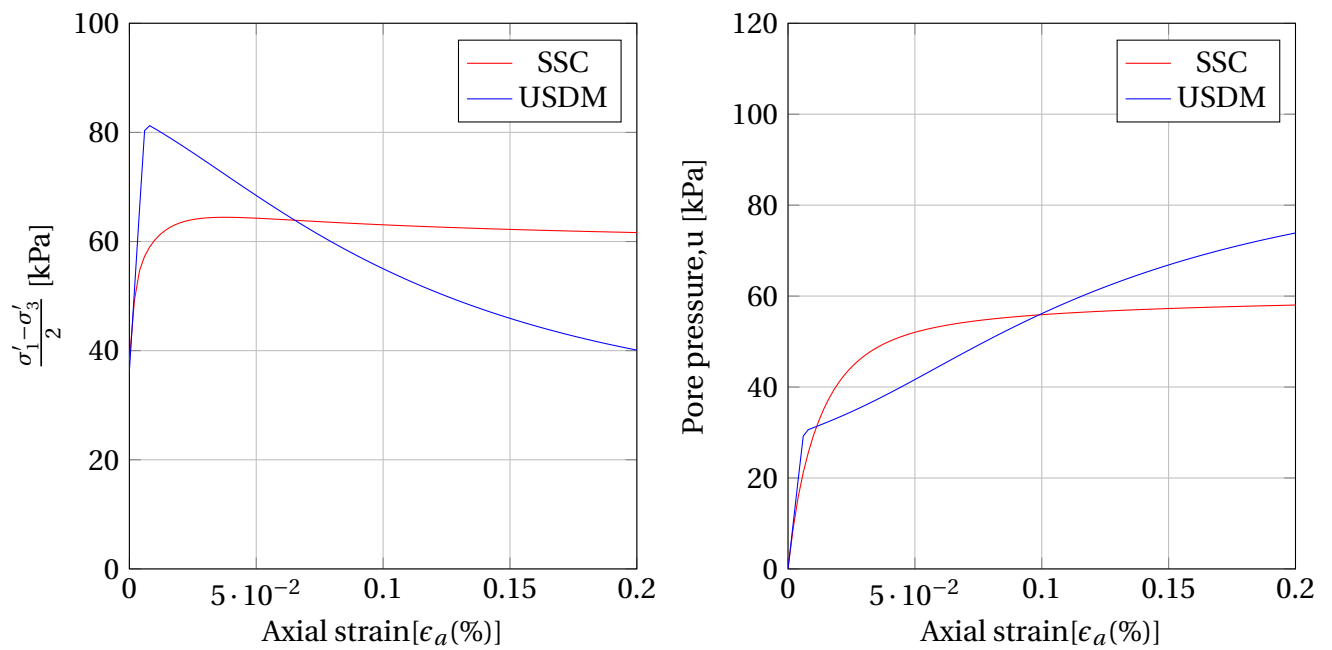


Figure C.12: Stress-strain relationship and pore pressure-strain for sample 2015 16.40 m. in Soil Test

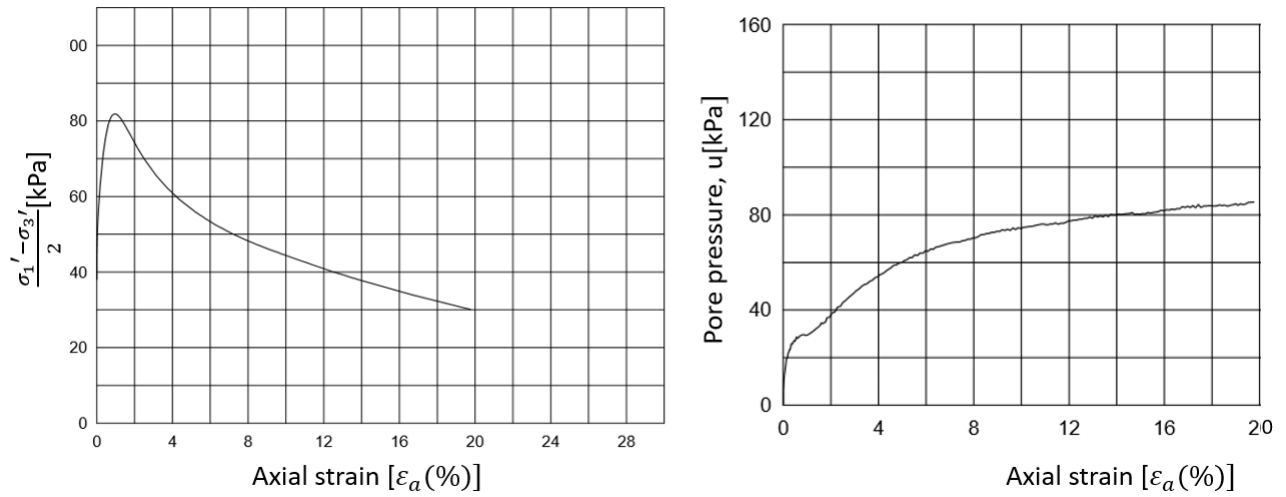


Figure C.13: Stress strain relationship and pore pressure development laboratory tests sample 2015 16.40 m. (Modified after [NGI \(2015\)](#))

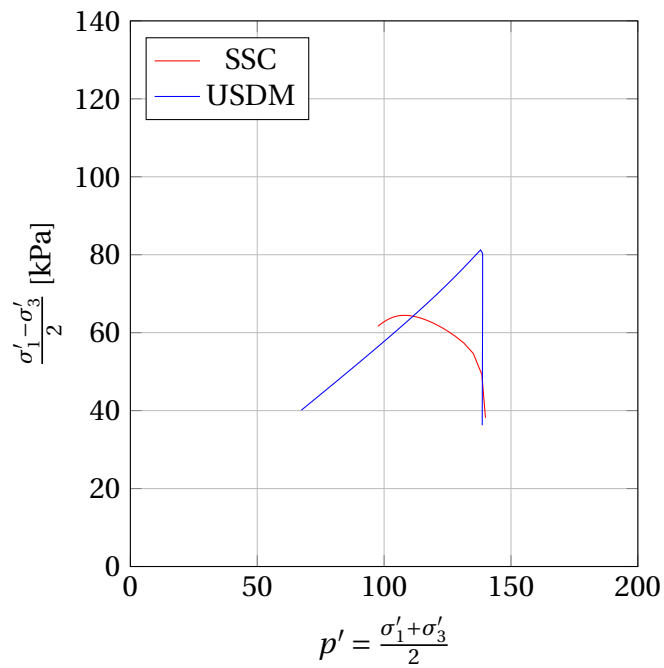


Figure C.14: Effective stress path SSC and USD M 2015 16.40 m. in Soil Test

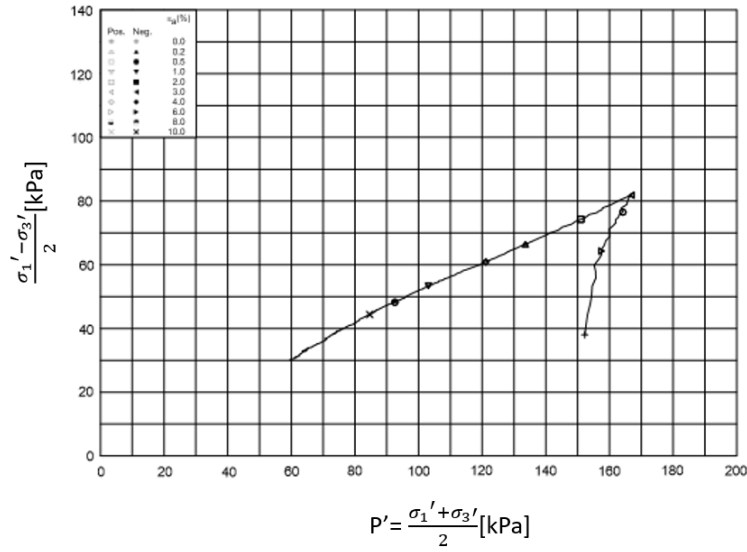


Figure C.15: Laboratory tests sample 2015 16.40 m. (Modified after NGI (2015))

Calibrated parameters can be seen in table C.3.

C.2.3 72mm Sample 2015 at Depth 9.55 m.

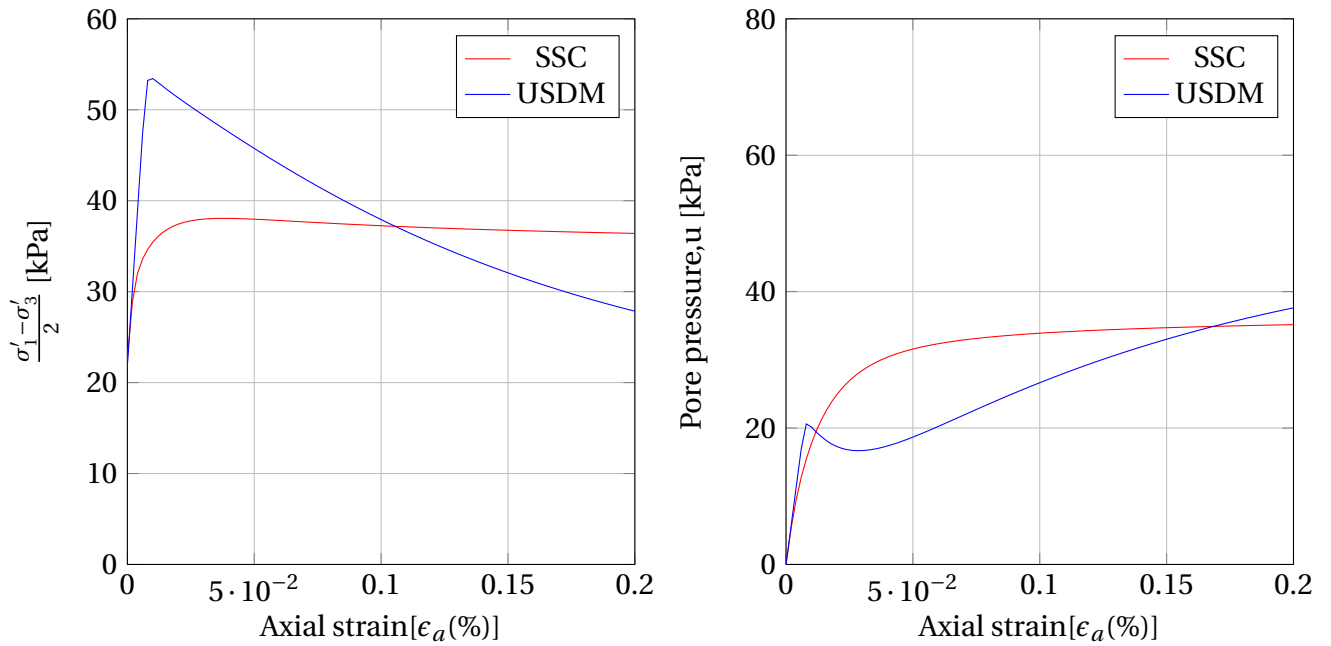


Figure C.16: Stress-strain relationship and pore pressure development for sample 2015 9.55 m. in Soil Test

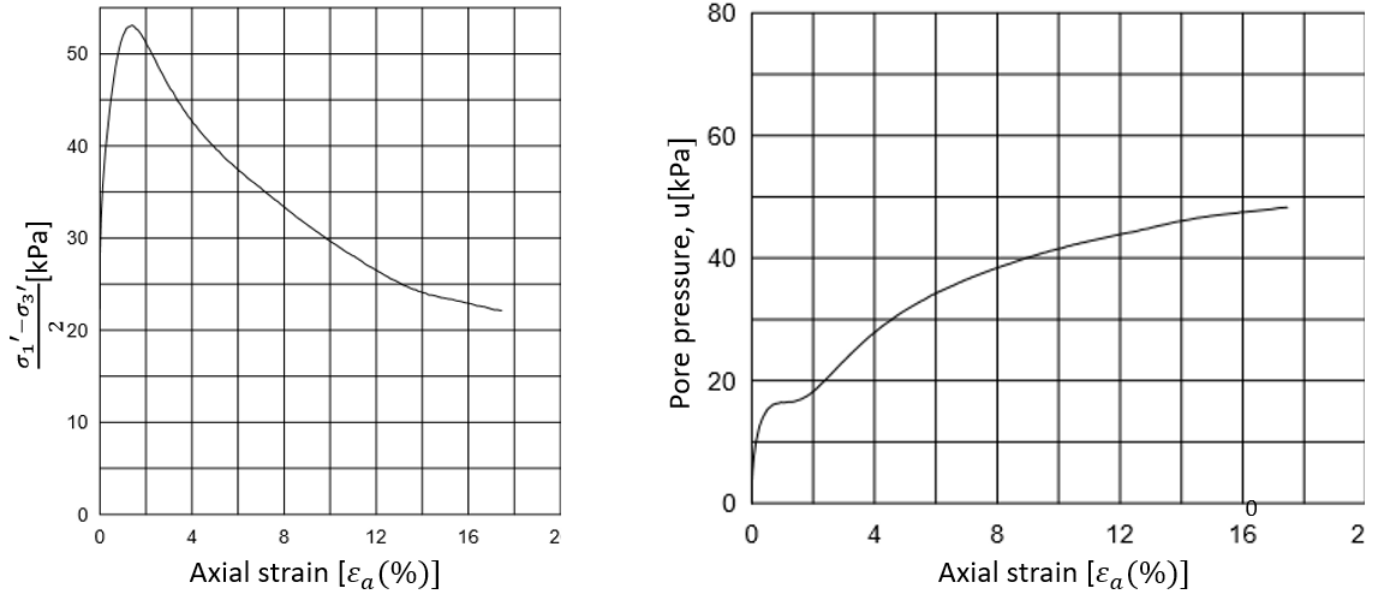


Figure C.17: Laboratory tests sample 2015 9.55 m. (Modified after [NGI \(2015\)](#))

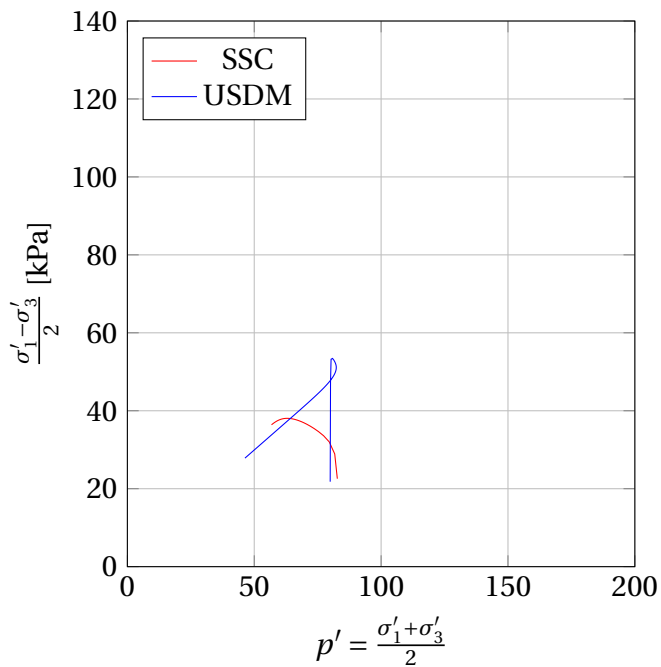


Figure C.18: Effective stress path SSC and USDM 2015 9.55 m. in Soil Test

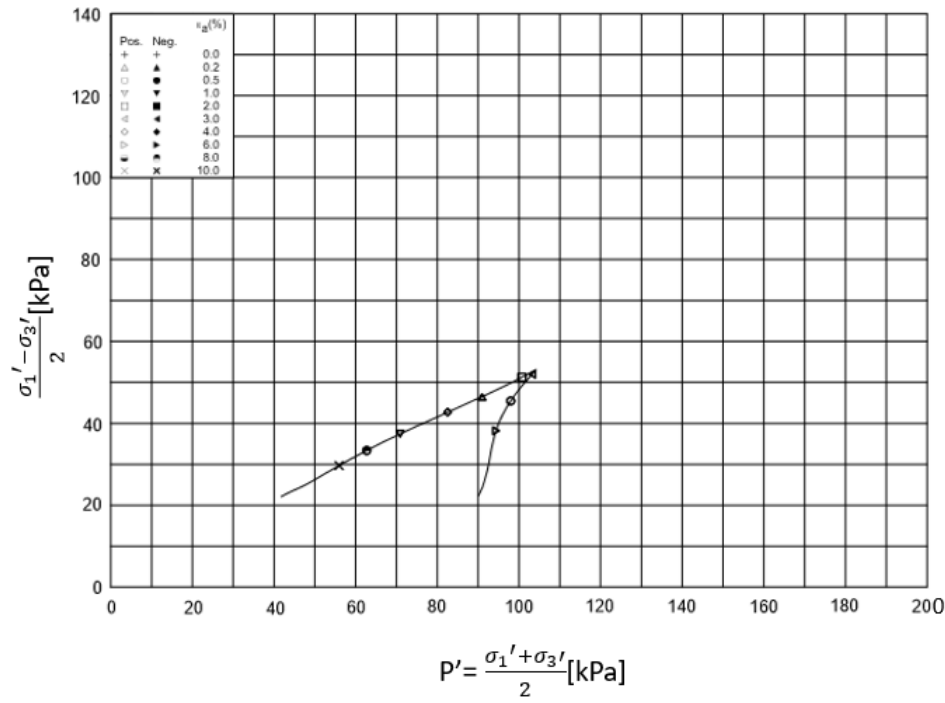


Figure C.19: Laboratory tests sample 2015 9.55 m. (Modified after NGI (2015))

Table C.3: Calibrated input parameters USDM

Parameters	16.40 m.	9.55 m.
ϕ_{cs}	31°	31°
ϕ_p	20°	22°
K_0^{NC}	0.53	0.53
r_{si}	510	510
x_0	5	5
POP	187	109
g^*	0.028	0.028
a_v	30	30
ω	0.3	0.25
μ	40	40
β_{k0nc}	0.1	0.1
τ	1.00	1.00
OCR_{max}	1.500	1.500

Appendix D

2-D Model

This appendix will show background data for modelling the 2D-model in section [6.1](#). Exact geometry is reconstructed through this data.

D.1 2-D Model

D.1.1 Measured Heights

The measured layers for dates presented in figure [6.5](#) is shown in [D.1](#). Each layer describes the measured height for the given time and the geometry is implemented in the 2D-Model. Date and time interval is given in table [D.1](#).

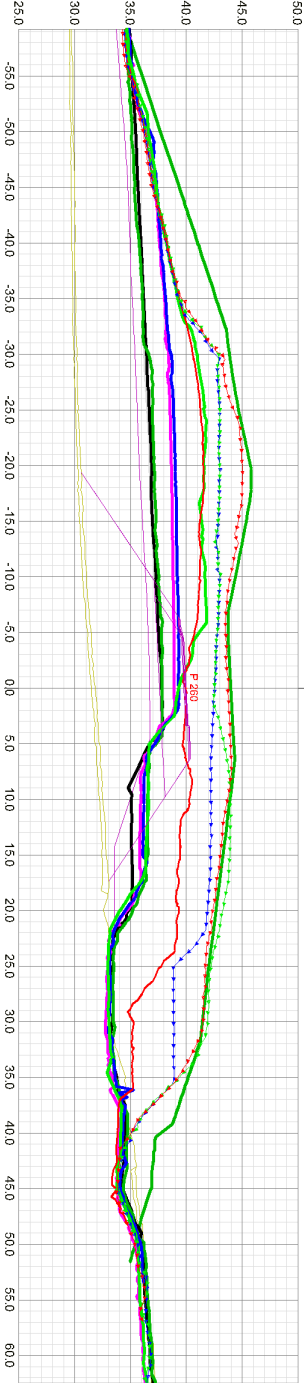


Figure D.1: Cross section through embankment with vertical drains (After NGI (2015)).

Table D.1: Load layers

Layer	Date	Time interval [Days]
0	2016-08-28	0
1	2016-10-25	56
2	2016-11-11	16
3	2016-11-21	10
4	2016-12-02	11
5	2017-01-05	34
6	2017-01-17	12
7	2017-01-25	8
8	2017-02-02	8
9	2017-02-13	11
10	2017-02-17	4
11	2017-03-20	31

D.1.2 Drone Photos

Drone photos used to recreate load application in phase 0-4 in section 6.3 is shown in figure D.2 to D.5.



Figure D.2: Drone photo 04.08.2016 (Statens Vegvesen, 2016).



Figure D.3: Drone photo 09.02.2016 (Statens Vegvesen, 2016).



Figure D.4: Drone photo 10.10.2016 (Statens Vegvesen, 2016).



Figure D.5: Drone photo 10.10.2016 (Statens Vegvesen, 2016).

Appendix E

Settlement

This appendix show background data for settlement calculations.

E.1 Settlement plates

The dates and displacement for the measurement of settlement plates are shown in table [E.1](#).

Table E.1: Settlement Plates

Dates	Settlement [mm]
07.09.2016	0
21.09.2016	14
17.10.2016	29
25.10.2017	62
31.01.2017	62
06.02.2017	56
13.02.2017	54
02.03.2017	55
06.03.2017	54
13.03.2017	57
20.03.2017	54
27.03.2017	54
03.04.2017	55
18.04.2017	53
24.04.2017	58
05.05.2017	58
11.05.2017	58

Bibliography

- Aalto, A., Rekonen, R., and Lojander, M. (1998). *The Calculations on Haarajoki Test Embankment with the Finite Element Program Plaxis 6.31*, pages 37–46. Springer Vienna, Vienna.
- Amundsen, H., Emdal, A., Sandven, R., and Thakur, V. (2015). On engineering characterisation of a low plastic sensitive soft clay. *GeoQuebec, Quebec*.
- Barron, R. (1948). The influence of drain wells on the consolidation of fine-grained soils. *Diss., Providence, US Eng. Office*.
- Barron, R. A. (1900). Consolidation of fine-grained soils by drain wells.
- Bjerrum, L. (1967). Engineering geology of norwegian normally-consolidated marine clays as related to settlements of buildings. *Geotechnique*, 17(2):83–118.
- Bjerrum, L. (1973). Problems of soil mechanics and construction on soft clays.
- Cudny, M. and Neher, H. P. (1998). Numerical analysis of a test embankment on soft ground using an anisotropic model with destructuration. In *Proc., Int. Workshop on Geotechnics of Soft Soils-Theory and Practice*, pages 265–270. VGE Verlag GmbH Essen, Germany.
- Grimstad, G. (2016). *EU CREEP project*, (PIAG_GA₂011 – 286397 – R4).
- Grimstad, G. and Degago, S. A non-associated creep model for structured anisotropic clay (n-sac). In *Proceedings of the 7th European Conference on Numerical Methods in Geotechnical Engineering*, pages 3–8.
- Hansbo, S. (1981). Consolidation of fine-frained soils by prefabricated drains. *Proceedings of 10th International Conference on Soil Mechanics and Foundation Engineering, Stockholm*, 3:677–682.

- Indraratna, B., Balasubramaniam, A. S., and Ratnayake, P. (1994). Performance of embankment stabilized with vertical drains on soft clay. *Journal of Geotechnical Engineering*, 120(2):257–273.
- Indraratna, B. and Redana, I. (2000). Numerical modeling of vertical drains with smear and well resistance installed in soft clay. *Canadian Geotechnical Journal*, 37(1):132–145.
- Indraratna, B. and Sathananthan, I. (2003). Comparison of field measurements and predicted performance beneath full-scale embankments. In *Proc., 6th Int. Symp. on Field Measurements in GeoMechanics*, pages 117–127.
- Janbu, N. (1969). The resistance concept applied to deformations of soils. In *Proceedings of the 7th International Conference on Soil Mechanics and Foundation Engineering, Mexico City*, volume 2529, pages 191–196.
- Janbu, N. (1985). Soil models in offshore engineering. *Géotechnique*, 35(3):241–281.
- Karlsrud, K. and Hernandez-Martinez, F. G. (2013). Strength and deformation properties of norwegian clays from laboratory tests on high-quality block samples. *Canadian Geotechnical Journal*, 50(12):1273–1293.
- Karstunen, M. and Koskinen, M. (2008). Plastic anisotropy of soft reconstituted clays. *Canadian Geotechnical Journal*, 45(3):314–328.
- Karstunen, M., Krenn, H., Wheeler, S. J., Koskinen, M., and Zentar, R. (2005). Effect of anisotropy and destructuration on the behavior of murro test embankment. *International Journal of Geomechanics*, 5(2):87–97.
- Leroueil, S., Tavenas, F., Brucy, F., La Rochelle, P., and ROY, M. (1979). Behavior of destructured natural clays. *Journal of Geotechnical and Geoenvironmental Engineering*, 105(ASCE 14657 Proceeding).
- Lin, D., Kim, H., and BALASUBRAMMANIAM, A. (2000). Numerical modeling of prefabricated vertical drain. *GEOTECHNICAL ENGINEERING*, 31(2).
- Liu, M. and Carter, J. (2003). Volumetric deformation of natural clays. *International Journal of Geomechanics*, 3(2):236–252.
- Mehli, M. (2015a). *EU CREEP project*, (PIAG-GA-2011-286397).
- Mehli, M. (2015b). Creep analysis of onsoy test fill. *EU Creep project*, (PIAG-GA-2011-286397).

- Mesri, G., Lo, D. O. K., and Feng, T.-W. Settlement of embankments on soft clays. In *Vertical and Horizontal Deformations of Foundations and Embankments*., pages 8–56. ASCE.
- NGI (2014a). Datarapport. (20130642-01-R).
- NGI (2014b). Grunnforhold og jordegenskaper. (20130642-09-R).
- NGI (2015). K36 røddevegbrua geoteknisk prosjekteringsrapport. (20130642-11-R).
- Nordal, S. (2016). Geotechnical engineering, advanced course, tba 4116, ntnu, 2016.
- of Civil Engineering Researche, D. C. and Codes. Cur publication 191.
- Plaxis (2016). *Material Models Manual*.
- Plaxis (2017). *2D Tutorial 04: Construction of a road embankment*.
- Steinar Hermann, N. (1996). Grunnforsterkning - økonomi og metoder. *Norske Sivilingeniørers Forening*.
- Tavenas, F, Jean, P, Leblond, P, and Leroueil, S. (1983). The permeability of natural soft clays. part ii: Permeability characteristics. *Canadian Geotechnical Journal*, 20(4):645–660.
- Terzaghi, K. (1943). *Theory of consolidation, in Theoretical Soil Mechanics*. John Wiley Sons, Inc.
- Tønnesen, J. (1991). Gravimetri for kartlegging av løsmassemekktighet i gaulosen. 21(211).
- Vegdirektoratet (2014). Grunnforsterkning, fyllinger og skraaninger. Haandbok(V221).
- Verruijt, A. (2008). Consolidation of soils. *Encyclopedia of Hydrological Sciences*.
- Wheeler, S. J., Näätänen, A., Karstunen, M., and Lojander, M. (2003). An anisotropic elastoplastic model for soft clays. *Canadian Geotechnical Journal*, 40(2):403–418.
- Zentar, R., K. M. W. C. S. H. and Koskinen, M. Comparison of two approaches for modelling, anisotropy of soft clays. *Proceedings of 8th International Symposium on Numerical Models in Geomechanics (NUMOG VIII), Rome 10-12 April, Edited by G.N. Pande and S. Pietruszzak*, pages = 115-121.